Sensitivity Analysis of Hydrodynamic Parameters on the Dynamic Response of the Semisubmersible Floating Offshore Wind turbine with the use of OpenFAST

MSc Thesis Report

Dimitra Karystinou

TUDelft Delft University of Technology

DELFT UNIVERSITY OF TECHNOLOGY

FACULTY OF ELECTRICAL ENGINEERING, MATHEMATICS AND COMPUTER
SCIENCE
WIND ENERGY GROUP, FACULTY OF AEROSPACE ENGINEERING, DELFT
UNIVERSITY OF TECHNOLOGY
MSC SUSTAINABLE ENERGY TECHNOLOGY

Sensitivity Analysis of Hydrodynamic Parameters on the Dynamic Response of the Semisubmersible Floating Offshore Wind Turbine with the use of OpenFAST

to obtain the degree of Master of Science in Sustainable Energy Technology
at Delft University of Technology

by

Name	Student Number
Dimitra Karystinou	5540739

Thesis Comittee

Prof.dr.ir Axelle Vire (Supevisor)
Dr.O.J (Oriol) Colomes Gene (Committee member)
L.(Likhitha) Ramesh Reddy (Daily Supervisor)

October 2023

An electronic version of this report is available at `http://repository.tudelft.nl/`.

TUDelft

Abstract

The advancement of floating wind turbine technology in recent years necessitates accurate predictions of their behaviour using various simulation tools. Utilizing multi-fidelity tools like OpenFAST allows for comprehensive calculations of the entire floating wind turbine structure. However, the precision of these calculations is challenged by the uncertainties associated with different system parameters.

The main goal of this research is to conduct a comprehensive exploration of various parameters, with a particular emphasis on hydrodynamic factors, and their impact on the structural and aerodynamic performance of semi-submersible floating wind turbines. To achieve this, an extensive sensitivity analysis approach is employed, utilizing the multi-fidelity model OpenFAST. The simulations are conducted on a semi-submersible floating wind turbine, specifically the one used in the OC4 experiment, featuring the 5MW NREL wind turbine. The Elementary Effects (EE) method is employed in this study to assess the significance of various factors. These factors include the hydrodynamic drag coefficients, wave height, peak wave period, wind speed, wind direction, current speed, current direction, and turbulence intensity. Their influence on the Damage Equivalent Load (DEL) of different loads acting on the floating offshore wind turbine (FOWT) is thoroughly examined.

The analysis conducted in this study has unveiled several key findings. The most influential parameters identified are the current speed, primarily impacting mooring line tension, and the significant wave height, which exhibits a balanced effect across various outputs, including hydrodynamic loads, tower loads, and rotor dynamics. Additionally, turbulence intensity emerges as a significant factor, particularly concerning rotor thrust and torque.

When employing the Morison equation, the order of parameter significance remains consistent with the hybrid theory (Potential + Drag). However, it is noteworthy that the added mass coefficients carry greater significance compared to the drag coefficient. Furthermore, simulations conducted using probability distributions for different locations confirm that wave height consistently ranks as the most significant parameter. However, the overall significance may vary and decrease in more severe environmental conditions.

The comparison with the OC3 spar platform revealed a similar pattern when examining the influence of current speed and significant wave height. Nonetheless, the simple hydrodynamic drag coefficient used for the whole platform also displayed significance, emphasizing the sensitivity of the spar platform loads to this modelling parameter. This significance is much higher than the corresponding one of the semisubmersible platform.

The research underscores it is imperative to mitigate the uncertainty associated with various parameters. This can be achieved through experimental verification and establishing correlations between modelling parameters and the specific conditions being simulated. Additionally, given that the most influential parameters are related to external conditions, it becomes crucial to simulate conditions that closely resemble the anticipated deployment location for the floating offshore wind turbine (FOWT). By doing so, the accuracy and reliability of the simulations will be enhanced to better inform FOWT design and deployment strategies.

Preface

As the journey of my master's program at TU Delft draws to a close, I find myself overwhelmed with gratitude and reflection. This path has been one of profound personal growth, intellectual development, and moments of challenge. This thesis stands as a testament to the dedication and effort that have carried me through, and I am deeply thankful for the guidance and encouragement I have received along this remarkable journey.

My interest in wind turbines was initially ignited during my studies, but it was within the pages of this thesis that the world of floating wind turbines was unveiled to me. Here, I had the privilege to dive deeper into this captivating field of study. This thesis encapsulates the wealth of knowledge and skills I have acquired throughout the MSc Sustainable Energy Technology program, flourishing within the rigorous academic environment at TU Delft.

First and foremost, I extend my gratitude to my supervisor, Prof.dr.ir Axelle Vire, for her unwavering guidance. Additionally, I am profoundly thankful to Likhitha Ramesh Reddy, for her invaluable feedback and whose mentorship has been fundamental for the entire process of the thesis. I would also like to express my appreciation to Dr. Oriol Colomes Gene for his valuable contribution as a committee member.

My heartfelt thanks go to my family, who has supported me throughout this challenging journey of pursuing a master's degree far from home. To my friends, your presence has illuminated even the darkest days.

Lastly, I wish to express my profound gratitude to the Onassis Foundation for their generous financial support, which made it possible for me to pursue my master's degree in the Netherlands, turning a dream into reality.

Delft, October 2023
Dimitra Karystinou

Contents

List of Figures

List of Tables

List of Abbreviations

List of Symbols

$sigma_u$ Turbulence standard deviation [m/s]

ϵ_n Random phase angle component [rad]

γ Peak shape parameter [-]

$_u$ Turbulence Intensity [%]

λ Wave length [m]

Λ_u Length scale parameter in Kaimal spectrum [m]

ω Angular frequency [rad/s]

ω_n Circular frequency component [rad/s]

ϕ Wave potential $[m^2/s]$

$\S_u$ Kaimal Spectrum $(m/s)^2/Hz$

ζ Wave elevation [m]

ζ_s Significant wave elevation [m]

ζ_{an} Wave amplitude component [m]

c Phase velocity $[m/s]$

c_g Phase group velocity $[m/s]$

E Total wave energy [J]

Fr Froude number [-]

g Gravity acceleration $[m/s^2]$

H Wave height [m]

h Water depth [m]

H_s Significant wave height [m]

K Kinematic wave energy [J]

k Wave number $[m^{-1}]$

k_n Wave number component [rad/m]]

KC Keulegan-Carpenter number [-]

m_n Spectral moments $[m^n]$

P Potential wave energy [J]

p Pressure $[N/m^2]$

Re   Reynolds number [-]

T_p Peak wave period [s]

u   Water velocity x-axis [m/s]

u_{tide} Tide current speed [m/s]

u_{wind} Wind current speed [m/s]

w   Water velocity z-axis [m/s]

Part I

Theory & Background

1 Introduction

1.1 Floating Wind Turbines

The rise in the energy demand combined with the constraints set by the Paris Agreement to reduce greenhouse gas emissions by 43% by 2030 has stimulated interest in renewable sources such as wind energy. Offshore wind has advanced tremendously in order to explore the greatest energy potential it offers. Over the next two decades, offshore wind power will develop significantly, increasing efforts to decarbonize energy systems and decrease air pollution as it becomes a larger fraction of the electricity supply. In fact, the potential of offshore wind amounts to 420,000 TWh per year worldwide, which is 18 times the current global electricity demand [1].

The Northern Sea has provided remarkably favourable circumstances for the development and commercialization of offshore wind technology because of its high-quality wind resources and relatively shallow waters and as a result Europe is the leading region in offshore wind. In the European Union (EU), the installed offshore wind capacity reached 14.6 GW in 2021 [2] and is expected to increase more than 25 times by 2030, with the use of the potential of the EU sea basins such as the North and the Baltic sea. On the other side, Asia, holding almost half of the market share, has commissioned several MW in China, Taiwan and Vietnam [3].

A significant aspect is that wind power is more potent at deeper water levels far away from the coast where the mean wind speeds are typically higher and constant [4]. Studies suggest that the greatest wind potential can be achieved in water depths where fixed-bottom offshore wind turbines are difficult to install. To be more specific, 80 % of the wind potential is located in depths of more than 60 meters, which is outside the feasible range for the majority of seabed-fixed (bottom-fixed) offshore foundations [1]. From this prospect, the development of Floating Offshore Wind Turbines (FOWT) is imperative, with 121.4MW of installed capacity at the end of 2021, the majority of which will be installed in Europe [3]. According to predictions of the Global Wind Energy Council, by 2030, 18.9 GW of floating wind will be installed, while DNV anticipates 264 GW of floating wind by 2050, which will be 15% of the total offshore wind [5].

Apart from the power generation, FOWTs concerning their social acceptance since they are not visible far away from land and they do not compete with human activity near the coast. Based on that, the first large-scale floating wind turbine concept was proposed by Professor William E. Heronemus in 1972 [6]. Although the idea was introduced around 50 years ago, floating wind turbines have been developed only in recent years. There are several floating wind farms in Europe and single FOWT systems used for projects [7]. The oldest one, Hywind Scotland, has five wind turbines with a total 30 MW capacity and is located near Peterhead, Scotland. It began operating in 2017 and also had a 57.1% capacity factor on average. Windfloat Atlantic, with a 25 MW capacity and the ability to power 60,000 consumers, was unveiled in Portugal in July 2020. Kincardine, which is also located in Scotland, is the largest currently online; it has a total capacity of 48 MW, enough to power 50,000 houses. These wind farms are depicted in Figure 1.1 along with the prospective floating wind farm in Norway, which is partially online and is expected to be the largest with a capacity of 95 MW.
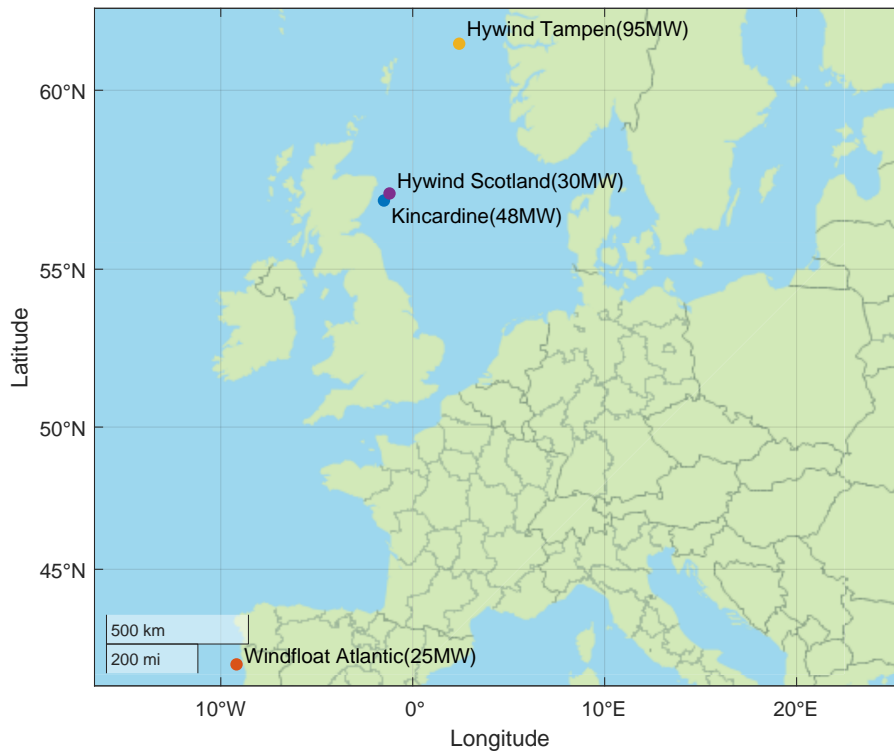
Figure 1.1: *Map of operational floating wind farms in Europe 2023*

1.2 FOWT structures

FOWTs consist of three main components: the wind turbine, the floating structure and the mooring system. All these come along with the anchoring and the electrical cables. The interaction of the FOWT components with the environment affects the structural performance and the power output of the wind turbine. Mooring systems, dynamic, suspended cables, and floating foundations for offshore wind all come in a variety of sizes, forms, and combinations.

Starting with floating structures, there are three main types of floaters.

- Spar

- Semi-submersible

- Tension Leg Platform (TLP)

Each one of them has unique characteristics and basic principles that make it appropriate for specific applications. Their characteristics in terms of depth, installation and cost are presented in Table 1.1 and the structural layout is depicted in Figure 1.2 .

Table 1.1: *Comparison of the different floating structures [4]*

Characteristics	Spar	Semisubmersible	TLP
Stability	Balance	Hydrostatics	Mooring
Min depth	Deeper (>100m)	Shallower(<50)	Medium(50-150m)
Periods	Good	Acceptable	Good
Fabrication	Simple structure	More complex	More complex

The primary properties used to compare the original structures are the stability, motion response, construction and installation aspects, depth independence, and mooring design. There are many
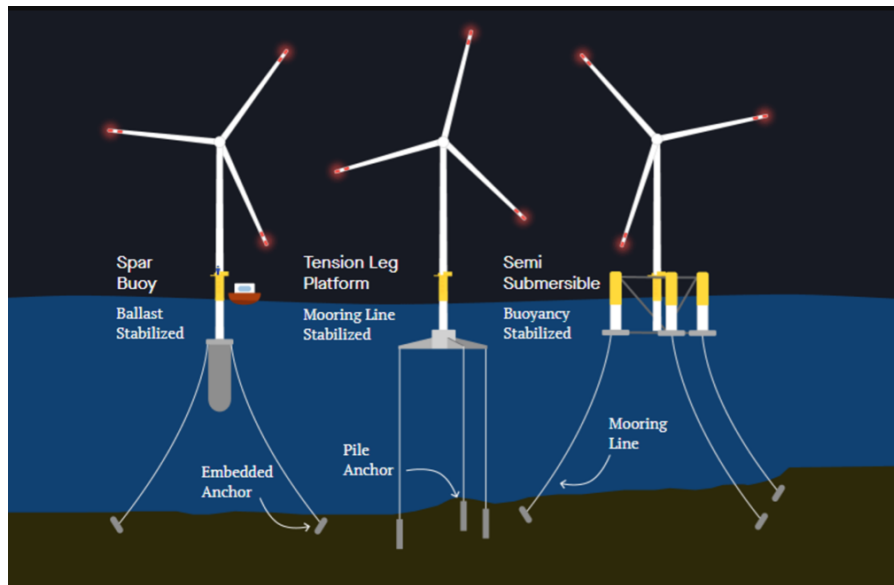
Figure 1.2: *Floating Structures Layout [8]*

more to be evaluated, such as the maturity of the design and its safety, which are also crucial for their selection.

Spar buoy design bases its stability on its centre of gravity, which is lower than the buoyancy centre [9]. This is achieved through a large upright cylinder with ballast weight in the lower part. Then catenary mooring wires are used to anchor the platform to the ocean floor firmly. Unlike the spar floater, semi-submersible bases its stability on distributed buoyancy provided by the wide submerged base structure of this type of floater. It consists of several cylinders while for added water plane stability, heave plates can be positioned at the base of the cylinders. The tension leg platform acquires stability through the tensioned mooring lines which are vertically anchored to the seabed. It also consists of a semi-submersible shallow structure that keeps the turbine in the right position.

The floating motion of each one of the floaters is also different. While stiff in translational motions, the spar floating structure is vulnerable to rotational motions. The semi-submersible structure is more sensitive to large wave-induced motions, with the tower top shifting considerably as a result of strong rotating motions caused by wave loading. On the contrary, TLP experiences small wave-induced oscillations and at the same time, it appears to be very rigid to rotational motions.

Their assembly and installation are also matters of significance. The spar is assembled on and offshore and then it may be towed to the site or not. The semi-submersible appears the most simple installation since it can be assembled on a dry dock and then towed to the site. TLP requires a more complex procedure since it is not self-stable.

Compared to the other two, the semi-submersible floater is additionally water depth independent, which means that it can be deployed in shallower waters as well. TLP is feasible in a range of 50m to 150m while the spar requires a water depth greater than 100m. The semi-submersible and spar structures usually have very long catenary mooring lines that are attached to drag-embedded (horizontally loaded) anchors. This results in higher costs. Instead, the TLP uses short vertical lines that to maintain a consistent tension between the anchors and buoyancy tank, they must carry a substantially heavier burden.

1.2.1 Semi-submersible structure

The semi-submersible floating structure appears to be more adaptable to changes in water depth when compared to the other floating structures. Because of this, it can be applied to a variety of

locations, from those in shallower to deeper ocean depths. Due to the higher surface area, the semi-submersible structure is more exposed to waves, hence it is important to examine how different ocean conditions would affect this kind of platform.

A more thorough examination of the semi-submersible structure is presented in Figure 1.3. Typically, three or four cylindrical columns with smaller beams connecting them together make up a semi-submersible construction. The wind turbine can be positioned either in the center of the floater or on top of one of the columns of the structure, which can be made of steel or even concrete. Heave suppression discs (heave plates) may be included at the foot of the columns because, as was already indicated, it is one of the most significant motions. The usage of catenary mooring lines, which are more challenging to construct in shallow water, is another feature.
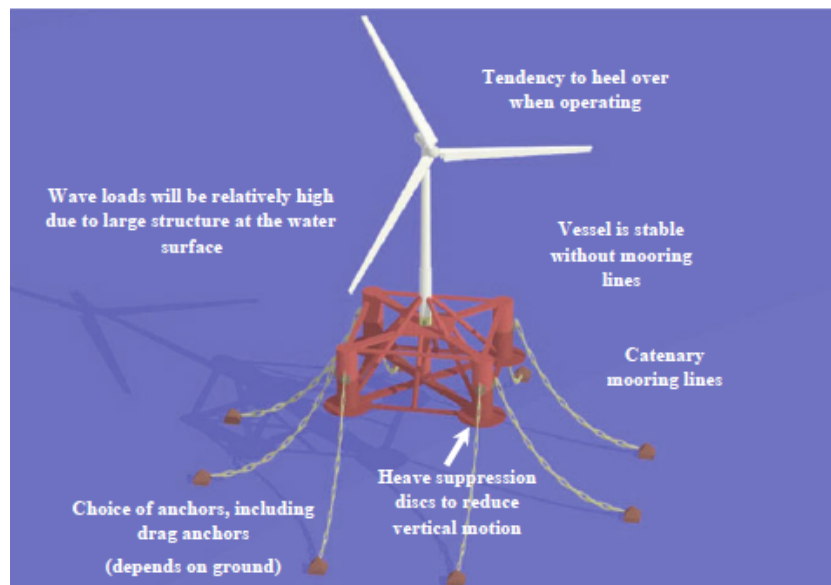
Figure 1.3: *Semis-submersible floating platform characteristics [4]*

There is a great amount of projects and structure layouts dedicated to the semi-submersible structure. Some of these structures are presented in Figure 1.4. As it is observed the design of the structure can differ while some extra components such as extra ballast components and heave dampers exist. The Tri-Floater that has been designed from GustoMSC [10] is a concept that promotes easy manufacturing and a scalable design while it does not use any extra ballast system. The SeaReed design of DCNS [11] is a different approach which consists of a central cylindrical column, that supports the wind turbine and three cylindrical columns connected with the central one through pontouns. The WindFloat is a type of floater that has been widely used in many projects and has been commercialized [12]. The design is the one, depicted in Figure 1.4c with three columns of which one supports the wind turbine. This platform also includes heave plates that dampen the wave motion and is 'turbine agnostic' meaning that it can support a wide range of wind turbine modifications.

1.3 Research Motivation

Despite the great wind potential in deeper waters, the technological development of FOWT systems is a major challenge. Due to their recent establishment, research and development on the FOWT and its alternative concepts is still underway. A correct prediction of the hydrodynamic behaviour and loading of the system impacts the design and manufacturing of the FOWT, especially for the floater itself. However, it is challenging to describe a coupled FOWT system, since the hydrodynamic response is debatable due to the stochastic nature of waves. This indicates a need to understand the various uncertainties of the hydrodynamic parameters that exist among the different models as well

(a) *Tri-floater concept [10]*   **(b)** *SeaReed Concept [11]*   **(c)** *WindFloat Concept [12]*
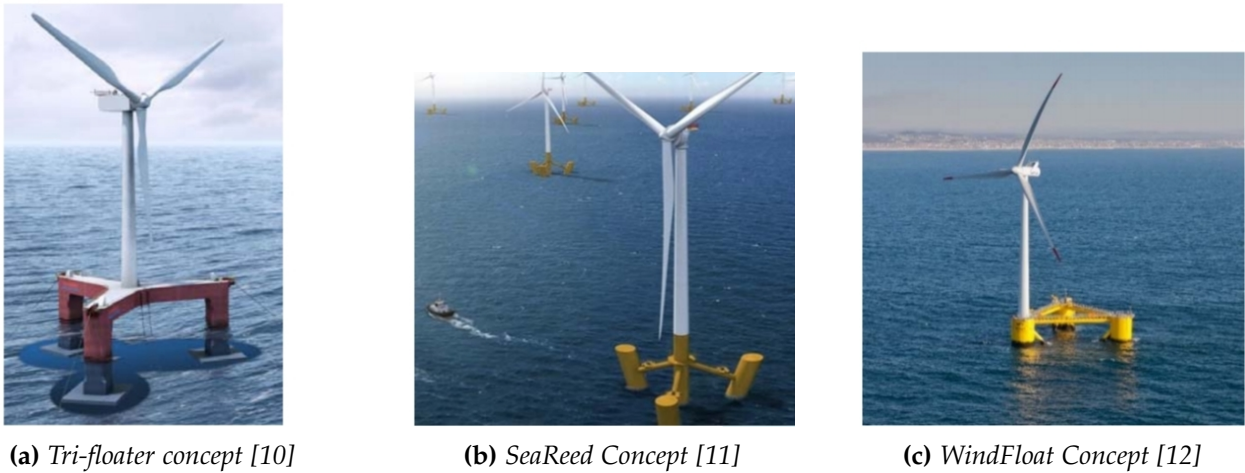
Figure 1.4: *Semi-submersible floating concepts*

as the exploration of different sea conditions in deep waters. In parallel, the role of inflow wind becomes particularly significant when it interacts with a floating structure, as opposed to a stable onshore installation.

Specifically for the case of the semi-submersible structure which is exposed to the wave motion, the need for relative research on hydrodynamic and aerodynamic loads is imperative. Several approaches have been developed and evaluated using different fidelity levels, while different hydrodynamic methods, namely Potential Flow Theory and Strip theory have been used. Nevertheless, choosing which method can accurately describe the overall loads with the least amount of computing expense is still necessary. A lot of effort has been devoted to the proper formulation of each of those methods and the proper tuning of their parameters under the consideration of wind and wave conditions.

It has been observed that the uncertainty associated with several parameters, encompassing both the modelling approach and the simulated environmental conditions, can substantially impact the behaviour of the floating offshore wind turbine (FOWT) system. Moreover, the multiparametric nature of this system makes it challenging to pinpoint which specific parameters exert the most significant influence.

For this reason, the project aims to identify the uncertain parameters within the FOWT model and investigate their impact in relation to varying external wind and metocean conditions. This will be achieved through the utilization of a medium-fidelity simulation tool, OpenFAST.

1.4 Research Objectives

The aforementioned motivation led to the problem statement of the thesis which can be described as follows:

The study aims to investigate the effect of different hydrodynamic parameters and environmental conditions on the hydrodynamic loads of a semi-submersible structure and the system's aerodynamic performance with the use of OpenFAST. The sensitivity of the different hydrodynamic parameters in combination with the external conditions from specific sites will be analyzed.

To better frame the problem the following research questions should be answered:

- Which input parameters have a wide range of variability?

- Which are the most significant input parameters with respect to the hydrodynamic loads, the mooring line tensions, the tower loads and rotor dynamics?

- What does the inclusion of turbulent wind introduce?

- What is the effect of the physical model on the significant parameter analysis?

- Can any conclusions be drawn when applying this analysis to a different type of floating platform?

- What does the location correlation add to the sensitivity analysis study?

1.5   Research Approach

The primary step of the research will include a literature review of the existing modelling approaches which will point out the properties that need further investigation. The numerical model will be verified with existing data from the literature and will be used as a reference throughout this work..

The initial part of the project will be approached with a sensitivity analysis which will measure the uncertainty of the different modelling parameters. This will be done with the Elementary Effects (EE) method which can scale the input parameters with respect to the influence they have on a specific output every time they change.

The second part is mostly relevant to the cases that would be simulated. For this part, different cases will be formulated based on real data from different locations that represent moderate, medium and severe wave and wind conditions. The measured sensitivity will then be compared and will also be correlated with the effect of the modelling parameters.

The overall approach of the research is presented in Figure 1.5 along with details of every step which will be analysed in the relevant chapters.

1.6   Report Layout

The thesis report is divided into two parts. The first one is dedicated to the literature review and the system definition while the second one focuses on the simulation tests and the sensitivity analysis results. In more detail:

PART I -Theory & Background

 Chapter 2 describes the basic wave theory developed to describe the sea motion and the basic equations used to describe the forces upon the floating structure.

In **Chapter 3** the existing numerical models are discussed and a thorough presentation of the up to date research is demonstrated. The motivation behind the thesis research is also presented.

Chapter 4 is dedicated to explaining the functionalities of the OpenFAST tool, focusing on the modules that will be used and modified in the simulations. The FOWT system is presented in more detail with the layout of the platform and the wind turbine characteristics. The inputs of the HydroDyn module are also discussed.

PART II -Simulations
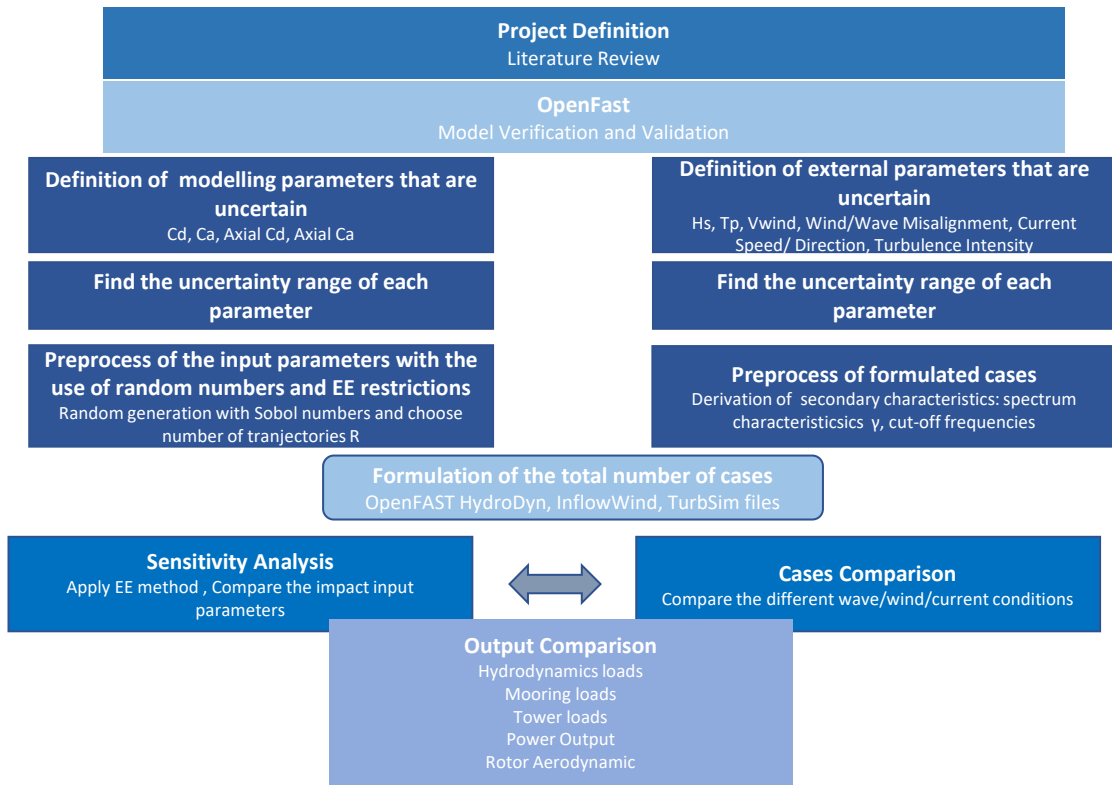
Figure 1.5: *Research Approach*

Chapter 5 presents the verification and the validation of the modelled system through a comparison with previous simulations and experiments of the same FOWT system. In this chapter, the basic idea of the different input parameters and their values is obtained.

Chapter 6 focuses on the uncertainty of the different parameters and the methodology of elementary effects methods used to measure their uncertainty. The chosen approach is analysed along with the post-process methodology.

In **Chapter 7** the results of the different simulations are analysed. Different cases and input and output parameters are discussed.

In **Chapter 8** a different formulation of cases is used, with realistic data from different locations and probability distributions for their selection.

Chapter 9 provides a comprehensive summary and conclusion of the project's findings while **Chapter 10** suggests areas of future research.

2   Wave Theory and Hydrodynamics

This chapter aims to introduce the different wave modelling techniques and to analyze the induced loads involved in the FOWT system. More specifically, Section 2.1 introduces the existing wave models and wave classifications depending on their characteristics. Section 2.2 discusses hydrodynamics by analysing the motions and forces on a floating body.

2.1   Wave models and Theory

Apart from the rotor motion similar to onshore wind turbines, FOWTs are also subjected to platform motion caused by sea state conditions. For this reason, it is important to explore the aero-hydro behaviour of the system.

2.1.1   Wave properties

Ocean waves are generated from the interaction between the wind and the sea and their analysis has been based on fluid mechanics. Waves can be generated in many ways and can be characterised based on their physical properties, such as the water depth h, the wavelength λ, the wave height H and relevant relations between those properties such as the wave steepness H/λ .

A first-order classification that applies to the waves that are produced by the wind divides them into two main categories: **sea** and **swell** [13]. Sea waves are those that are primarily created by the local wind patterns and are distinguished by their short crests and irregularity. On the other hand, swell waves might exist far from the area where they were created. They have longer crest lengths and are more regular. In addition to these two categories, water depth can be used to define waves Figure 2.1. The waves with a ratio of water depth h to a wavelength λ of more than 1/2 are known as deep water waves (short). Shallow water waves (long) have a ratio of h/λ less than 1/20.
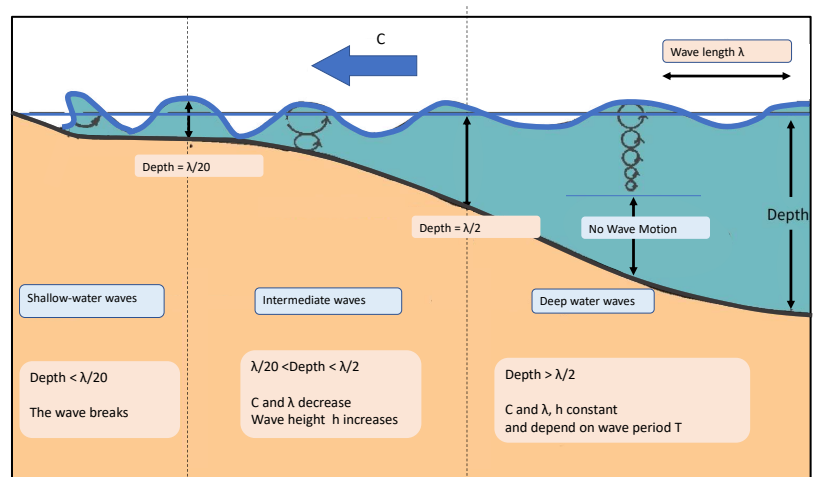
Figure 2.1: *Deep and Shallow water regions*

In shallow water depths, water particles can be influenced by the sea bottom, resulting in a huge difference in the speed of the upper particles, which move fast, to the lower ones, which have reduced speed. This results in the so-called breaking wave, which practically means that the top of

the wave spills over and falls down on the front surface.

There are three primary circumstances that lead to the breaking waves forming. The wave crest forming an angle less than 120 degrees is one cause. The wave height to wavelength ratio H/λ (steepness) falling below 1/7 is a secondary cause. Thirdly, breaking waves can occur when the wave height is more than three-fourths of the water depth (H > 3/4 D).

In addition to this fundamental division, the waves are separated into regular and irregular waves. This division has been used to build up different wave models and describe their behaviour mathematically.

2.1.2 Regular Waves

The simplest way to describe waves is with the use of a simple sinusoidal function. Regular or harmonic waves are single wave components with a given wave direction, height, and period. Usually, they are described with a sinusoidal function. Their characteristic shape can be described by a crest which is the highest point of the wave and a trough, which is the lowest point. The distance between two continuous crests gives the wavelength as shown in Figure 2.2, while the wave height is the vertical distance between the crest and the trough. The wave elevation is described by Equation 2.1 where ζ_a is the amplitude of the wave elevation as shown in Figure 2.2, $k = 2\pi/\lambda$ is the wave number (rad/m), $\omega = 2\pi/T$ is the angle velocity (rad/s).

$$\zeta(x,t) = \zeta_a \cos(kx - \omega t) \tag{2.1}$$
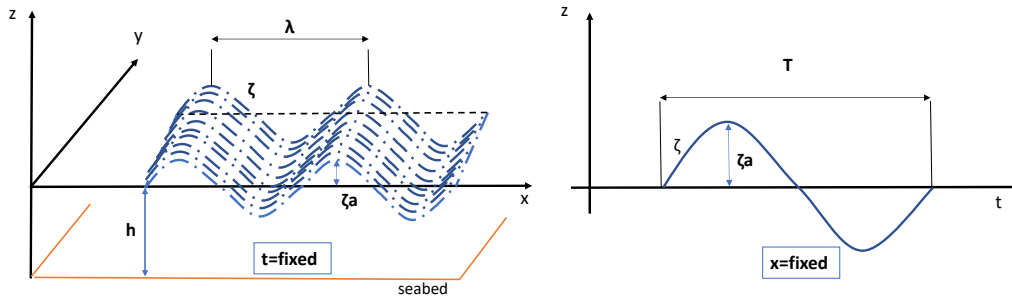
Figure 2.2: *Regular Wave Definition [13]*

Potential Flow Theory

In order to analyze the hydrodynamic behaviour of floating structures, the potential flow theory can be used. Potential flow theory is a linearized method that can be applied to regular waves. Based on the aforementioned expression Equation 2.1 for the wave elevation of regular waves the fundamental expressions of the potential flow theory can be derived. The potential theory has two main assumptions. The first indicates that the water surface is very small and this means that the wave steepness which is described by the ratio of wave height to wavelength H/λ is also small, this allows the neglection of some second-order terms. The second one is that a linear relationship between frequency components is considered and all nonlinearities are ignored. Starting with the equation, the wave can also be described with the use of potential Equation 2.2, where Φ is the wave potential of the wave, the derivative of which in the different direction gives the velocity.

$$\Phi(x,z,t) = \frac{\zeta_a g}{\omega} \cdot \frac{\cosh k(h+z)}{\cosh kh} \cdot \sin(kx - \omega t) \tag{2.2}$$

This form of the first order potential flow solution is based on the following fundamental assumptions:

a) **Continuity condition** or **Laplace** which is described as $\nabla^2 \phi = 0$

b) **Sea-bed boundary condition** which states that the vertical velocity at the sea bed is zero

c) **Free Surface dynamic boundary condition** which states that the pressure at the surface should be atmospheric

d) **Free Surface kinematic boundary condition** which states that the vertical velocity of the water particles at the free surface of the fluid is equal to the vertical velocity of the free surface itself.

With the above assumptions several equations can be derived. The dispersion relationship described by Equation 2.3 provides a relation between the angular wave frequency and the wave number.

$$\omega^2 = k \cdot g \cdot \tanh kh \tag{2.3}$$

While the phase velocity is calculated in Equation 2.4. With the approximation for shallow waters $\tanh hk = hk$ and for deep waters $\tanh hk = 1$ the expressions can be simplified more as presented in Equation 2.5 and Equation 2.6.

$$c = \sqrt{\frac{g}{k} \cdot \tanh kh} \tag{2.4}$$

$$\underbrace{c = \frac{g}{h}}_{\text{Shallow water}} \tag{2.5} \qquad \underbrace{c = \sqrt{\frac{g}{k}} = \frac{g}{\omega}}_{\text{Deep water}} \tag{2.6}$$

The afformentioned expressions lead to the wave kinematics and pressure relationships presented in Table 2.1.

Table 2.1: *Wave expressions for deep and shallow water depths*

Deep Water	Shallow water
$u = \zeta_a \omega \cdot e^{kz} \cdot \cos(kx - \omega t)$ (2.7)	$u = \zeta_a \omega \cdot \dfrac{1}{kh} \cdot \cos(kx - \omega t)$ (2.8)
$w = \zeta_a \omega \cdot e^{kz} \cdot \sin(kx - \omega t)$	$w = \zeta_a \omega \cdot \left(1 + \dfrac{z}{h}\right) \cdot \sin(kx - \omega t)$
$p = -\rho g z + \frac{1}{2}\rho g \zeta_a^2 \omega^2 \cdot e^{2kz} + \rho g \zeta_a \cdot e^{kz} \cdot \cos(kx - \omega t)$ (2.9)	$p = -\rho g z + \rho g \zeta_a \cdot \cos(kx - \omega t)$ (2.10)

Diffraction and Radiation

In the case of larger structures, scattering is important and the diffraction and the radiation effects should be considered. Diffraction and radiation effects are significant in floating structures in the case of structures close to the sea surface such as the semi-submersible structure. Diffraction is defined as the change in wave direction as it passes through a barrier and its effects are considered relevant when $kD > 1.3$ or $D/\lambda > 0.2$. On the other hand, radiation is when the floating body

oscillates in still water producing waves that radiate away from it.

With those considerations, the potential can be split into three different parts, the radiation potential, the wave potential and the diffraction potential. Therefore the potential flow theory can incorporate these elements and obtain an expression for loads of the floating structure counting the contribution of each element separately.

$$\Phi(x,y,z,t) = \Phi_R(x,y,z,t) + \Phi_D(x,y,z,t) + \Phi_W(x,y,z,t) \tag{2.11}$$

With the aforementioned considerations the derived forces calculated from the integration of pressure over the submerged surface would be represented for each component respectively with the addition of hydrostatic buoyancy as presented in Equation 2.12.

$$F = \underbrace{F_R}_{\text{Radiated waves}} + \underbrace{F_D}_{\text{Diffracted waves}} + \underbrace{F_W}_{\text{Incident waves}} + \underbrace{F_S}_{\text{Hydrostatic Buoyancy}} \tag{2.12}$$

2.1.3 Irregular Waves

The potential flow theory is, as stated before, a well-defined theory to describe linear regular waves. However, under actual conditions, waves are erratic with the elevation of the water of Figure 2.3 rather than a sinusoidal one. The sea is always changing throughout time without repeating itself, and the wavelength varies between two subsequent crests. Because of this, irregular waves are important because they can simulate realistic conditions and predict the nonlinear hydrodynamic response of floating structures.
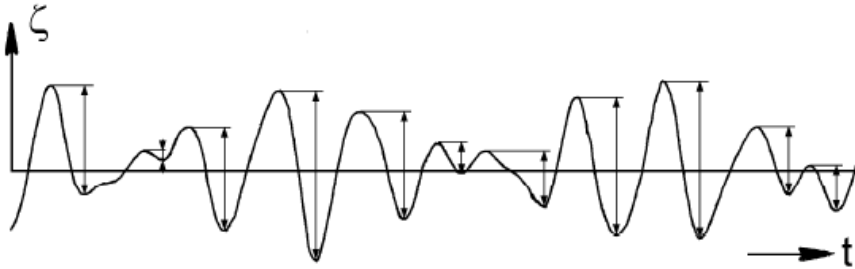
Figure 2.3: *Irregular Waves elevation [13]*

Statistics

In general irregular waves can be described with the superposition of multiple sinusoidal waves. In this case, due to the complexity of the multiple waves used, a statistical analysis is required. The mathematical representation used to describe the distribution of wave energy across different frequencies is the wave spectrum. Starting with the basic parameters used to describe the wave characteristics, the significant wave height, H_s is the average height of the highest $1/3$ of the waves in the wave record. It is equal to four times the standard deviation as shown in Equation 2.13 and Equation 2.14. Another important parameter is the peak period, T_P which is the period that the spectral energy that is the highest in the wave spectrum and it represents the dominant wave period.

$$\sigma = \sqrt{\frac{1}{N-1}\sum_{n=1}^{N}\zeta_n^2} \tag{2.13}$$

$$H_{1/3} = H_s = 4\sigma$$
$$\zeta_{\alpha_{1/3}} = \zeta_{\alpha_s} = 2\sigma \tag{2.14}$$

As a natural phenomenon wave elevation can be described from Gaussian distribution as the sum of independent harmonic waves. From this assumption, the wave height distribution is considered to be the Rayleigh distribution. Rayleigh distribution is mostly used in the case of a small range of frequencies and can express the wave amplitude and the wave height as well as presented in Equation 2.15 and Equation 2.16.

$$P\left[\zeta_\alpha > \alpha\right] = exp\left(-\frac{\alpha^2}{2\sigma^2}\right) \tag{2.15}$$

$$P\left[H_w > H\right] = exp(-2\left(\frac{H}{H_s}\right)^2) \tag{2.16}$$

The maximum wave height, which cannot simply be taken to be un-limited, is a vital component. In reality, the maximum depends to the frequency of appearance which is derived from the Rayleigh distribution. The most commonly used representation is the wave height that occurs once per 1000 waves, over a 3-hour period wave. The greatest wave height obtained using the Rayleigh distribution is $H_{max} = 1.86H_s$. These properties are important for the long-term analysis of waves.
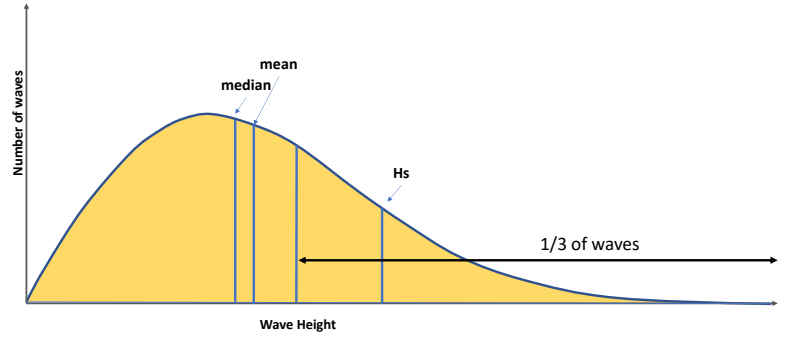
Figure 2.4: *Rayleigh distribution of wave height*

$$P\left[H_w > H_{max}\right] = exp(-2\left(\frac{H_{max}}{H_s}\right)^2) = 1/1000 \tag{2.17}$$

Wave Spectra

Since the study is in the time domain it is too complicated because different components of different frequencies are added up, and the frequency domain is used to describe the waves. Equation 2.18 describes the wave elevation in the time domain where ζ_{α_n} is the wave amplitude for every n, k_n is the wave number, ω_n is the circular frequency, ϵ_n is the random phase angle.

$$\zeta(t) = \sum_{n=1}^{N} \zeta_{\alpha_n} \cos(k_n x - \omega_n t + \epsilon_n) \tag{2.18}$$

In the frequency domain, it can be transformed to the spectrum formulation and give Equation 2.19.

$$S_\zeta(\omega_n)d\omega = \frac{1}{2}\zeta_{\alpha_n}^2 \tag{2.19}$$

Firstly, the spectral moments are described as the integral of the wave energy spectrum multiplied by the frequency to the n-th power and are expressed mathematically from the Equation 2.20.

$$m_n(\omega) = \int_{\infty}^{0} \omega^n S(\omega) d\omega \tag{2.20}$$

The zero-order spectral moment gives the area under the spectral curve, while the first order is the static moment and the second order is the moment of inertia. With these considered a group of significant parameters can be described.

Table 2.2: *Wave spectrum characteristics*

Parameter	Equation
RMS Wave Elevation	$\sigma_\zeta = \sqrt{m_{0\zeta}}$ (2.21)
Significant wave amplitude	$\zeta_{a_s} = 2\sqrt{m_{0\zeta}}$ (2.22)
Significant wave height	$H_s = 4\sqrt{m_{0\zeta}}$ (2.23)
Mean wave period	$T_1 = 2\pi \frac{m_{0\zeta}}{m_{1\zeta}}$ (2.24)
Mean zero-crossing period	$T_2 = 2\pi\sqrt{\frac{m_{0\zeta}}{m_{2\zeta}}}$ (2.25)

There are specific wave spectra used to describe open sea conditions. The Pierson-Moskowitz (PM) or Bretschneider is a mathematical model used to describe the ocean wave spectrum [14]. It is mostly used for fully developed wind sea and it is described by Equation 2.26 where H_s is the significant wave height as was defined previously, f_p is the peak frequency (Hz), f is the frequency (Hz) [15]. It is also characterised by the balance between wind energy input and wave dissipation.

$$S_{PM}(f) = 0.3125 \cdot H_s^2 \cdot f_p^4 \cdot f^{-5} exp\left(-1.25\left(\frac{f_p}{f}\right)^4\right) \tag{2.26}$$

Similar to the PM spectrum the Joint North Sea Wave Project (JONSWAP) spectrum is used mostly in cases of growing sea and therefore cannot be applied to swell waves. In this type of spectrum due to the growing wave, there is a net energy input. The spectrum is described by Equation 2.27 as a modification of the PM spectrum, with γ being the peak shape parameter and $\sigma = 0.07$ for $f < f_p$ or $\sigma = 0.09$ for $f > f_p$.

$$S_{JS}(f) = 0.3125 \cdot H_s^2 \cdot T_p \cdot \left(\frac{f}{f_p}\right)^{-5} exp\left(-1.25\left(\frac{f_p}{f}\right)^4\right)(1 - 0.287\ln\gamma)\gamma^{exp\left(-0.5\left(\frac{\frac{f}{f_p}-1}{\sigma}\right)^2\right)} \tag{2.27}$$

The peak shape parameter is derived from Equation 2.28.

$$\gamma = \begin{cases} 5 & \frac{T_p}{\sqrt{H_s}} \leq 3.6 \\ exp\left(5.75 - 1.15\frac{T_p}{\sqrt{H_s}}\right) & 3.6 \leq \frac{T_p}{\sqrt{H_s}} \leq 5 \\ 1 & \frac{T_p}{\sqrt{H_s}} > 5 \end{cases} \tag{2.28}$$

A comparison between the two spectra is presented in Figure 2.5 for a significant wave height $H_s = 4m$ and three different peak periods of 6, 8 and 10 sec. It can be observed that the JONSWAP spectrum has a more noteworthy peak.

2.1.4 Currents

Apart from the waves, ocean currents are another environmental phenomenon that needs to be considered. There are three main reasons that lead to the occurrence of a current. The ocean circulation
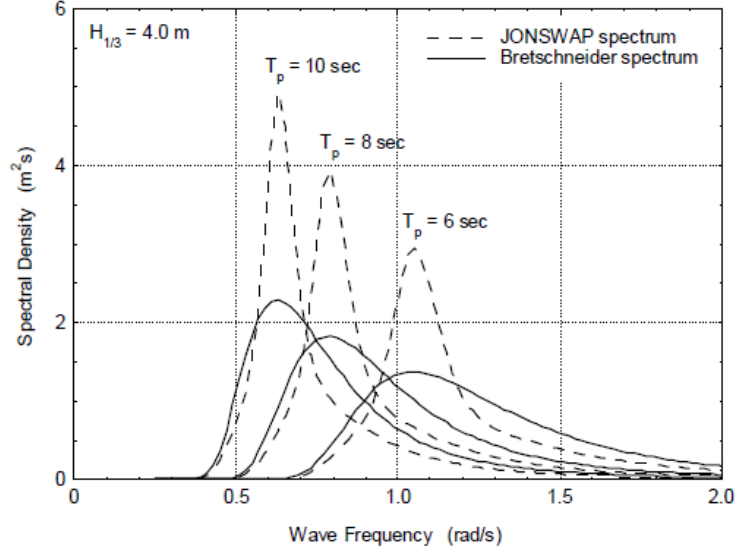
Figure 2.5: *Comparison between PM and JONSWAP spectrum [13]*

system, produces a continuous current, the cyclical variation in lunar and solar gravity, which results in tidal currents, wind, and differences in seawater density. In a more general description, the current velocity can be described as the superposition of a tide and a wind current as presented in Equation 2.29 and Equation 2.30 and is valid for water levels $z < 0$.

$$u_{tide} = u_{tide0} \left(\frac{h+z}{h} \right)^{1/7} \tag{2.29}$$

where u_{tide0} is the velocity at still water level (SWL) and h is the depth at SWL

The wind current is provided by Equation 2.30 and describes a linear distribution of the velocity from a reference depth h_0 till the water level $z = 0$.

$$u_{wind} = u_{wind0} \left(\frac{h_0 + z}{h_0} \right) \tag{2.30}$$

where u_{wind0} is the current's velocity in still water level (SWL) and is proportional the average wind speed of 10m $u_{wind0} = kU_0$ and h_0 is the reference depth for wind-generated current

2.2 Hydrodynamics

The general description of waves can lead to several hydrodynamic approaches. Hydrodynamics examines the motion of the seawater and the forces that are imposed on the floating structure through their interaction. As will be presented in this section, the relative motion between the floating wind turbine and the sea causes time-varying loads to be applied to the floating structure, which moves the structure and extra fluid motion.

2.2.1 Degrees of freedom of FOWT

There are multiple loads that are exerted in a floating wind turbine. The wind-induced loads are the typical loads experienced in every wind turbine in all three different rotor axes (thrust, torque and yaw). This includes all the mean and dynamic components and shear and bending moments as well. Apart from those there are wave-induced loads which are produced from the wave conditions

lead to both the static and the dynamic components and both shear and bending moments.

All the aforementioned loads create motions of the floating structure upon six degrees of freedom (DOF). As presented in Figure 2.6, the degrees of freedom are:

- Surge describes the motion parallel to x-axis

- Sway describes the motion parallel to y-axis

- Heave describes the motion parallel to z-axis

- Roll describes the motion around to x-axis

- Pitch describes the motion around to y-axis

- Yaw describes the motion around to z-axis
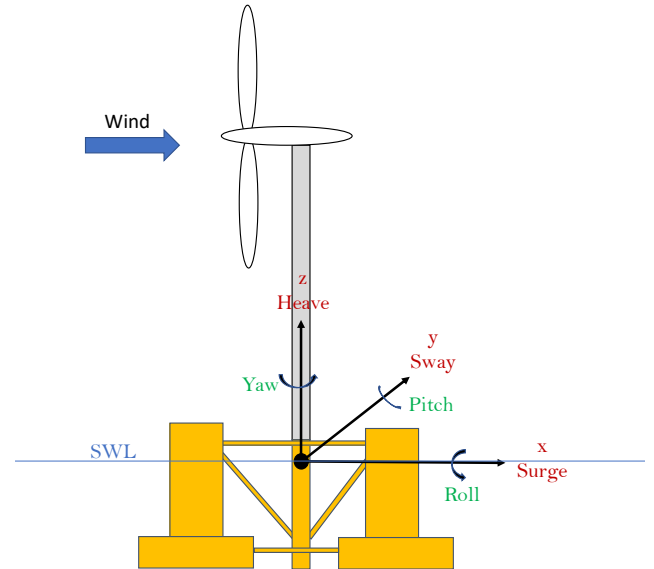
Figure 2.6: *Degrees of freedom of FOWT [4]*

2.2.2 Stability

The floating of the semi-submersible structure as it was described in Section 1.2 is based on its buoyancy. This effectively implies that the gravitational force and the buoyant force, as described by Archimedes' principle, are in balance. Equation 2.31 represents this balance and should be always active to ensure static stability in the vertical axis of the structure.

$$F_B - F_G = \rho g V - mg = 0 \tag{2.31}$$

In the case of disturbances such as wind, waves and currents the structure is rotated and needs to be balanced again. Although the forces in the z-axis are still the same, the centres of the forces are not coincident. The Centre of Gravity (COG) on x-axis is defined as the product of the individual masses times their positions divided by the total mass (Equation 2.32). On the other hand, the Centre of Buoyancy (COB) is defined as the product of the individual volumes of the submerged parts times the positions of their volumetric centre divided by the total volume displacement (Equation 2.33).

$$COG_x = \frac{\sum_n (x_n dm_n)}{\sum_n dm_n} \tag{2.32}$$

$$COB_y = \frac{\sum_n (y_n dV_n)}{\sum_n dV_n} \tag{2.33}$$

In the case that the structure rotates there is a misalignment between the two centres, which creates a moment capable of returning the structure back to the initial position to ensure the floating stability. In more detail, under the rotation of the floating body by an angle ϕ, the center of buoyancy is moved with response to the vertical misalignment axis of the two centres by GZ as shown in Figure 2.7. Based on this, the floating stability of the structure can be measured with the use of metacentric height which is the distance GN_ϕ, the COG to the metacentre N_ϕ. The metacentre represents the

intersection of the vertical lines of the centre of gravity G and the new offset centre of buoyancy B_ϕ. Therefore, from the rotational stability, it can be derived that the moments M_s described by Equation 2.34 should be equal to the buoyancy force multiplied by the lever arm indicating the misalignment of the two centres.

$$M = \rho g V \cdot \overline{GZ} \tag{2.34}$$

where
GZ is the stability lever arm and can be expressed as a function of the heel angle ϕ , and the metacentre N_ϕ, $\overline{GZ} = \overline{GN_\phi} \sin \phi$ which are presented in Figure 2.7.
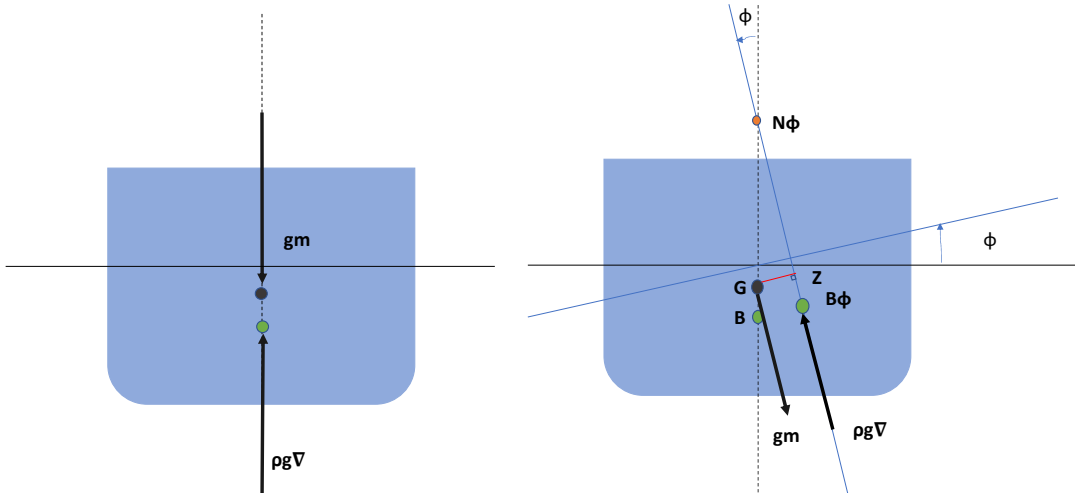
Figure 2.7: *Rotational Equilibrium of a floating body [13]*

2.2.3   Motion and Load equations

In addition to the static stability of a floating body, it is important to explore the basic equations of motions with respect to loads. According to Newton's second law, the vertical motion of the buoy is described by Equation 2.35. In this approach, the motion of the structure is the result of the superposition of the hydromechanical forces which are induced by the harmonic oscillations of the structure in still water and the wave exciting forces which are created by the upcoming ocean waves.

$$\frac{d}{dt}(\rho \nabla \dot{z}) = \rho \nabla \ddot{z} = F_h + F_w \tag{2.35}$$

Considering only the oscillation of a floating buoy in the heave direction the linear equation of motion without the existence of any external force (free decay in still water) is described by Equation 2.36. The motion of the body is described by the vertical displacement z with $\dot{z}$ being the velocity and the $\ddot{z}$ being the acceleration. Firstly, the term $b\dot{z}$ is triggered by the hydrodynamic reaction that arises from the body's motion with respect to the water. The body's vertical oscillations produce waves which convey energy, and also take energy away from the oscillations of the (free) buoy, causing its motion to cease. In a linear system, this so-called wave damping is proportional to the velocity of the body $\dot{z}$ by the hydrodynamic coefficient b. The term $\alpha\ddot{z}$ is also a result of the hydrodynamic behaviour of the body. This force is generated by the acceleration of water molecules close to the body and this part of the force does not lose energy and it resembles a standing wave system close to the floating body. The coefficient α, also known as the hydrodynamic mass or additional mass, has the dimension of a mass and is added to the solid mass of the structure. Finally, the term cz describes the restoring force which is proportional to the displacement z.

$$(m + \alpha)\ddot{z} + b\dot{z} + cz = 0 \tag{2.36}$$

where:

z is the vertical displacement (m), $m = \rho A_w T$ is the solid mass of the boy structure (kg), A_w the water plane area (m^2), α is the hydrodynamic mass coefficient (kg), b is the hydrodynamic damping coefficient (kg/s), $c = \rho g A_w$ is the restoring spring coefficient (kg/s^2), T is the length of the body under the water(draft) m

With the existence of a sinusoidal external heave force the equation of motion can be transformed as seen in Equation 2.37.

$$(m + \alpha)\ddot{z} + b\dot{z} + cz = F_\alpha \sin(\omega t + \epsilon_{F_z}) \tag{2.37}$$

During the forced heave, the vertical motion of the model is described through a sinusoidal relation $z(t) = z_\alpha \sin(\omega t)$. By applying this to Equation 2.37 the coefficients can be defined based on the external force characteristics, apart from the restoring coefficient which is merely dependent on the geometrical characteristics.

$$
\begin{aligned}
\alpha &= \frac{c - F_\alpha/z_\alpha \cos \epsilon_{F_z}}{\omega^2} - m \\
b &= \frac{F_\alpha/z_\alpha \sin \epsilon_{F_z}}{\omega} \\
c &= \rho g A_w
\end{aligned}
\tag{2.38}
$$

Under the exposure to waves the force at the bottom the floating body is derived from Equation 2.9 for deep water and it is described by Equation 2.39.

$$F = (\rho g T + \rho g \zeta_\alpha e^{-kT} \cos(kx - \omega t)) A_w \tag{2.39}$$

The harmonic part is the wave force called the Froude-Krilov force and it is considered to be calculated by multiplying the spring coefficient with the effective wave elevation. However, due to the reason that waves are diffracted there are additional terms that are needed to describe the wave force with components proportional to the acceleration and the velocity. With all the aforementioned the wave equation is described by Equation 2.40 with ζ^* indicated as the reduced or effective wave elevation.

$$F_w = \alpha \ddot{\zeta}^* + b\dot{\zeta}^* + c\zeta^* \tag{2.40}$$

All of the aforementioned equations can be combined and give the total equation of motion Equation 2.41.

$$(m + \alpha)\ddot{z} + b\dot{z} + cz = \alpha \ddot{\zeta}^* + b\dot{\zeta}^* + c\zeta^* \tag{2.41}$$

When studying a FOWT system other external forces have to be considered. In fact, the excitation forces are a sum of hydrostatic forces, hydrodynamic loads, mooring forces, and aerodynamic loads as presented in Equation 2.42. The hydrostatics along with the mooring describe the restoring loads and therefore the system restoring coefficient includes the mooring stiffness as well as the static contribution of the whole FOWT system. The hydrodynamics can describe both ocean waves and currents while the aerodynamics depend on the existing wind conditions.

$$F_{ext} = F_{hydrostatics} + F_{hydrodynamics} + F_{moorings} + F_{aerodynamics} \tag{2.42}$$

Morison equation

Potential wave theory, as it was presented in Section 2.1.2, reconstructs the motion caused by the presence of radiation, diffraction forces, hydrostatic buoyancy, and incident waves. The damping and additional mass over the six degrees of freedom are derived from radiation and diffraction characteristics and employed in the system's equation of motion. However, the presence of viscous effects is completely ruled out, which might result in an underestimation of the system's damping. Consequently, several techniques have been developed to take this into consideration. For identifying which elements are important a diagram has been developed as shown in Figure 2.8. It describes whether diffraction or drag is most important based on the wave characteristics and the characteristic dimension of the buoy.
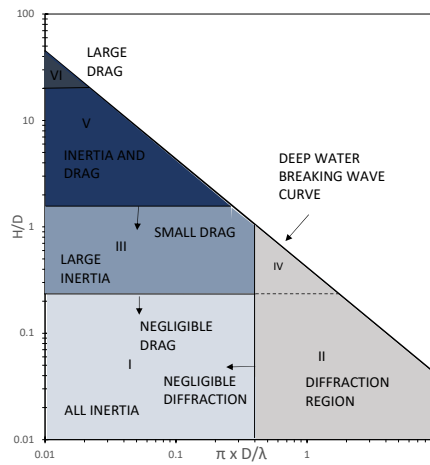
Figure 2.8: *Different wave force regimes D is the characteristic dimension, H is the wave height, and λ is the wave length*

Morison's representation is an empirical approach that can be used to describe the forces on an offshore structure. Although it is mostly used for fixed bottom applications, the Morison equation can also be applied to floating structures to directly compute the linear wave loads and viscous-drag loads. It is mostly, limited to slender structures bodies where the dimensions of the structure are significantly smaller than the wavelength, specifically $D/\lambda < 0.2$. In this case, diffraction is negligible and as presented in Figure 2.8. The Morison equation considers the force derived from the superposition of inertia and drag forces.

$$F(t) = \underbrace{\frac{\pi}{4}\rho C_M D^2 \cdot \dot{u}(t)}_{\text{Inertia term}} + \underbrace{\frac{1}{2}\rho C_D D \cdot u(t)|u(t)|}_{\text{Drag term}} \qquad (2.43)$$

The pressure gradient and the disturbance force are the two primary types of inertia forces that result from the ocean's flow accelerations. The Froude-Krilov force, which was discussed previously, is what causes the pressure gradient, which is created by the pressure around a body. Since the body's shape pushes the fluid to move around it and creates local velocities, the disturbance is the body's force applied to the water. These two forces have the same value however their significance to the inertial force is different. For the Froude-Krilov force, it is considered to be 1, while for the disturbance the significance is C_α which is the coefficient of added mass and it is usually less than 1. The sum of $1 + C_\alpha$ equals to C_M which is the inertia coefficient.

The drag forces are proportional to the square of velocity U^2, and the characteristic diameter D and

it is considered to be caused by a current.

The drag and the inertia coefficient are fundamental for the Morison equation and therefore it is helpful to be defined through non-dimension numbers. Reynolds number, Froude number and Keulefan Carpenter number are some that can be used to describe the coefficients.

1. Reynolds number is expressed by Equation 2.44 where u_α is the velocity amplitude m/s, D is the characteristic diameter m and v is the kinematic viscosity m^2/s

$$Re = \frac{u_\alpha D}{v} \tag{2.44}$$

2. Froude number can be defined in Equation 2.45 where g is the acceleration of gravity m/s^2

$$Fr = \frac{u_\alpha}{\sqrt{gD}} \tag{2.45}$$

3. Keulegan Carpenter number is expressed by Equation 2.46 where x_α is the water displacement amplitude m

$$KC = \frac{2\pi x_\alpha}{D} \tag{2.46}$$

Inertia and drag dominance which is also shown in Figure 2.8, can be expressed through the Keulegan-Carpenter number, as shown in Equation 2.48. This is a significant point, which can possibly simplify the Morison equation by neglecting some terms.

$$\frac{F_{drag_\alpha}}{F_{inertia_\alpha}} = \frac{\frac{1}{2}\rho C_D D \cdot u_\alpha |u_\alpha|}{\frac{\pi}{4}\rho C_M D^2 \cdot \dot{u}_\alpha} = \frac{\frac{1}{2}\rho C_D D \cdot u_\alpha |u_\alpha|}{\frac{\pi}{4}\rho C_M D^2 \cdot \omega u_\alpha} = \frac{2C_D |u_\alpha|}{\pi C_M D \omega} \tag{2.47}$$

The maximum value of $|u_\alpha|$ is u_α, while $\omega = 2\pi T$ and $u_\alpha = \omega x_\alpha$ the expression can be reformulated.

$$\frac{F_{drag_\alpha}}{F_{inertia_\alpha}} = \frac{1}{\pi^2}\frac{C_D}{C_M}\frac{u_\alpha T}{D} = \frac{1}{\pi^2}\frac{C_D}{C_M}KC \tag{2.48}$$

Considering that $\frac{1}{\pi^2}$ is around $1/10$, and that C_D is more than half the C_M the two forces are equal when KC varies between 15 to 20. In more detail:

- For KC < 3 the inertia force is dominant. In this case, compared to the diameter, the flow does not move far enough to produce significant boundary layers or vortices and the drag force can be ignored. The potential flow theory is still valid.

- For range, 3 < KC < 15, a linearized approach of the drag force can be applied.

- For higher range, 15 < KC < 45 , the complete Morison equation is applied.

- For higher KC values, KC > 45, the drag force is the primary force, while inertia can be neglected. At this point, the flow behaves more like a uniform flow.

3   Related research review & Literature Gap

The theory that was introduced in Chapter 2 can be applied with different numerical approaches. In this chapter, an insight into the different numerical approaches (Section 3.1) is presented with an emphasis on the research that is currently conducted on the accuracy and the aspects of those models (Section 3.2). The chapter concludes with the research gap that led would be the main of focus of the thesis simulations (Section 3.3).

3.1   Numerical Models

In order to develop solid technology on FOWT, their modelling is essential since it is the main indicator of the ultimate loads and fatigue damage of the structure. The two primary approaches for modelling FOWT are numerical methods and physical testing. Numerical tools calibrated with physical testing can be used to explore the design space by running more design load cases.

For the analysis of floating wind turbines, there have been multiple tools developed, combining structural dynamics, aerodynamics, hydrodynamics and mooring dynamics. Fatigue, Aerodynamics, Structures, and Turbulence (FAST), SIMPACK, Bladed, SIMA workbench and HAWC2 are some of the multi-fidelity tools [16]. Each one of them uses different modelling approaches for each one of the sections as shown in Table 3.1. Computational Fluid Dynamics (CFD) can also be used for a high-fidelity approach to aerodynamic and hydrodynamic analysis.

As observed in Table 3.1 the different software uses different approaches for hydrodynamics, aerodynamics and structure dynamics which determine the fidelity level of the simulations. For hydrodynamics, which is the main objective of the present thesis, all software use the Potential Flow Theory and the Morison equation. Implementing these theories requires tuning different modelling parameters such as drag coefficients, added mass matrices and hydrostatic properties. There are frequency domain tools that explicitly focus on the floater and the definition of the hydrodynamic coefficients such as WAMIT [17], NEMOH [18] and Ansys AQWA [19] which can provide input to the time-domain mid-fidelity tools. This kind of tool solve the radiation/diffraction problem and calculate the added mass and damping for different range of frequencies and wave directions. The radiation/diffraction defined coefficients could be used as an input in the potential flow solution, however, the viscous effect should be accounted for as well. Depending on the structure and the application the viscous effects (drag coefficients) are determined through the Re and KC numbers. The calculation and the selection of the hydrodynamic coefficient are significant for measuring the FOWT performance and the research efforts have been put into measuring their effect in the correct prediction of the FOWT performance.

3.2   Related research

There are several projects, devoted to the performance analysis of this system, have examined several aspects concerning the aero-hydro dynamic performance. The projects OC4 (Offshore Code Comparison Collaboration Continuation) and OC5 (Offshore Code Comparison Collaboration Continu-

Table 3.1: *Software tools for FOWT [16]*

Software	Hydrodynamics	Aerodynamics	Structure
FAST	PF+ME	BEMT + GDW/FVW	RB+Modal/FEM+Dyn/QS
HAWC2	PF+ME	BEMT + GDW	FEM+Dyn
SIMA	PF+ME	BEMT	FEM+Dyn
Bladed	With SIMA	BEMT + GDW	Modal
SIMPACK	With HydroDyn	AeroDyn/AeroModule	FEM
Orcaflex	PF+ME	With FAST	RB+FEM+Dyn
Flexcom	PF+ME	With FAST	RB+FEM+Dyn

ation with Correlation project) have been carried out in previous years and have used the National Renewable Energy Laboratory (NREL) 5MW wind turbine and different platforms to verify and validate different tools and methods. More precisely, OC4 included verifying the accuracy of different offshore wind turbine modelling tools by comparing the different codes previously mentioned [20] for a semisubmersible structure. Several load cases, including free-decay tests, currents, and irregular waves coupled to and uncoupled from the wind, were simulated during this study using a variety of codes, including the FAST code. The findings allowed for the identification of the system's natural frequencies and motions that are susceptible to resonance. From those comparisons, it was concluded Morison equation and potential flow solution can provide equivalent results while the choice of drag should be member-dependent.

OC5 focused on validating the tools used for modelling offshore wind systems through the comparison of simulated responses of select system designs to physical test data [21]. In this study, a scaled-down physical model of the system (Floater and Wind turbine) was constructed and tested under different cases and the results were compared to the ones obtained from simulations. The results of the simulations comply with those of the experiments, however, there is an under-prediction of around 20% in the global loads. This under-prediction is crucial in pitch and surge natural frequencies which have natural frequencies outside the linear wave excitation region and therefore are excited from non-linear hydrodynamic loads. This suggests that second-order terms should be carefully modelled and not disregarded.

This underestimation has sparked a lot of research on its main causes and has led to the OC6 project (OC5 with unCertaitny). Simulations conducted have proposed that the proper tuning of the drag coefficients is crucial to the prediction of low-frequencies responses [22]. However, it is difficult to find a coefficient that can effectively predict the response in both free-decays and irregular wave conditions [23]. Several approaches have been proposed such as depth-dependent drag coefficients with the use of larger drag coefficients close to the SWL [24] and the modification of the Quadratic Transfer Functions (QTF) which are responsible for calculating the second-order terms. In this case, the QTF can be calculated with CFD and then added to a multi-fidelity tool such as OpenFAST [25]. More research conducted in relation to OC6 proposed that the low-frequency forces in the transverse flow are mostly related to viscous drag and can therefore be correctly predicted with the increase of drag coefficient near this point and the addition of wave-stretching [26].

Although there has been extensive research on the approach of low frequencies with an emphasis on drag, further research on those models has identified other dependencies as well. The way that quadratic damping is implemented seems to have an effect on the load prediction [27]. The drag coefficient in the Morison equation does not account for Degrees Of Freedom (DOF) dependency, therefore a quadratic damping matrix seems to address more accurately the loads compared to experimental results. The complementary effect of the different degrees of freedom can also be addressed with the use of multi-directional waves instead of uni-directional ones which tend to overpredict the global loads [28]. On the other hand, the uncertainty of drag seems to have negligible effects on large structures but there is a need for research on small and slenderer floaters [29].

The second-order dynamics apart from their contribution to lower frequencies, appear to be sensitive to water-depth changes [30] with their effectiveness being greater in shallower water. The use of coupled models that take wind conditions into account is also crucial since it might alter predictions of total loads.

Recent research has concentrated on assessing the sensitivity of various parameters related to both the wind turbine and the floating platform, employing the OpenFAST framework [31] [32]. This research serves as a valuable reference for the current study. The investigation delves into the influence of several parameters, encompassing aspects of wind, waves, and current, as well as intrinsic model characteristics like system mass, centre of mass, and blade properties. The findings from this research highlight that the most impactful input parameter is the standard deviation of turbulent wind, closely followed by current speed and the system's centre of mass in the x-direction.

3.3 Research gap

The aforementioned work demonstrates that there is still a need for exploring the effect of different hydrodynamic parameters in order to make more accurate predictions of FOWT behaviour. Especially for mid-fidelity tools the proper tune of the parameters can be crucial for load prediction. Although it appears that the main issue with mid-fidelity tools is the underprediction of low-frequency hydrodynamic loads, which has been attributed to the proper selection of the drag coefficient, other properties of the hydrodynamic models seem to have a great impact as well. The effect of added mass coefficients which are derived from the potential flow theory can be different for different wave amplitudes, while the axial drag and added mass coefficients might also need to be adjusted for different wave conditions. At the same time, other aspects such as wave stretching can also affect the results.

On the other hand, the inclusiveness of the research is limited since most of the simulations have focused only on specific load cases. Moreover, the hydrodynamic parameters have not been studied extensively for coupled cases, and therefore the interaction between hydrodynamic parameters and wind effect has not been explored. Finally, the currents have a limited representation in the literature including the uncertainty of the parameters.

This gap in research is related to the lack of experimental and full-scale data to compare with, however, there can be other methods implemented to give an indication of the performance on a global scale. Those include the uncertainty of the different parameters and at the same time will cover a wide range of possible wave /wind cases. This led to the current thesis which will focus on the effect of the different parameters on the overall performance through a sensitivity analysis. While there exists a sensitivity analysis for semi-submersible Floating Offshore Wind Turbines (FOWT), the current project aims to take this analysis to a more comprehensive level. Firstly, it will place a greater emphasis on the hydrodynamic parameters, thoroughly examining each individual member. Furthermore, the study will delve into comparing different theoretical approaches, including a sensitivity analysis utilizing the Morison equation. Additionally, sensitivity analysis will extend to a spar platform, facilitating a comparative study between the two types. The research will encompass a wide range of scenarios, incorporating diverse environmental conditions that FOWTs may encounter.

A correlation between the ocean waves and the modelling approach could not only predict the possible response of the FOWT but also give a more in-depth analysis of the model features that are uncertain. Therefore, it is considered quite important to identify those uncertain features and study their effect on the FOWT performance. Additionally, it might bring the standardization of the modelling approaches applied to FOWT one step closer.

4 OpenFAST & System Properties

This chapter will discuss the primary computational tool, OpenFAST, used in the simulation and analyze the employed hydrodynamic and aerodynamic techniques. There will also be a description of the system that OpenFAST will replicate.

4.1 OpenFAST

From all the different tools, FAST (Fatigue, Aerodynamics, Structures, and Turbulence) that has been developed by National Renewable Energy Laboratory (NREL) is a multi-fidelity, multiphysics tool. FAST was first created to forecast loads for on-land and offshore bottom-mounted wind turbines, but its functionality was expanded with the addition of new modules to allow for the modelling of FOWTs. To enable coupled nonlinear aero-hydro-servo-elastic analysis in the time domain, the code consists of modules representing various FOWT characteristics. As shown in Figure 4.1 there are external conditions concerning the wind and the waves, which are translated into an applied load which is then coupled and gives several outputs relevant to the power generation and the wind and wave motion.
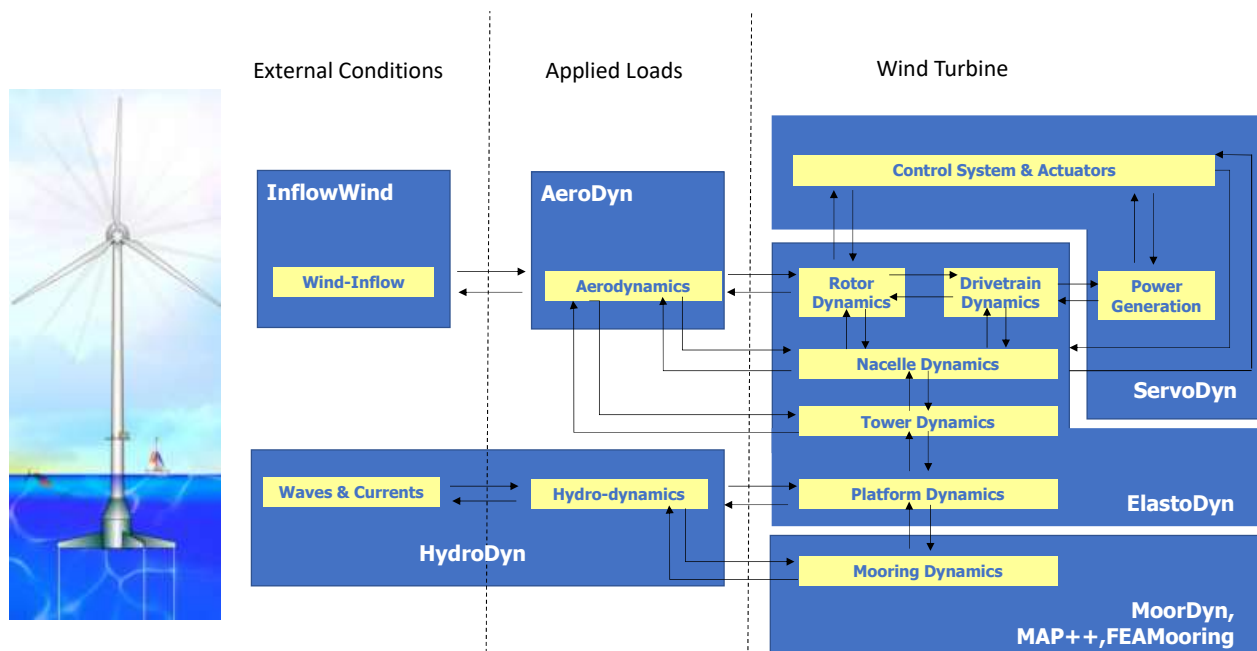
Figure 4.1: *OpenFast Modules*

OpenFAST is the tool used to run all the simulations using the FAST code. Its main modules are AeroDyn, HydroDyn, InlfowWind, ElastoDyn, ServoDyn and MoorDyn. All of these combined can successfully module a floating wind turbine system and model its behaviour. For the current study, the primary focus will be on the external conditions and the applied loads meaning that the HydroDyn and AeroDyn modules will be mostly studied. In the following section, a more detailed analysis of the modelling options will be given

4.1.1 HydroDyn Module

HydroDyn is the module responsible for calculating the hydrodynamic loads and the platform motion with the wave characteristics as an input [33]. This module allows the different hydrodynamic modelling approaches to be applied and measure their effect on the FOWT. In more detail, the HydroDyn provides the ability to define specific sea conditions which will then be used to calculate the motions and loads. Starting with the wave condition, it is possible to simulate regular and irregular waves JONSWAP and PM spectrums, as well as user-defined input data of wave motions. The basic characteristics that are required for the definition of the sea conditions are the wave height H (significant wave height H_s for irregular waves), the period T (peak period T_p for irregular waves), the peak shape parameter γ in case of spectrum, the direction and the directional spreading if applied. It is also possible to add currents to the water motion by providing the velocity in the SWL and the water depth.

The HydroDyn main approach to reach the solution is the Potential theory and the Morison equation (Strip Theory) as they were described in Chapter 2. The potential flow theory is used for substructures that are large compared to typical wavelengths. The potential-flow hydrodynamic loads include linear hydrodynamic restoring, added mass and damping contributions from linear wave radiation, and the incident-wave excitation from the first and second-order diffraction [33]. This solution requires hydrodynamic coefficients which are precalculated from separate codes such as WAMIT.

Second-order components that are crucial for identifying excitations at lower or higher frequencies can be added to the potential flow theory's first-order solution. The mean-drift forces, the Newman approximation, and the full QTF are the three separate methods used in OpenFAST to generate the quadratic terms as quadratic transfer functions (Quadratic Transfer Function). The quickest method is the mean-drift approach, which only considers diagonal terms (where frequencies and direction are the same). The significance of the drift loads is due to the presence of low-frequency components that may generate sluggish drift motions. Similarly, Newman's approach only needs those diagonal elements as input but it extrapolates them to acquire the off-diagonal elements as well. However, for large QTF terms, it underestimates the off-diagonal components. Therefore, the full QTF method may be more appropriate. This method is more computationally intensive, but it enables obtaining the sum frequency QFT, which is significant for capturing the high frequencies.

The second solution method is the Morison equation which is expressed through the Strip theory and used for structures with small diameters relative to a typical wavelength. In this case, the fluid-inertia, added-mass and viscous-drag components of Morison's equation are included in the strip-theory loads. Moreover, axial loads from tapered members and static buoyancy loads can be added, while hydrodynamic loads are also applied as lumped loads on member endpoints (joints). Flooding or ballasting of members and the effects of marine growth can also be included. It should be mentioned that in some cases, the potential-flow theory is combined with the viscous-drag components of the strip theory for a more inclusive approach.

4.1.2 AeroDyn and InflowWind

AeroDyn module offers aero-elastic modelling of horizontal-axis turbines in the time domain. It can also be used as a standalone module to calculate the aerodynamic performance of the wind turbine uncoupled with the OpenFAST and the rest of the modules. In the present thesis, this module along with InflowWInd will be used to add wind effect combined with the hydrodynamics.

The AeroDyn module assumes the turbine geometry consists of a single tower supporting a one-, two-, or three-bladed rotor. It is used to determine the aerodynamic loads on the tower and blades with calculations subjected to the principles of actuator lines. In this aerodynamic approach, the

Modelling Approach		
Potential Flow Theory	Strip Theory (Morison Equation)	Hybrid
$F_{WRP} = F_w + F_{HS} + F_{RD_n} + F_{AM}$	$F = F_I + F_D + F_B + F_{MG}$ $+F_{F\_B} + F_{AM-M} + F_{AM\_MG} + F_{AM\_F}$	$F = F_D + F_{F\_B} + F_{AM\_F}$
Wave Excitation Hydrostatic Radiation Added mass	Inertia Force Drag Force Buoyancy Force Weight of Marine Growth Fluid Ballasting Added Mass Added Mass marine growth Added Mass Fluid Balancing	Drag Force Fluid Ballasting Added Mass Fluid Balancing
2nd order Mean-Drift Newman Approximation Full QTF	2nd order Full QTF	2nd order Full QTF

Figure 4.2: *Modelling Methods of HydroDyn module [33]*

three-dimensional (3D) flow around a body is approximated by local two-dimensional (2D) flow at cross sections, and the distributed pressure and shear stresses are approximated by lift forces, drag forces, and pitching moments lumped at a node in a 2D cross-section [34].

The most significant part of the AeroDyn module is the rotor wake modelling which defines the modelling approach for calculating the forces upon the wind turbine. In Aerodyn, wake modelling is conducted through three main methodologies: theBlade Element Momentum (BEM) theory, the Dynamic Blade Element Momentum (DBEM) theory and the cOnvecting LAgrangian Filaments (OLAF).

BEM theory is widely used to calculate aerodynamic forces with the combination of principles from blade element theory and momentum theory. In blade element theory the thrust force and the torque around an annulus dr, are defined from Equation 4.1 and Equation 4.2, respectively.

$$dT = B\frac{1}{2}\rho V_{total}^2 (C_l \cos\phi + C_d \sin\phi) c dr \qquad (4.1)$$

$$dQ = B\frac{1}{2}\rho V_{total}^2 (C_l \sin\phi - C_d \cos\phi) c r dr \qquad (4.2)$$

where B is the number of blades, V_{total} is the total speed upon a blade as the geometrical superposition of the wind speed and the rotational speed, C_l is the lift coefficient of the blade, C_d is the drag coefficient of the blade, ϕ is the inflow angle, c is the chord and r is the radius.

On the other hand, in the momentum theory the same properties are defined from Equation 4.3 and Equation 4.4 , with the consideration of some extra corrections such as Prandtl tip-loss, Prandtl hub-loss, and Pitt and Peters skewed-wake.

$$dT = 4\pi r \rho U_\infty^2 (1-a) a F dr \qquad (4.3)$$

$$dQ = 4\pi r^3 \rho U_\infty \Omega (1-a) a' F dr \qquad (4.4)$$

where, U_∞ is the wind speed, Ω is the rotational rotor speed, a is the axial induction factor, a' is the tangential induction factor and F is the correction factor to the induced velocity based on the tip-loss model and hub-loss

To solve these equations an iteration process is followed. Starting with an estimation for the induction factors a and a', the inflow angle can be calculated, along with the local angle of attack. Followed by this, the tip and hub-loss factors can be calculated, while the lift and drag coefficients can be found based on the angle of attack. The new induction factors can then be calculated through the balance of the blade element and momentum theory equations. The resulting induction factors are compared to the initial estimation and the iteration process is continued till the results converge.

Apart from BEM models OpenFAST is also possible to use a different approach which is Free Vortex Wake (FVW) models. The main module is the cOnvecting LAngrangian Filaments (OLAF). The increase in the rotor size involves large blade deflections which result in swept areas that differ from the rotor plane and affect the near wake. This situation violates the assumptions used by BEM theory and there is a need for a more robust approach such as OLAF. It should be noted that this approach is out of the scope of the thesis and therefore it will not be used.

In addition to rotor aerodynamics, OpenFAST employs additional techniques to determine the lift and drag coefficients of airfoils. Using static aerodynamics, which uses tables with the necessary data for each airfoil, is the easiest method. The coefficients are determined as a function of the Reynolds number and the angle of attack. However, the fluctuation in wind speed over the rotor disk causes unstable or oscillatory angles of attack time histories on wind turbine blade airfoil sections, which results in dynamic stall occurrences. Vertical wind, yaw misalignment, horizontal and vertical wind shears, and wind turbulence are the sources of these fluctuations in velocity. Different unsteady airfoil aerodynamic models are offered by the AeroDyn module, making it possible to model those phenomena in the lift and drag coefficient calculations.

It is worth mentioning that AeroDyn also simulates the wind turbine tower's effect on the blades' aerodynamics. This is performed with the use of a potential flow solution around a cylinder as the basic flow field, combined with a tower dam model for the upwind effect and a downwind wake model based on tower drag coefficient Cd.

A significant part of the aerodynamics is the input wind data defined in the InflowWind file. Different wind conditions can be simulated such as steady wind or fluctuating wind with turbulence addition and shear phenomenons. InflowWind supports different formats such as uniform, binary TurbSim full-field (FF), binary Bladed-style FF, and HAWC formatted binary FF wind files. Based on the wind type that is chosen different input parameters need to be defined, such as the horizontal wind and the reference height. The purpose of this module is to simulate accurately the wind conditions and therefore the wind type used will be based on the available data that will be obtained for the different studied locations.

When dealing with turbulent wind conditions, TurbSim is a valuable tool for generating necessary files. TurbSim offers flexibility in modifying parameters to create full-field wind data files. Among various turbulent models, the Kaimal spectrum is commonly utilized due to its effectiveness in characterizing atmospheric turbulence [35]. The Kaimal spectrum is defined by the equation presented in Equation 4.5, where Λ_u represents a length scale parameter, and U corresponds to the mean wind speed at the hub height [36].

$$S_u(f) = \frac{4\sigma_u^2 \frac{\Lambda_u}{U}}{\left(1 + 6f\frac{\Lambda_u}{U}\right)^{\frac{5}{3}}} \tag{4.5}$$

4.1.3 Wind Turbine Modules

The wind turbine modules as presented in Figure 4.1 contain the ServoDyn, the ElastoDyn and the MoorDyn modules. ServoDyn implements wind turbine control, such as the Pitch control and the Generator and Torque control. The ElastoDyn defines different modelling options, geometries and active DOFs of the different substructures such as the tower, the nacelle, the blades and the platform. At the same time, it sets the initial conditions of the simulation. MoorDyn simulates the mooring of the platform, including the lines and their physical properties.

These sections refer to the system characteristics and therefore will not be studied in the present report. However, they will be used to obtain the total performance of the FOWT.

4.2 Wind Turbine and Platform Properties

For the conceptual study of offshore wind turbines, the National Renewable Energy Laboratory (NREL) has developed a baseline wind turbine widely used in projects to evaluate the performance and response under specific aerodynamic and hydrodynamic conditions [37]. The NREL 5MW wind turbine is a three-bladed upwind turbine with variable-speed and variable blade-pitch-to-feather-controlled. The characteristics of the wind turbine are presented in Table 4.1. It has been used in several projects and has already been simulated in OpenFAST, making it an ideal choice for studying different cases.

Table 4.1: *NREL 5MW Properties ([37])*

Rated Power	5MW
No Blades	3
Rotor Diameter	126m
Hub- Height	90m
Rated speed	11.4 m/s
Cut-in wind speed	3 m/s
Cut-out wind speed	25 m/s
Cut-in rotor speed	6.9 rpm
Cut-out rotor speed	12.1 rpm
Rated Tip Speed	80 m/s
Rotor Mass	110,000 kg
Nacelle Mass	240,000 kg
Tower Mass	347,460 kg

For simulating the aforementioned floating wind turbine as a semi-submersible floating structure, a floating platform has been developed to support the rotor-nacelle assembly and the tower. The platform layout is presented in Figure 4.3, where a scaled construction of the structure is shown [38]. The floating platform consists of a main column, which is attached to the tower at the centre of the structure. Three offset columns surround this and are connected to the main through pontoons and cross members. These smaller structures are two sets of three pontoons connecting the offset columns at the top and the bottom, along with another two sets of three pontoons connecting the offset to the main. Additionally, there are three cross braces connecting the bottom of the main to the top of the offset. The structure's total height is supposed to be 32m, with the first 20m under the SWL. The total mass includes the ballast water and has been considered carefully to ensure the buoyancy of the system taking into account the weight of the rotor-nacelle assembly, the tower, the floating platform and the mooring system.

Along with the floating platform's physical qualities, it is important to characterize its hydrostatic and hydrodynamic parameters. The core of hydrostatics is the stability of the system's equilibrium
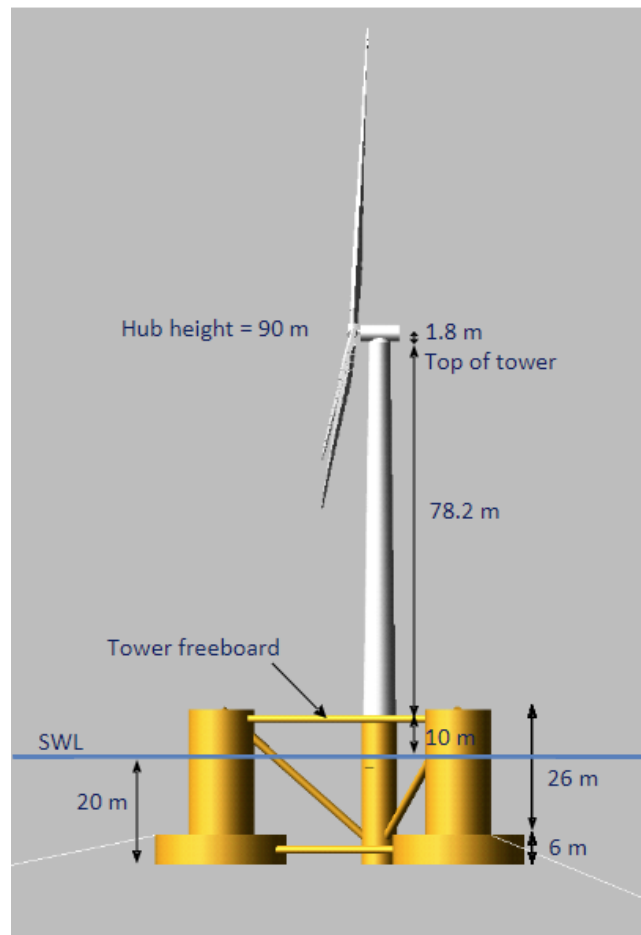
Figure 4.3: *Layout of the whole structure designed for the OC4 and OC5 projects[39]*

while taking into account the effects of gravity, the displaced volume, and the shape of the water plane at the centre of buoyancy (COB). The hydrostatic restoring matrix (6x6) that is generated as a result of this balance is utilised as an input in OpenFAST. It should be noted that due to the symmetry of the structure and the alignment of the COB with the tower centre line only the heave, the roll and the pitch diagonals of the matrix are non-zero.

On the other hand, the inputs that are relevant to hydrodynamics rely exclusively on the hydrodynamic approach used. The potential flow hypothesis demands additional mass effects, radiation, and wave excitation. They are predefined by WAMIT, which addresses the linear potential-flow radiation and diffraction issues when modeling various excitation tests. Added mass and damping matrices (6x6) that are dependent on wave frequency are provided by the radiation problem, whereas a hydrodynamic wave-excitation vector that is dependent on both wave frequency and direction is provided by the diffraction problem[38].

In cases where the radiation damping is negligible and flow separations can occur Morison's Equation can be applied. In this case, the added mass coefficient C_a and the viscous-drag coefficient C_d have been predefined for the transverse flow as well as the axial (heave) direction. The added mass was selected such that it agrees with the potential flow added mass and it was verified through simulations. The viscous drag was defined through Reynolds number relations for the different members of the platform. The detailed are presented in Table 4.2.
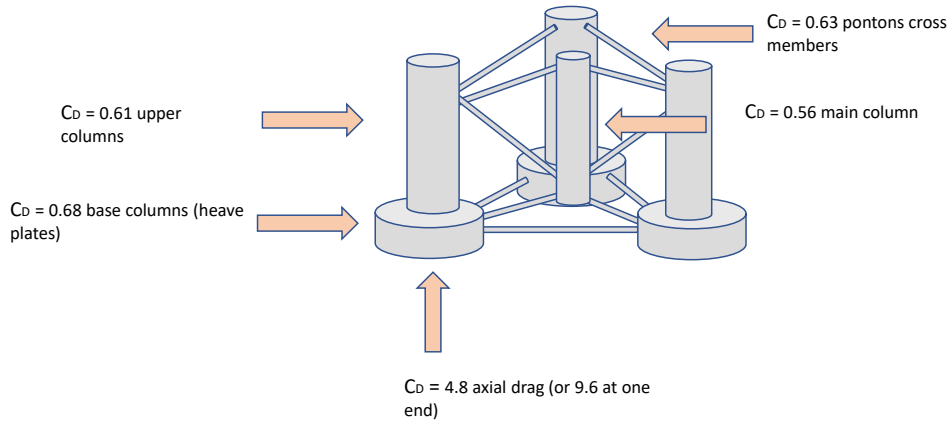
Figure 4.4: *Drag coefficients on the different parts of the floater according to the system description [38]*

Table 4.2: *Semisubmersible Floating Structure for OC4 project*

General Properties	
Platform mass, including ballast	1.3473E+7 kg
Displaced volume (V_o)	13917 m^3
Center of Buoyancy (COB) below SWL	13.5 m
Hydrostatic restoring matrix	
Heave ($C_{33}^{Hydrostatic}$)	3.836E+06 N/m
Roll ($C_{44}^{Hydrostatic}$)	-3.776E+08 N-m/rad
Pitch($C_{55}^{Hydrostatic}$)	-3.776E+08 N-m/rad
Morrison coeffients	
Added Mass coefficient (C_a) all members	0.63
Drag coefficient (C_d) main column	0.56
Drag coefficient (C_d) upper columns	0.61
Drag coefficient (C_d) base columns	0.68
Drag coefficient (C_d) pontoons and cross members	0.63
Axial added mass coefficient (C_{az}) base column	1
Axial drag coefficient (C_{dz}) base column	4.8
Additional Quadratic Damping	
Additional quadratic drag in surge (B_{11}^{quad})	3.95E+5 Ns^2/m^2
Additional quadratic drag in sway (B_{22}^{quad})	3.95E+5 Ns^2/m^2
Additional quadratic drag in heave (B_{33}^{quad})	3.88E+6Ns^2/m^2
Additional quadratic drag in roll (B_{44}^{quad})	3.70E+10 Nms^2/rad^2
Additional quadratic drag in pitch (B_{55}^{quad})	3.70E+10 Nms^2/rad^2
Additional quadratic drag in yaw (B_{66}^{quad})	4.08E+9 Nms^2/rad^2

Part II

Simulations

5   Model Verification & Validation

In the context of the research, it is important to conduct a model verification process before simulating various sea conditions and models. The purpose of this verification serves two different goals. Firstly it will ensure that the simulations running with the selected version of the OpenFAST align with previous simulation results, such as those of the OC4 project and the experimental results of OC5 and OC6 projects. Secondly, it will be used as a point of reference for the different theories applied. Consequently, a comparison, of the natural frequencies and the free-decay responses will be presented. In addition, a comparison with the experimental results will also be demonstrated and the differences between those will be discussed in this chapter.

5.1   Verification with NREL FAST simulations

The first step towards verification is to obtain relevant simulation data that can be used as benchmark data for the comparison to the model. The OC4 project, as was mentioned, was developed to evaluate the Morison equation and Potential Flow theory with the use of mid-fidelity tools, including the simulations with the FAST code. Those simulations were dedicated to the selected semisubmersible floater with the NREL 5MW wind turbine and therefore are the ideal choice for conducting the verification.

The set of simulation cases that were conducted in OC4 project encompassed various scenarios to assess the behaviour of the model. Still water conditions, wave conditions, and simulations where wind coupling were considered. Under those terms, those simulations were also chosen for the model verification for a better representation of the different scenarios.

5.1.1   Free-decay tests

Still water simulations (free-decay tests) allow the evaluation of the model's response in the absence of any external force, providing insights into the system's characteristics. The free-decay tests provide the natural frequencies over the platform six degrees of freedom which are significant for the analysis of the dynamic performance of the system. In addition, they are essential in the verification of the models since they are indicative properties.

Considering that the same set-up is used for the model in OpenFAST the comparison between the two models is expected to give almost identical results. During the OC4 project, four free decay tests were simulated in the surge, heave, pitch and yaw directions. In these tests, it is considered that there is no wind and there is still water while the platform is moved by some meters or degrees in one of the directions and the motion is documented. It should be noted that the simulations were modelled with only the 6 DOFs of platform motion active and all the other DOFs of the wind turbine were turned off. The properties of the model as referred to in Table 4.2 were simulated with 0.0125s timestep. The initial conditions for those tests are described in Table 5.1.

An important aspect of the simulations is the mooring dynamics model. It was decided to run the simulations with MAP++ over MoorDyn due to differences observed between those two mooring approximations. MoorDyn is a dynamic method of mooring calculations on the contrary MAP++ is

a quasi-static approach. Although it is expected that MoorDyn is more accurate, for the comparison of the free-decay tests, some discrepancies were noticed, which led to the use of MAP++.

Table 5.1: *Initial offsets of modes of motion for the selected free-decay test and simulation properties*

Motion DOF	Initial Offset	Simulation Time
Surge Decay	Surge = 22m	1200s
Heave Decay	Heave = 6m	300s
Pitch Decay	Pitch = 8 deg	300s
Yaw Decay	Yaw = 8 deg	900s

The NREL results were first compared to potential flow theory in combination with the Morison equation referred to as hybrid theory in HyrdoDyn module. This means that the model uses the predefined WAMIT files of the floating platform with the addition of the drag coefficients of the platform's members. Those drag coefficients have been determined in the system definition as was mentioned in Chapter 4. This is the main setup under which the OC4 simulations from NREL were conducted. The dominant motions that correspond to each of the free decay tests are presented in Figure 5.1.

By observing the results in Figure 5.1, the natural frequencies and the damping ratios are clearly in close compliance in the majority of simulations. More specifically, there are minor variations in surge amplitude that are also seen in pitch and yaw, along with a slight change in time, although heave is the same. The modifications between the various openFAST versions have been identified as the primary cause of those minor variances. In fact, OpenFAST v3.5.0 was used to recreate the present simulations while NREL simulations were run using FAST v8. Improvements in the implementation of the HydroDyn solution throughout the course of OpenFAST's multiple versions fully account for the minor variations found.

From the free decay tests presented above, the natural frequencies for sway and roll were also computed and contrasted with those offered by NREL for completeness. Overall, the natural periods of the 6 DOF are presented in Table 5.2 and are quite similar, with a few slight variations and with a maximum error of 5% observed in sway natural frequency. This small discrepancy is attributed to the modelling modifications of the earlier version of OpenFAST that has been used at the NREL OC4 project.

Table 5.2: *Natural Frequencies comparison between NREL and OpenFAST 3.5.0 simulations*

Natural Period (Frequencies)	NREL	Hybrid (OpenFAST 3.5.0)
Surge	104.8s	105.4s
Sway	113s	107.5s
Heave	17.9s	17.8s
Roll	26.9s	26.05s
Pitch	25.7s	26.05s
Yaw	79s	78.05s

5.1.2 Comparison of hydrodynamic theories

The verification analysis was also conducted between the different modelling approaches of the HydroDyn module. OpenFAST encompasses three different approaches, namely potential flow theory, strip theory and hybrid which is a combination of the two. Among these the most widely used is the hybrid theory due to each versatility in different geometries and shapes of floaters. The hybrid
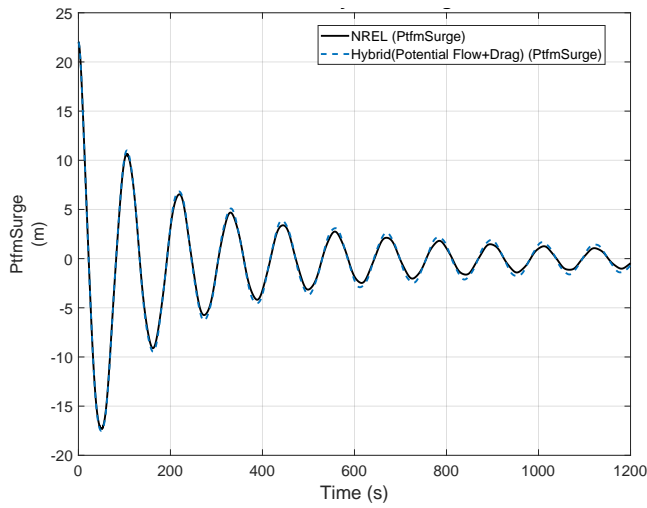
(a) *Surge Free Decay Test, Platform surge motion (m)*
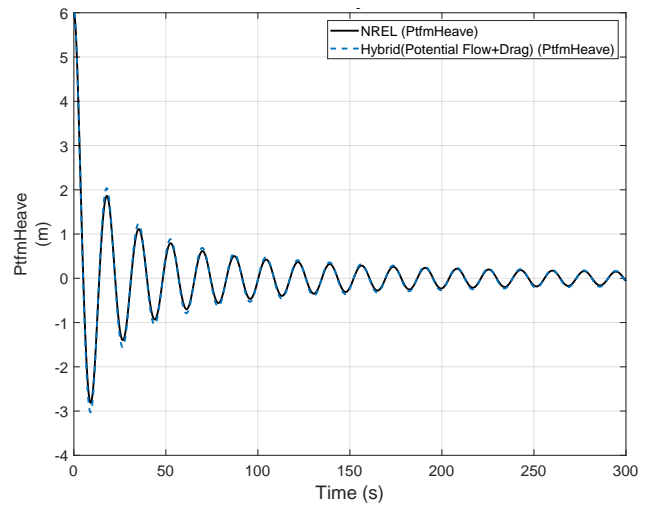
(b) *Heave Free Decay Test, Platform heave motion (m)*
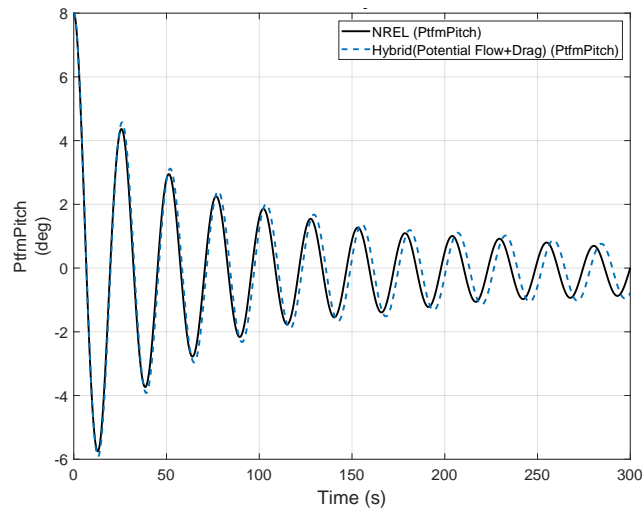
(c) *Pitch Free Decay Test, Platform pitch motion (deg)*
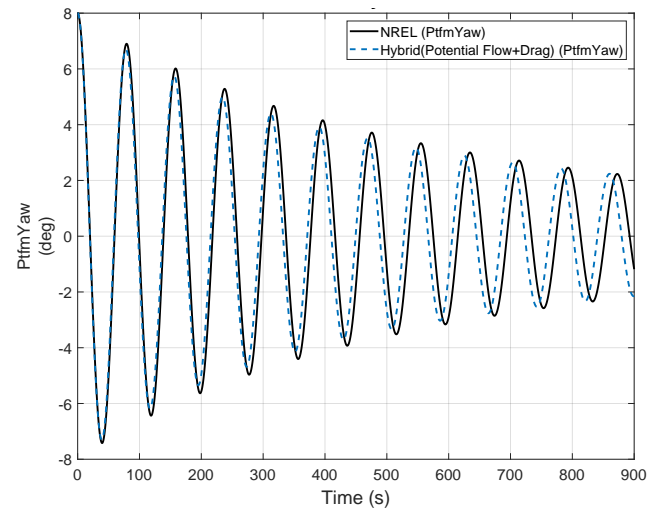
(d) *Yaw Free Decay Test, Platform yaw motion (deg)*

Figure 5.1: *Comparison of free decay tests between NREL OC4 simulations and Hybrid theory with OpenFAST 3.5.0 version represented as the floating platform motion among different directions*

Table 5.3: *Damping ratio comparison between NREL and OpenFAST 3.5.0 simulations*

Damping Ratio	NREL	Hybrid (OpenFAST 3.5.0)
Surge	0.0407	0.03615
Heave	0.0249	0.0241
Pitch	0.0292	0.0285
Yaw	0.0179	0.0175

theory makes use of the diffraction-radiation problem derived by WAMIT, which is the potential flow theory input, and the viscous effects, which are represented by the drag coefficients of the Morison equation (Strip theory).

While the potential flow theory allows for application to different types of floaters, the Morison equation, although less suitable for larger and complex structures, offers a more direct approach. The requirement for a detailed frequency-dependent solution from WAMIT in the case of potential flow theory can be replaced with the simple definition of drag and added mass coefficients. Its simplicity underlines the importance of the Morison equation and the need for investigating further its application.

(a) *Surge Free Decay Test, Platform surge motion (m)*

(b) *Heave Free Decay Test, Platform heave motion (m)*

(c) *Pitch Free Decay Test, Platform pitch motion (deg)*

(d) *Yaw Free Decay Test, Platform yaw motion (deg)*

Figure 5.2: *Comparison of free decay tests between hybrid solution (Potential Flow + Drag Coefficients) and Strip theory solution represented as the floating platform motion among different directions*

Within this framework, the free-decay tests were also simulated using the Morison equation, incorporating the coefficients as defined in Table 4.2. Figure 5.2 demonstrates the difference in the free-decay tests of the hybrid and strip theory approach in the 4 DOFs. The figure demonstrated a remarkable similarity, indicating the Morison equation is applicable to the present structure and can yield comparable results. The largest discrepancies are located in the yaw free-decay test where the damping ratio is significantly lower. The cause of this difference can be attributed to the values of the coefficients used. Specifically, the added mass, derived from the potential flow solution, may not be highly accurate as it is represented by a constant value. For this reason, it should be one of the parameters that require further investigation. However, it should be noticed that in all other simulations, the hybrid and Morison equation approaches are in agreement. This observation supports the statement that the differences with the NREL OC4 simulation are attributed to the version of OpenFAST utilized.

The free-decay tests were also performed with the application of the potential-flow theory only. In this case, only the radiation-diffraction solution is considered through the predefined WAMIT files. Since the drag coefficients are ignored the viscous damping is not considered. It has been noticed that viscous-induced damping is dominating for the specific semisubmersible structure. Hence, it should be added through the quadratic damping matrix presented in Table 4.2 to obtain equivalent outputs. The comparison between all of the theories is presented in Figure 5.3 and the total comparison between the natural periods calculated for the different theories is presented in Table 5.4. What is observed is that for the four main motions, namely surge, heave, pitch, and

(a) *Surge Free Decay Test, Platform surge motion (m)*
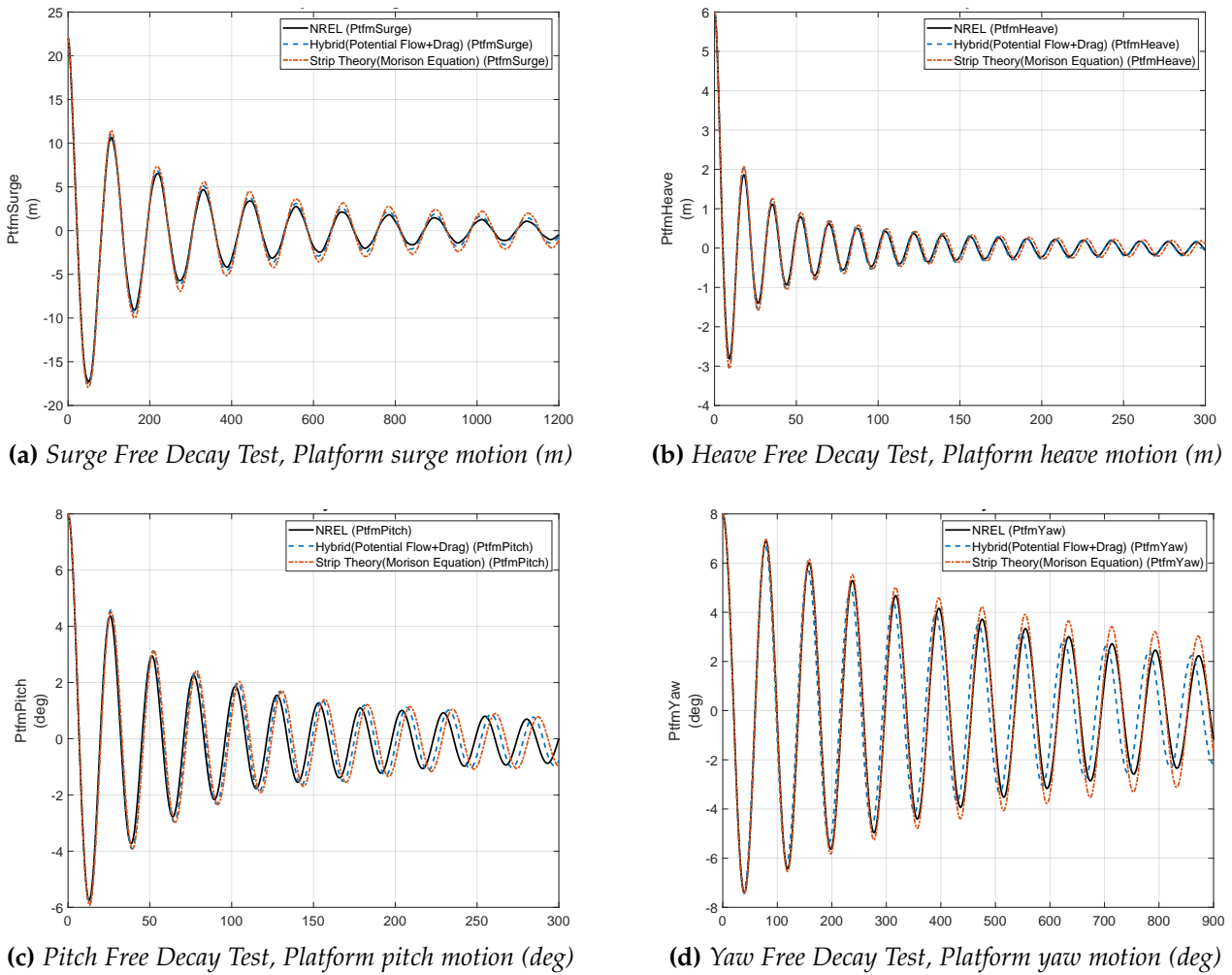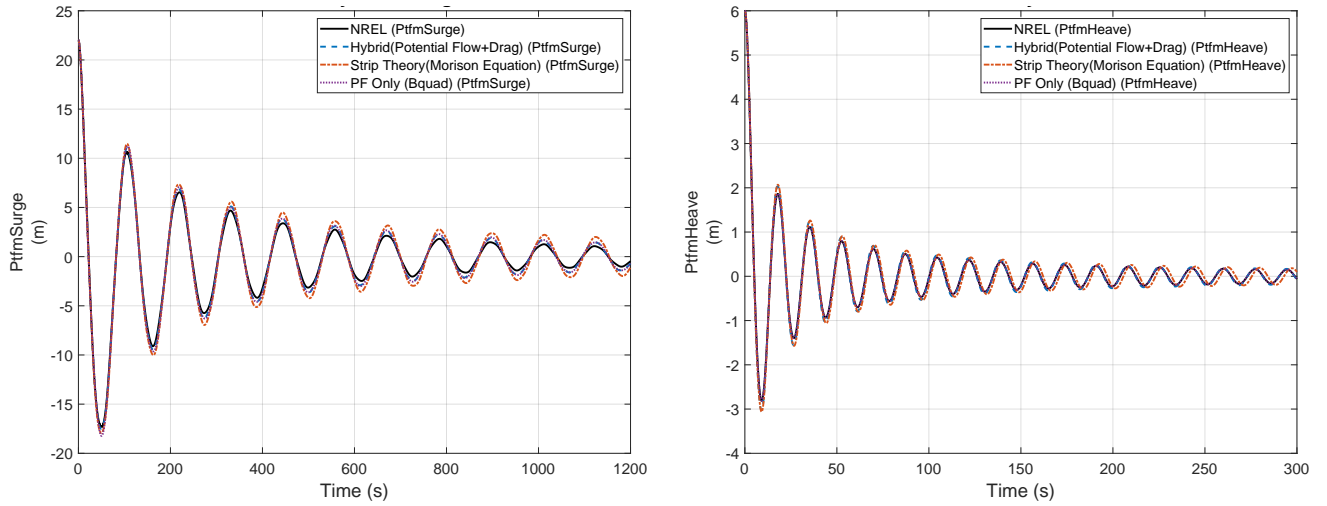

(b) *Heave Free Decay Test, Platform heave motion (m)*

Figure 5.3: *Comparison of free decay tests between hybrid solution (Potential Flow + Drag Coefficients), Strip theory solution (Morison equation) and Potential flow solution represented as the floating platform motion among different directions*

yaw, there is alignment between the natural periods obtained using the hybrid and strip theory, suggesting that the two theories are equivalent, at least for the free decay tests. A close agreement in natural periods is also noted for surge, heave, and yaw motions when using potential flow theory alone. However, in the case of pitch motion, when employing potential theory exclusively, a natural period of 40 seconds is observed, which is 15 seconds longer than the values obtained with the other approaches. This discrepancy in pitch motion could be attributed to the model setup when using potential flow theory alone, which may require additional modifications to accurately predict the pitch motion. Further investigation is recommended to identify the problem. It is worth noting that the strip and hybrid theories, which employ member-based attribution, have longer simulation runtimes but may provide more accurate calculations of the motions.

Table 5.4: *Natural Frequencies comparison between different hydrodynamic theories in OpenFAST 3.5.0 and the NREL OC4 project*

Natural Period (Frequencies)	NREL	Hybrid	Strip Theory	Potential Flow Theory
Surge	104.8s	105.25s	104.6s	106.9s
Heave	17.9s	17.8s	17.95s	17.9s
Pitch	25.7s	26.5s	26.25s	40s
Yaw	79s	78.35s	78.35s	79.15s

5.1.3 Wind and Wave simulations

Apart from the free-decay tests, other load cases were also incorporated into the model verification. More specifically, within the frame of OC4 project, several cases including waves and wind were simulated. The outputs of those simulations were used to verify the model's behaviour under different environmental conditions.

In more detail, load case 2.2 as simulated in OC4, with a JONSWAP spectrum, of wave height $H_s = 6m$, peak period $T_p = 10sec$, and peak shape parameter $\gamma = 2.87$, was simulated and compared with the NREL simulation results. When simulating irregular waves it is advised to run simulations for at least 60 minutes [33]. Therefore, the model runs for 4600 seconds, excluding 1000 seconds of transient behaviour. Similarly to the previous simulation, the timestep was set to 0.0125sec while the hybrid modelling approach with potential flow theory in combination with
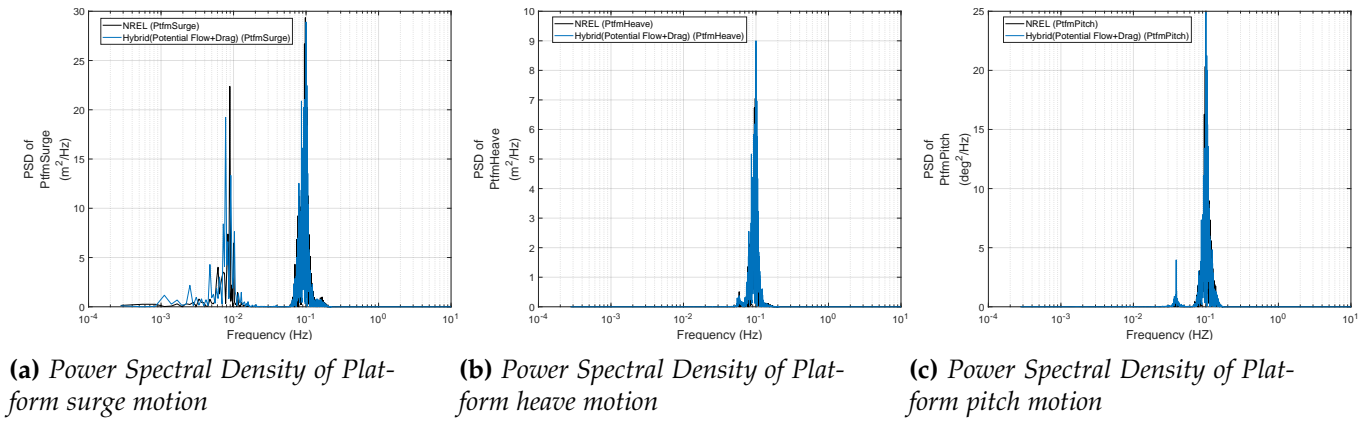
(a) *Power Spectral Density of Platform surge motion*

(b) *Power Spectral Density of Platform heave motion*

(c) *Power Spectral Density of Platform pitch motion*

Figure 5.4: *Comparison of load case 2.2 ($H_s = 6m$, $T_p = 10sec$, $\gamma = 2.87$) between OpenFAST 3.3.0 version hybrid model and NREL (OC4) results with the use of power spectral density (PSD) diagrams of the platfrom motions*

member-defined drag coefficients was used. It is important to note that for this load case, only wave conditions are simulated, and still air is considered..

In the case of irregular phenomena the comparison between the different load cases can be done in the frequency domain for a better representation of the wave frequency. For this reason, the Power Spectral Density (PSD) for each of the outputs can be calculated. The PSD is calculated by applying Fast Fourier Transformation (FFT) to the time-domain output and then calculating the power of this measurement. As a result, an insight into the resonance frequencies can be obtained. The comparison between the power spectral densities of the surge, heave and pitch motions are presented in Figure 5.4. It should be mentioned that all the graphs were generated with the use of the Matlab Toolbox that has been built for analyzing OpenFAST simulation data. The peaks are very similar and appear at the same frequencies. The smaller peaks are observed in the natural frequencies that were calculated in the free-decay tests. However, the dominating resonance is detected around 0.1 Hz which is the frequency corresponding to the peak period of the irregular waves that are simulated.

In addition to the wave conditions mentioned above, coupled simulations were also performed. This means that wind was also considered and used for the verification of the model. More specifically, load cases 3.2 and 3.3, as presented in OC4 code comparison [20], with irregular wave conditions and turbulent wind were regenerated. With the same simulation properties as in the previous cases the simulation runs for 4600 seconds with 0.0125 seconds of timestep. Two different wind speeds were simulated, $V = 11.4 m/s$ which is the near-rated wind speed of the wind turbine and $V = 18 m/s$ which is the above-rated wind speed. The wind files were generated with the use of TurbSim. Nevertheless, it should be mentioned that the wind files were generated with different turbulent models than the ones of the OC4 project simulations. In more detail, instead of the Mann model of the NREL simulations, the IEC Kaimal model was used.

For the verification of wind simulations blade and tower-related outputs were considered for the comparison. Some representative results are demonstrated in Figure 5.5, with respect to the blade deflection for case 3.2. In this case, the PSD diagrams are displayed. It can be noticed that there is a compliance of the simulation with the results derived during the OC4 project, with the peaks located around the same frequencies. A more general overview is also presented at Table 5.5 where the mean response values of different outputs are compared. It can be noticed that the values are very similar with only small variations. The most significant difference is observed in the surge motion of the platform and certain tower moments, with the most significant error found in the top tower moment in the y-direction, showing a deviation of up to 60%. Those differences can be attributed to the different wind files that were used as can be shown from their mean values in all directions, which can have an effect on the calculated moment at the base of the tower.

Table 5.5: *Mean response comparison between NREL OC4 project simulations and OpenFAST 3.5.0 version for Load Case 3.3*

Input	NREL	OpenFAST 3.5.0 (Hybrid)
Wind velocity x-direction	17.89 m/s	18.15 m
Wind velocity y-direction	0.022 m/s	0.063 m/s
Wind velocity z-direction	0.053 m/s	0.025 m/s
Output	**NREL**	**OpenFAST 3.5.0 (Hybrid)**
Platform Surge	4.48 m	6.0 m
Platform Pitch	1.71 deg	2.02 deg
Tower Base Moment x-direction	6601 Nm	8294 Nm
Tower Base Moment y-direction	38782 Nm	43467 Nm
Tower Top Moment x-direction	4214 Nm	4289 Nm
Tower Top Moment y-direction	1057 Nm	1690 Nm
Out-of Plane Blade Deflection (1)	1.70 m	1.64 m
In-Plane Blade Deflection (1)	-0.55 m	-0.53 m
Fairlead Tension 1	1017.9 kN	994.2 kN
Fairlead Tension 2	1349.7 kN	1454.6 kN
Fairlead Tension 3	1008.4 kN	971.3 kN
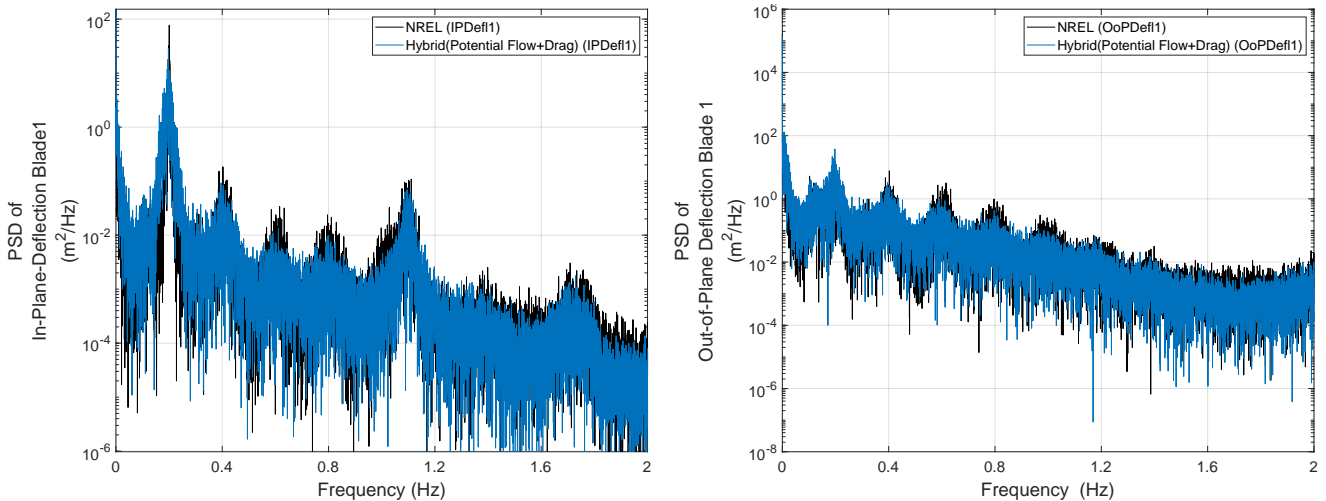
(a) *Power Spectral Density of In-plane Deflection of Blade 1*

(b) *Power Spectral Density of Out-of-plane Deflection of Blade 1*

Figure 5.5: *Comparison of load case 3.2 ($H_s = 6m$, $T_p = 10sec$, $\gamma = 2.87$, Turbulent wind $V = 11.4m/s$) between OpenFAST 3.5.0 version hybrid model solution and NREL (OC4) results with the use of PSD of the in-plane and out-of-plane deflections*

5.2 Validation with the use of experimental results

An additional step is to validate the OpenFAST results with existing experimental outputs. Validation efforts have been undertaken in the OC5 and OC6 projects, where various tests were conducted on a scaled experimental model and compared with the full-scale model simulations in OpenFAST. These analyses made it possible to detect any discrepancies between simulations and realistic tests and explore the limitations of the modelling approach. Although the results from the tests have been thoroughly analysed and it has been concluded that OpenFAST underestimates some low frequencies [21], they are utilized here for a more comprehensive evaluation of the modelling set-up.

In order to compare the model to experimental results the FOWT build-in model in OpenFAST had to be modified. The new inputs are described in Table 5.6 highlighting modifications on the floater and mooring properties. In more detail, the platform mass along with the moments of inertia had to be adjusted while the mooring lines are completely different with respect to their size and properties. These adjustments were required due to the fact that the experimental results are based on a scaled model, which, when extrapolated to full scale, has to be modified properly to get the equivalent model [40]. In addition to modifying structural parameters, changes to the HydroDyn inputs are required to achieve the same level of damping observed in the experimental setup [41]. The drag coefficient of the members was fluctuating around 0.6 in the OC4 simulations while for the experimental simulations, different values were employed. A drag coefficient of 1.6 for the heave plates (base columns) and 0.4 for the rest of the members had to be chosen. This range between the two set-ups underscores the significance of the drag coefficients in accurately representing the hydrodynamic behaviour of the system. This apparent difference in the selected drag coefficient further highlights the requirement for a thorough analysis and evaluation of the drag coefficient as one of the key characteristics of the systems.

Table 5.6: *Properties of OpenFAST full-scale model for experimental model comparison*

Properties	
Floater Properties	
Mass,m	1.40715E7 kg
Displaced Volume, V	1.39180E4 m3
Vertical Center of Gravity, VCG (from SWL)	-7.53 m
Roll Moment of Inertia, I_{xx} about CG	1.28980E10 kg/m2
Pitch Moment of Inertia, I_{yy} about CG	1.2851E10 kg/m2
Yaw Moment of Inertia, I_{zz} about CG	1.4189E10 kg/m2
Mooring Properties	
EA	2.710624E6 N
Unstretched length	55.432m
Equilibrium length	78.388m
Diameter	0.0040m
Mass Density	0.12 kg/m
HydroDyn Inputs	
Additional linear damping surge	75000 N
Additional linear damping pitch	31E06
Axial drag coefficient	8.20
Drag coefficient member, Cd	0.4
Drag coefficient base columns, Cd	1.6

In the validation, the free decay tests were conducted for the surge, heave, and pitch directions. The initial offset over the different degrees of freedom for those free decay tests is presented in Table 5.7. It was observed that the response over time could be reproduced with almost identical behaviour, particularly in the surge direction. In general, from the comparison between the experimental results for the three degrees of freedom, there is a close relevance between the results.

Overall, the OpenFAST model demonstrates appropriate reproduction of the experimental results in terms of free decay simulations. This indicates that the model is capable of accurately capturing the dynamics of the system. However, it should be mentioned that in the comparative analysis between experimental and OpenFAST simulations under load cases, there are findings where the model fails to predict certain peaks, particularly under low-frequency conditions, as was mentioned [21]. This suggests that further improvements or refinements may be necessary to enhance the accuracy and predictive capabilities of the model in such scenarios.

Table 5.7: *Initial offset of the degrees of freedom of the different motion for the free decay tests in surge, pitch and heave direction*

Load Case	Surge (m)	Sway (m)	Heave (m)	Roll (deg)	Pitch (deg)	Yaw (deg)
Surge	-5.0539	0.9128	0.0068	0.0764	0.7403	0.2514
Heave	0.0768	-0.3213	-2.1687	0.1995	0.2739	0.1441
Pitch	-2.0729	0.0648	-0.0870	-0.0902	-5.6719	0.0026
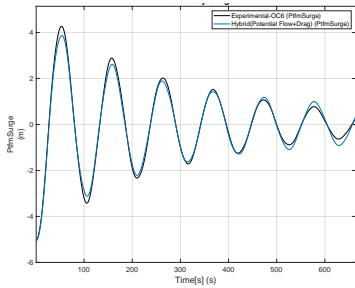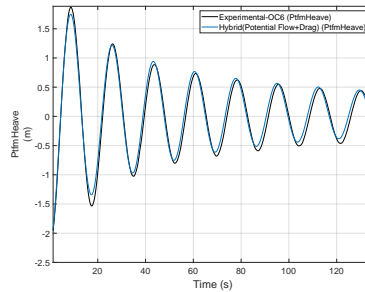
(a) *Free Decay Surge*   **(b)** *Free Decay Heave*   **(c)** *Free Decay Pitch*
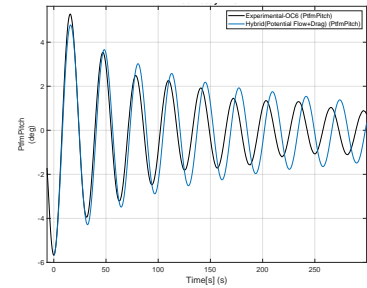
Figure 5.6: *Comparison of free decay test between OC6 experimental results and openFAST simulations*

6 Significant Parameters Analysis

The dependence of performance on the modelling inputs creates great uncertainty in the measured results and the reliability of the FOWT response. In order to comprehend the effect of uncertainties, a sensitivity analysis over different input parameters is conducted. This analysis identifies the significance of different inputs over specific outputs.

6.1 Elementary Effects Method Description

A sensitivity analysis could be a useful tool for determining how various parameters affect the FOWT's response. In reality, a number of input parameters related to both environmental factors and modelling parameters might impact the system, and it can be challenging to identify which of those elements may be responsible. The majority of sensitivity analysis techniques, such as Monte Carlo, are computationally costly and need a significant number of simulations.

Because of this, a different strategy—the elementary effects method—is used. The elementary effects (EE) approach is a screening technique that rates various inputs according to their corresponding influence on a given output, rather than explicitly measuring the variance of that result [42]. This enables determining the most important factors and focusing the research on them.

This method has previously been applied, primarily focusing on aerodynamic parameters[32], and more recently extended to include other modelling parameters relevant to floating wind turbines [31] using the OpenFAST and the same type of floating wind turbine. Therefore, it is a well-established method that can be effectively employed for the comprehensive analysis of the existing multiparameter system.

Each output of FOWT system such as the platform motions, the hydrodynamic, the tower and the mooring loads and the power generation is a function of different input properties. Based on that the elementary effects method can be described as follows:

1. The set of input parameters is selected and is normalized so all the variables take values between zero and one

2. A number of trajectories R is chosen. The trajectories represent the different initial number sets of the input parameters. Each trajectory is generated randomly with a selected random generator or sampling method.

3. For each trajectory R, only one input parameter is changed by a fixed step size $\Delta = 1/R$, until every parameter change once.

4. The resulting set of numbers is used as an input and the different simulations run to measure the outputs. The output that is measured for every case set and the elementary effects are calculated through Equation 6.1. The EE is calculated for every parameter i, meaning that in the end, every parameter has R different EE calculated.

$$EE_i(x) = \frac{f(x + \Delta e_i) - f(x)}{\Delta}$$

(6.1)

where f is the output that is studied and the input variables $x, x + \Delta ei$ is the difference between the time steps

5. The elementary effect statistics over all of the trajectories are then calculated with the mean effect μ_i^* and the standard deviation σ_i. As a result, every parameter has a total effect. The statistics are plotted and used to rank the parameters.

$$
\begin{aligned}
\mu_i^* &= \sum_{r=1}^{R} \left| \frac{EE_i\left(x_r\right)}{R} \right|, \\
\sigma_i &= \sqrt{\sum_{r=1}^{R} \frac{\left(EE_i\left(x_r\right) - \mu_i\right)^2}{R}}.
\end{aligned}
\tag{6.2}
$$

A detailed graph of the method is presented in Figure 6.1

6.2 Elementary Effects method objectives

The main objective of performing a sensitivity analysis is to identify which inputs and outputs are most important. This involves identifying the main input parameters that affect the FOWT system. It is important to carefully decide which input and output parameters to include in the analysis in order to obtain meaningful conclusions. In addition to input and output selection, the ranges of the assigned parameters and the sampling method can have an impact on the analysis results. Choosing appropriate ranges ensures that the full range of potential values and their effect on the system are considered. The sampling method should ensure that all the possible combinations of values are examined and it can influence the robustness and reliability of the analysis. Once the sensitivity analysis is performed and the results are obtained, the post-process analysis of those results has to be carefully decided for their most effective interpretation. The post-process analysis may involve statistical analysis or other techniques to facilitate the understanding of the relations between the parameters and the system behaviour.

By addressing the selection of parameters, the sampling method and the post-process analysis, the sensitivity analysis can provide valuable information on the performance of the system.

6.2.1 Selection of parameters

As presented in Section 3.3 there are several parameters that require further studying with respect to their impact on the hydrodynamic analysis. Those can be divided into the modelling properties such as the hydrodynamic coefficients and the wave/wind properties which are related to the external conditions applied to the system. A detailed table with the parameters and their range is presented in Table 6.1.

As can be observed the main parameters that will be studied involve the drag coefficients and the added mass coefficients for every member and in the axial direction (heave). Their uncertainty is presented in several studies in which different values have been chosen based on the conditions that were simulated. With respect to the drag coefficients, the OC4 project (Table 4.2) has selected values ranging from 0.56 to 0.68 for different components. However, when comparing the code with CFD simulations that only consider currents, different ranges have been proposed [43]. These ranges not only differ between the upper and lower sections of the floating structure but also between the front and back parts, with values ranging from 0.320 to 0.922. Other CFD simulations have indicated that the drag coefficient is underestimated and values exceeding 1 should be taken into account [44]. As a result, a range of 0.3 to 1.6 should be considered for simulations. Similarly, although the axial drag has not been extensively studied, it falls within the range of 2.5 to 5 in the same studies, which
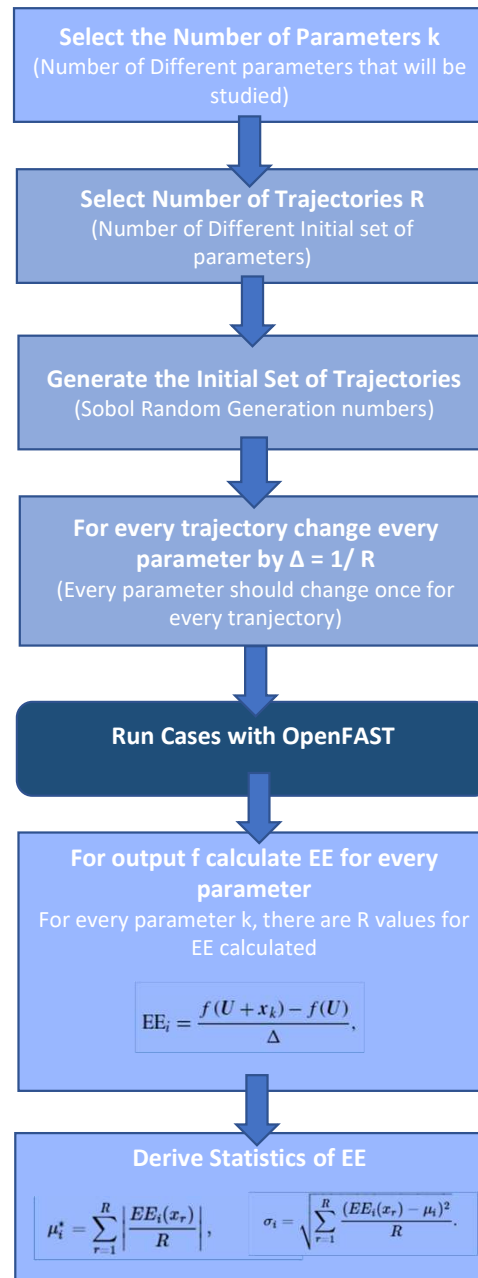
Figure 6.1: *Elementary Effects Method flowchart*

will be varied between 5 and 10 as an input in OpenFAST.

The range of observed values for the added mass is smaller compared to other parameters. The added mass coefficient is specifically used when applying the Morison equation instead of the potential flow theory which relies on predefined WAMIT matrices. In the case of the Morison equation, the added mass coefficient is calculated with respect to the potential flow solution. However, this is a global value that may not accurately represent all the cases. Therefore, research suggests that different values can be selected based on the simulated case [44]. Considering this, a range of 0.5 to 1.3 can be examined for the traverse direction and 0.3 to 1.3 for the axial direction .

The observed environmental conditions can exhibit considerable variations. In this analysis, a wide

range of conditions will be simulated, including significant wave heights ranging from 0.13m to 14.18m and peak wave periods spanning from 2.18s to 21.2s. The wind speeds range from 0m/s to 25m/s including the functional range of the wind turbine between cut-in and cut-off speeds but also cases where minimum or no wind speed is applied. These ranges have been established based on a comprehensive examination of potential floating wind turbine locations worldwide, and further analysis will be presented in the subsequent stages. To encompass all possible scenarios, the wind wave misalignment range has been set from 0 to 90 degrees. The selection of the current speed is extracted from previous research findings [31].

Table 6.1: *Ranges of the different input parameters of the OpenFAST model of NREL 5MW Semisubmersible FOWT*

Parameters	min	max
Modelling Parametres		
Cd (Members)	0.3	1.6
Cdz (Axial)	5	10
Ca (Members)	0.5	1.3
Caz (Axial)	0.3	1.3
External Conditions		
Hs (m)	0.13	14.8
Tp (s)	2.18	21.22
Wind Speed (m/s)	0	25
Wind/Wave misalignment (deg)	0	90
Current Speed (m/s)	0	2
Current Direction (deg)	0	90
Turbulent Intensity (%)	0	15

6.2.2 Sampling Method

The selection of trajectories involves the definition of the different combinations of cases that will be performed. By definition, the Elementary Effects method uses the trajectories approach. The trajectories approach starts with the generation of a number R of vectors with different input values k. Those initial values are selected randomly and should not be repeated. For each one of the trajectories, every parameter has to change by a value Δ. When the first, input changes in the next step it remains changed while the next parameter is changed by delta. At the end of the procedure, for every trajectory in total $k + 1$ cases have been created including the initial condition, which leads to $R(k + 1)$ cases in total.

Although the trajectories method is widely used there have been alternative approaches developed which might enhance the reliability of the results. The radial method is such an approach, which has the same starting points as the trajectories method. However, instead of keeping the modified values at each step, the input parameter changes only once and then it reverts back to its initial value. The primary objective of the radial method is to isolate and examine the impact of a specific parameter without considering the potential influence of other parameters. A graphic representation of the two methods is presented in Figure 6.2 where the behaviour of the sampling procedure in the hyperspace considering that there are three parameters is shown. Given these considerations, the radial method was employed while a fixed Δ of 10% the total range of each parameter was considered.

Apart from the method used to formulate the total number of different inputs, the initial selection of the random numbers is a matter of concern. The initial pool of trajectories is generated with Sobol random numbers generator which is a quasi-random low discrepancy sequence which distributes samples uniformly across the input space. This method was chosen since it has already
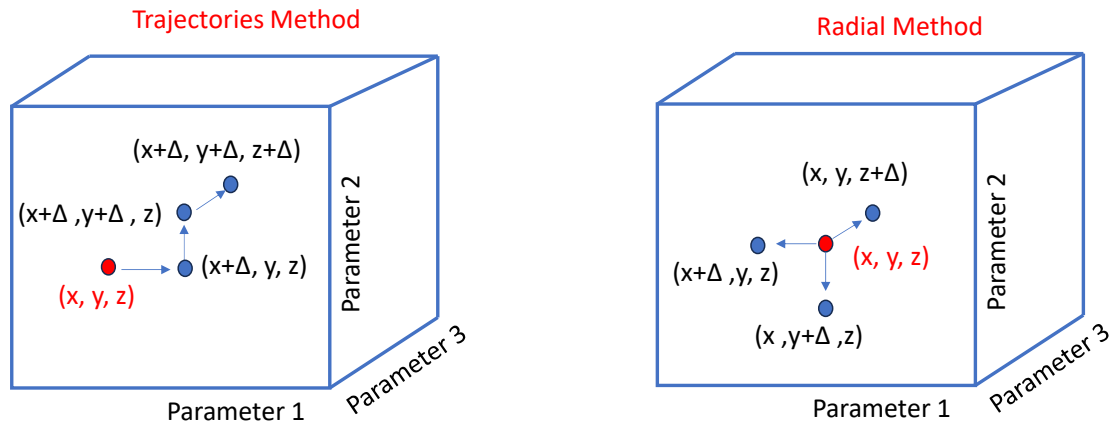
Trajectories Method

(x+Δ, y+Δ, z+Δ)

(x+Δ ,y+Δ , z)

(x+Δ, y, z)

(x, y, z)

Parameter 2

Parameter 1

Parameter 3

Radial Method

(x, y, z+Δ)

(x+Δ ,y, z)

(x, y, z)

(x ,y+Δ ,z)

Parameter 2

Parameter 1

Parameter 3

Figure 6.2: *Sampling method comparison in the hyperspace considering three parameters are studied.*

been used in previous research that uses the EE method [32]. From this pool, the initial vectors are selected in a way that maximizes their dissimilarity, ensuring a broad range of conditions is covered.

6.2.3 Post-process of EE resutls

The post-process of the simulations is the most significant aspect of the analysis. The first step includes the determination of the outputs that are worth being studied with regard to the FOWT performance. Since the most crucial aspect is related to the system's hydrodynamic performance, the platform motions will be considered. In addition, the hydrodynamic loads for the surge and the pitch direction should also be included in the analysis. The mooring line tensions are also important for the evaluation of the system while loads that affect the tower such as the tower top and base moments should also be counted. Finally, some representative loads with respect to aerodynamics such as the rotor thrust and torque and the power generation would be taken into account. The total output parameters that are considered are presented in Table 6.2 with their corresponding abbreviation.

Table 6.2: *Output parameters considered in the analysis*

Output Parameters	Abbrevation
Axial Hydrodynamic Force z	HydroFxi
Hydrodynamic Moment x	HydroMxi
Hydrodynamic Moment y	HydroMyi
Hydrodynamic Moment xy	HydroTotMoment
Tower Base Moment x ,Side-side (roll)	TwrBsMxt
Tower Base Moment y,Fore-aft (pitch)	TwrBsMyt
Total Tower Base Moment xy	TwrBsTotMoment
Tower Top Moment x	YawBrMxp
Tower Top Moment y	YawBrMyp
Total Tower Top Moment xy	YawTotMoment
Mooring Line Tensions	T[1], T[2], T[3]
Total Mooring Line Tension	TensionTotal
Rotor Thrust	RotTorq
Rotor Torque	RotThrust
Power Generation	PwrGen

For the comparison of the effects of the different parameters the Damage Equivalent Load (DEL) will be used. DEL is a method for evaluating the fatigue damage experienced by a structure subjected to repetitive loading. It quantifies the cumulative damage by considering the number of equivalent cycles until failure. In case of irregular cycles such as those encountered in simulations, the rainflow counting method is utilized to calculate the count of equivalent cycles within a defined time domain load output, considering different load ranges. The DEL of a time-series load output j is calculated as presented in Equation 6.3. L_{ji}^R is the cycle load range, n_j^{STeq} is the total equivalent fatigue counts for time series j and n_{ji} is the fatigue counts for every cycle of the time series j. The slope of the Whoeler fatigue curve is described by m and takes different values according to the material properties. Therefore for the tower m equals 3.5, for the mooring lines 3, 10 for blade flapwise and 8 for blade edgewise moments.

$$DEL_j^{ST} = \left(\frac{\sum_i \left(n_{ji} \left(L_{ji}^R \right)^m \right)}{n_j^{STeq}} \right)^{\frac{1}{m}} \tag{6.3}$$

To ensure a fair comparison of the impacts of various input parameters, the mean value and standard deviation are computed. However, it is important to consider that the outputs may have different ranges, necessitating the use of a supplementary standardized elementary effects method. This method involves normalizing the results, allowing for the observation of the relative importance across different outputs [45]. Normalization is accomplished using Equation Equation 6.4. In this equation, the mean Elementary Effect (EE), which has been computed from the Damage Equivalent Load (DEL), is divided by the standard deviation of the output.

$$SEE_j^{ST} = \mu_i^* / \sigma_j \tag{6.4}$$

7 Results & Discussion

7.1 Elementary Effects Method Results

The elementary effects method was used to analyze the effects of the different inputs that were referred to in Chapter 6 over specific outputs. As described, OpenFAST uses different theories for the application of hydrodynamics, and not all of the theories use all the parameters. The added mass coefficient is only used when the Morison equation is applied. For this reason, different approaches were used with combinations of the theories for the comparison of the results.

7.1.1 Hybrid Theory solution

The sensitivity analysis was initially conducted using the hybrid model that integrated the potential theory and drag coefficient. This required considering the drag coefficients of various members along with external factors such as wave characteristics, wind speed, wind/wave misalignment, current speed, and direction. The depth-dependent current was used for the ocean current type with 10 meters of reference while the directional spreading was active during the simulations. For those simulations, a steady wind was used with a vertical shear exponential of a=0.11. It should be noted that 20 different initial points were used the choice of which will also be explained in Section 7.1.4.

An indicative diagram of the significance of each input parameter with respect to different outputs is presented in Figure 7.1. For this specific graph, the DEL values of the time series output have been calculated and then the EE have been derived with the formulas used in Equation 6.3. To facilitate the comparison, the resulting values were normalized following the methodology detailed in Equation 6.4. The findings reveal that the impact of different parameters varies across the different outputs. Notably, the influence of external parameters, such as environmental conditions, surpasses that of the model-specific parameters such as the drag coefficients.

More specifically, the current speed emerges as the most influential parameter, particularly concerning the mooring line tension. The mooring line tension is also affected significantly by many other parameters as well, such as the drag coefficient of all the columns and the wave height and peak period. The focus of the analysis is primarily on mooring line number one, but it is important to consider the overall effect on all three mooring lines. Figure 7.2 provides an illustration of the relationship between the input parameters and the tension in all three mooring lines. The mooring line tension is influenced by the current speed due to its direct exposure to the prevailing currents. As the current speed increases, the forces exerted on the platform become more significant. This, in turn, leads to increased platform motion and subsequently higher mooring line tension. The correlation between the mooring line tension and the current velocity is non-linear which results in such a high influence[46]. It can also be observed that all the different mooring lines have the same sensitivity which is justified by the symmetrical layout of the structure and the mooring lines (Figure 7.2b). This feature also explains why the sensitivity of the current direction is not as significant.

An interesting aspect of the analysis is observed at the effect of the wave parameters. The significant wave height and the peak wave period as well as the wind/wave direction represented by the wave direction have a significant effect on the studied outputs, surpassing the effect of the wind
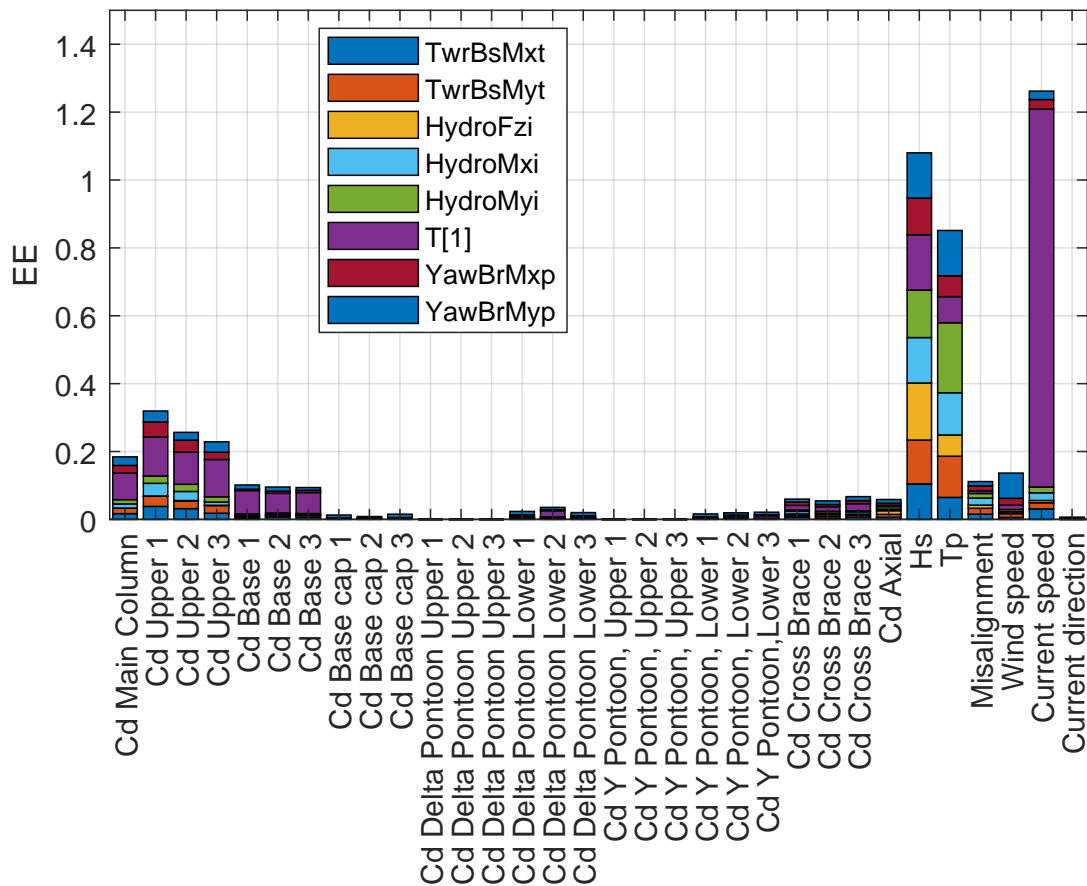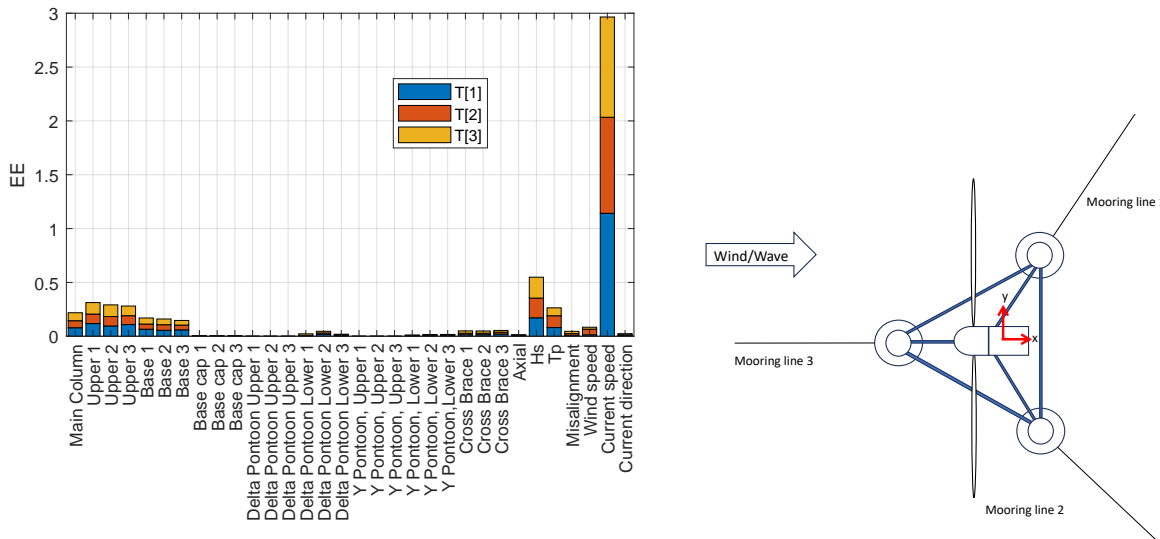
Figure 7.1: *Total Normalized EE significance of the input parameters (member hydrodynamic drag coefficients and external conditions) with respect to the DEL values of the tower and hydrodynamic loads and mooring line tensions.*

speed. This observation signifies that the external hydrodynamic conditions are the main factors determining the loading of the floating structure and the tower of the wind turbine. This underlies the importance of wave conditions when designing and assessing a floating wind turbine, which should be further analysed under different conditions.

Wind speed is another significant parameter that also affects many different outputs. It mostly affects the tower's top pitch moment which is reasonable since the wind always points in that direction. However, the wind is still not the main parameter affecting the pitch top tower moment since the significant wave height and the peak wave parameter have a higher effect. The direction of waves and wind which have been expressed as their misalignment (adjusting only wave direction), equally affects the different outputs but the total effect is relatively small.

From the studied drag coefficients the upper and the base members appear more significant. However, the exact position of those also affects since not all of the base or upper drag coefficients affect the same. To better understand and interpret the effect an explanatory diagram of the different floater members is presented in Figure 7.3. It can be observed that the front upper drag coefficient is the most sensitive parameter with respect to the other two upper columns and all three base columns which have equal significance. This appears to be in contrast with the findings of recent sensitivity analysis conducted[31], in which the bottom drag coefficients are more sensitive compared to the upper. However, it should be mentioned that this analysis does not focus on the member but only on the separation between the top and bottom drag coefficients. It can be observed

(a) *Total Normalized EE significance of the input parameters (member hydrodynamic drag coefficients and external conditions) with respect to the DEL values of all three mooring line tensions*

(b) *Mooring lines layout of NREL 5MW FOWT platform*

Figure 7.2: *Mooring lines tension EE analysis*

that the secondary elements of the structure such as the pontoons and the cross braces have little or no effect on the studied outputs. On the contrary, the main column and the three columns including the upper and the base part (heave plates) mainly affect the mooring line tension followed by an effect on tower and hydrodynamic loads. The effect on the tower top moment is quite interesting and signifies the importance of the floater parameters to the whole structural dynamics of the FOWT system. The axial coefficient which applies to the bottom of the structure and is mostly related to the axial damping of the structure has a small effect compared to the traverse direction coefficients.
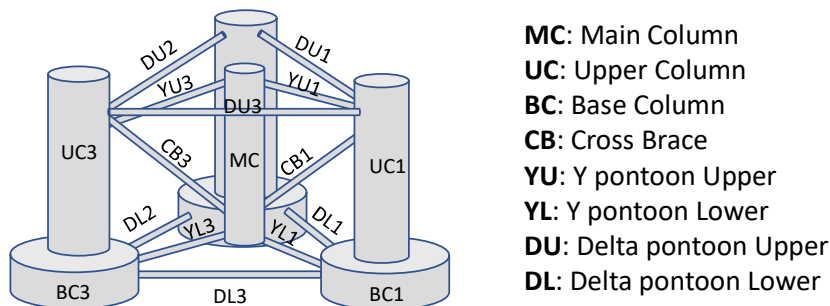

MC: Main Column
UC: Upper Column
BC: Base Column
CB: Cross Brace
YU: Y pontoon Upper
YL: Y pontoon Lower
DU: Delta pontoon Upper
DL: Delta pontoon Lower

Figure 7.3: *OC4 Platform layout and members*

In analyzing the impact on power generation, the Elementary Effects calculation was conducted using mean values. The wind speed, being the crucial determinant of the power curve, is anticipated to significantly influence power extraction. Nevertheless, it remains intriguing to explore the extent to which the power generation of a given wind condition is influenced by the variability in the other parameters. This exploration is facilitated by the radial approach employed, where a single parameter is altered in each iteration. Figure 7.4 represents the effect of all the input parameters on the power output excluding wind. Evidently, external conditions continue to play a pivotal role in influencing power generation. Notably, the peak period is essential in terms of impact, followed by wave height and current speed. This noteworthy observation underlines the significance of peak

wave periods and wave heights, along with the current speed, in shaping the extracted power profile. This insight highlights that even minor fluctuations in wave conditions or current speed possess the potential to yield substantial variations in the power output. One possible explanation for this phenomenon could be attributed to the platform's dynamic behavior. In specific scenarios, the platform may undergo pitching motions, potentially leading to a reduction in wind speed experienced by the rotor due to wind shear effects.
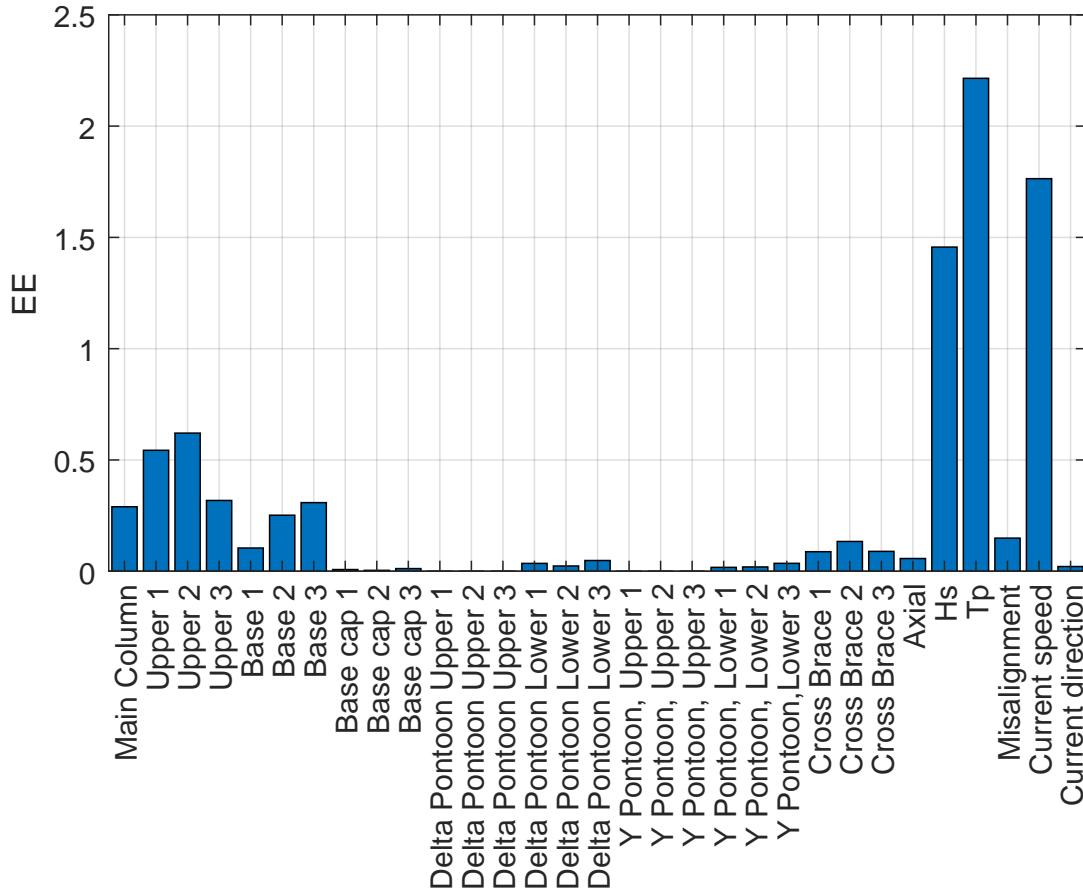

Figure 7.4: *Normalized EE significance of the input parameters (member hydrodynamic drag coefficients and external conditions) with respect to the power generation*

7.1.2   Influence of the physical model on the significant parameter analysis

Although the results clearly indicate the most significant parameters, the second-order elements were used in the wave simulations. To identify the influence of the physical model on the ranking of the sensitivity, the simulations were executed both with and without the incorporation of the quadratic transfer functions approach. Those elements were added with the use of Morison 2nd-order because the predefined WAMIT files do not include changes in the wave direction. The compared results are presented in Figure 7.5 where all the different outputs of Figure 7.1 are summed up. The order of parameter significance remains consistent across various inputs. However, a subtle difference in the resulting Elementary Effects (EE) is noticeable when second-order elements are considered. The inclusion of these elements may yield a different Damage Equivalent Load (DEL) and affect the identification of critical variables. In the current simulation, neglecting second-order elements tends to underestimate the outcomes slightly in all of the outputs apart from the current speed where a significant underestimation is observed. While their inclusion might enhance safety considerations, the disparity is negligible. Hence, it can be reasonably assumed that a comparable sensitivity analysis can be obtained without employing second-order elements, allowing for expe-
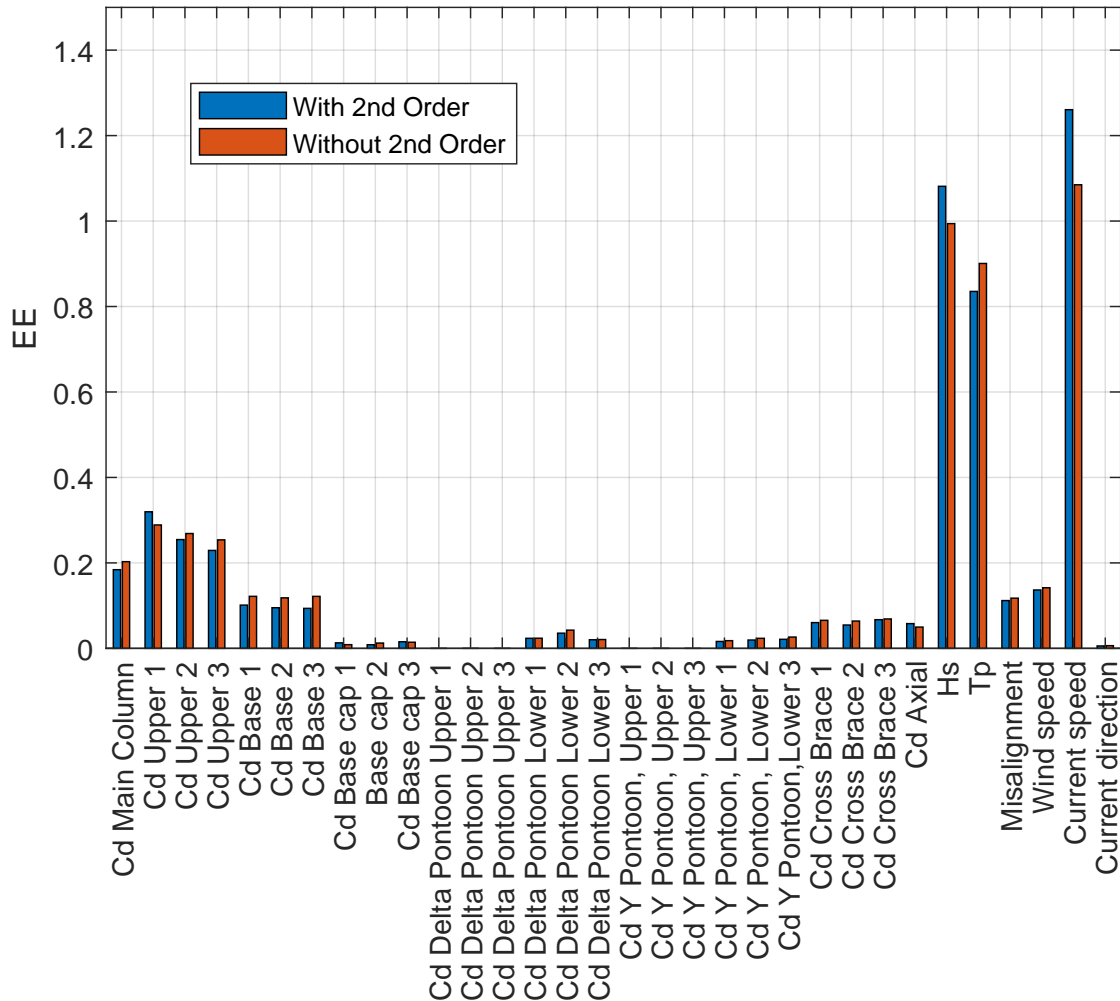
dited results in subsequent simulations.

Figure 7.5: *Combined Normalized EE significance of the input parameters (member hydrodynamic drag coefficients and external conditions) with respect to the DEL values with and without the use of 2nd-order hydrodynamic elements*

Morison equation solution

Apart from the hybrid theory, the sensitivity of the added mass coefficients was also examined through the Morison Equation-only approach. The resulting significant analysis for those parameters is presented in Figure 7.6, with the total normalized Elementary Effects of the DEL of the different loads. The simulation with the same assumptions as in potential flow theory, considering second-order elements and steady wind.

It can be observed that the variation of the external met-ocean conditions continues to exert a discernible influence on the structural loads. Notably, when considering the impact of the current speed, it becomes evident that its primary effect is on the mooring line tension, overshadowing its impact on other variables. Additionally, the significant wave height and the peak period equally affect the different loads of the tower and the floater. On the contrary, the wind speed's impact is comparatively minimal, thereby contributing less significantly to load variations. The misalignment factor, while exerting a marginal influence on different outputs, collectively presents a relatively minor effect compared to the aforementioned variables.

Similarly, the significance of the drag coefficient is equivalent to that of the hybrid (potential + drag coefficient) approach. This intriguing alignment of significance underscores the reliability of both theories, each yielding comparable outcomes despite their distinct methodologies. The drag coefficient uncertainty of the main columns along with the upper and base columns mainly affects the mooring line tension but also exerts an impact on the hydrodynamic and tower loads. On the other hand, the delta upper pontoons and the Y upper pontoons can be safely neglected due to their negligible effect on the studied parameters.

Undoubtedly, an important aspect lies in the influence of the added mass coefficients. The concept of added mass entails the supplementary mass that a structure undergoes during oscillation caused by waves. This phenomenon can be perceived as an augmentation of the structure's inertia. It is worth delving into the theory behind this effect: as a structure moves through the water, it displaces a certain volume, leading to water movement around it. This interplay causes an apparent increase in mass due to the inertia of the water that is set in motion.

Within the analysis, the added mass coefficient is much more influential, overshadowing the impact of drag coefficients. In more detail, it becomes evident that the added mass of the upper columns exerts a significant influence not only on mooring line tensions but also on the resultant loads of the floater and the tower structure. This could be attributed to the position of the upper columns, where their interaction with water and oscillation dynamics contribute to pronounced alterations in the structure's behaviour.

Furthermore, a notably substantial finding emerges in the axial added mass, which surpasses the influence of all other parameters. The axial added mass pertains to the inertia linked to vertical oscillations of the structure. Consequently, its accurate specification holds immense significance for the resultant loads. Any uncertainties surrounding such parameters could potentially lead to substantial disparities in anticipated loads, consequently affecting the fatigue analysis of the structure by either overestimating or underestimating the loads' impact.

Hence, the correct determination of the associated added mass coefficient in accordance with the simulated conditions is crucial. This underscores the potential benefit of employing the potential flow theory, which calculates the added mass considering frequency. It also emphasizes the necessity for rigorous verification of the coefficients' validity. This process is pivotal for ensuring accurate load estimations, contributing to a more precise assessment of the floating wind turbine's structural integrity and operational lifespan.

7.1.3 Turbulent wind

As was mentioned the wind simulated so far was steady shear wind. To emulate more realistic conditions turbulent wind was included as well. The inclusion of turbulent wind introduces additional fluctuations in the wind speed, consequently impacting the loads experienced by the tower top, rotor nacelle assembly, and the power generation process. The IEC Kaimal spectrum was adopted, and the corresponding files were generated using TurbSim. The introduction of turbulent wind brings additional variables that may impact the targeted outputs. Notably, recent research [31] emphasizes the central role of the standard deviation of turbulent wind in influencing the structural behaviour of floating wind turbines. Calculated from the turbulence intensity and mean wind speed, the standard deviation is incorporated into TurbSim via intensity parameterization as described in Equation 7.1. In offshore wind locations, turbulence intensity can range from 1% to 15% [47]. Building upon this, new test cases were formulated considering turbulence intensity. Following the previous simulations, cases involving the delta upper pontoons and y upper pontoons were excluded due to negligible effects. In addition, the total moments are calculated by taking the geometric sum of the components in the xy directions, while for mooring line tensions, the sum of all three directions is considered. This rationalization led to a reduction in the total number of
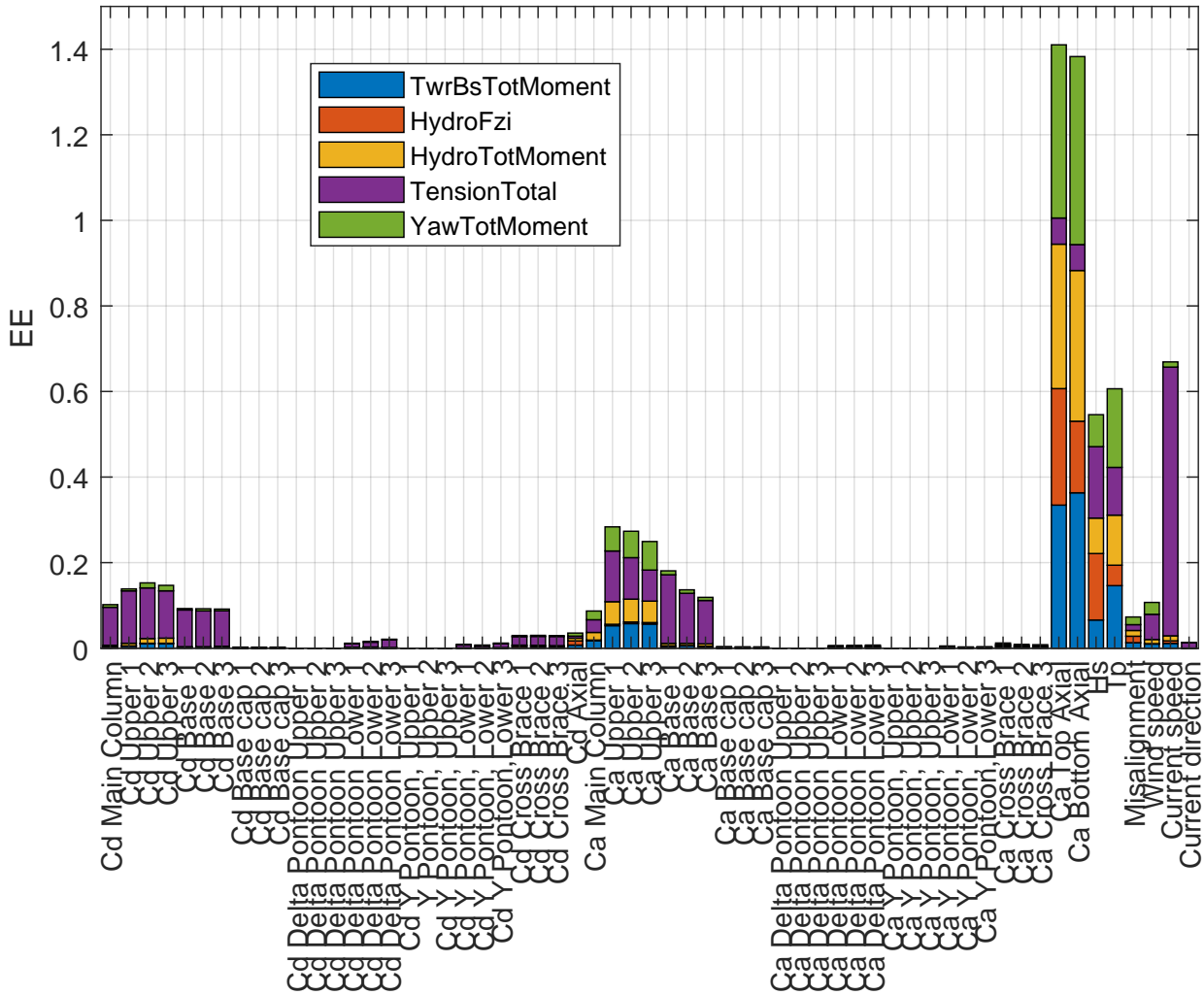
Figure 7.6: *Total Normalized EE significance of the input parameters (member hydrodynamic drag coefficients, member added mass coefficients and external conditions) with respect to the DEL values of the tower and hydrodynamic loads and mooring line tensions for the Morison equation solution approach*

cases. In terms of wind profile, a roughness of $z_0 = 0.0001m$ and a log profile exponent of $a = 0.11$ were considered [47].

$$I_u = \frac{\sigma_u}{U} \tag{7.1}$$

The results are shown in Figure 7.7 revealing a resemblance to the effects observed in the case of steady wind conditions. Notably, the dominance of the current speed's impact on mooring line tension remains intact, marking it as the most significant parameter. The current speed effect in the mooring line tension is dominant creating the most significant effect. Simultaneously, the significant wave height, accompanied by the peak wave period, appears to equally influence the hydrodynamic and tower loads, thus underlining their connection. The introduction of the turbulence intensity which is equivalent to the turbulence standard deviation seems to affect the top tower moment and the rotor torque. It is worth noting that the sensitivity of the hydrodynamic drag coefficients does have a minor impact on the rotor torque. This minor influence could be attributed to the motion of the floater, which affects the overall position of the entire system and is also dependent on the hydrodynamic drag. This motion, especially considering wind shear effects, might result in slight exposure to different positions where different wind speeds exist. Further investigation is recommended, and this is explored in more detail in Chapter 8, where more realistic scenarios are simulated.
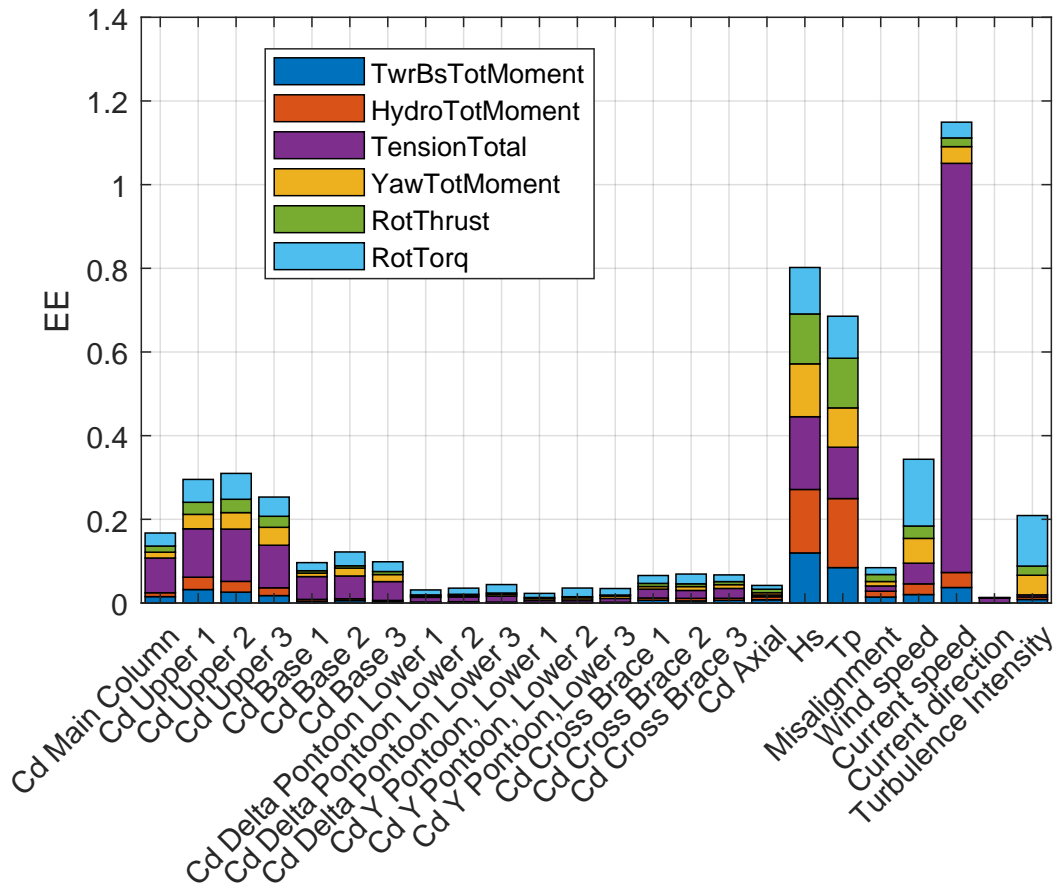
Figure 7.7: *Total Normalized EE significance of the input parameters (member hydrodynamic drag coefficients and external conditions) with respect to the DEL values of the tower and hydrodynamic loads and mooring line tensions with the turbulent wind consideration*

7.1.4 Number of starting points and random seeds independence

Within the framework of the analysis, the number of starting sampling points and the simulation seeds were examined. The independence of those parameters is important for the final results as it ensures the reliability of the analysis.

In Figure Figure 7.8, the convergence of results for varying numbers of initial starting points is illustrated. The value of R, representing the number of starting points, significantly influences the total count of simulations and consequently impacts the final outcome. More starting points lead to a broader examination of cases, resulting in a more comprehensive range of results. The plot reveals that the significance of parameters stabilizes after 12 trajectories. Notably, mooring line tension displays the highest variation, particularly in relation to the current speed, which emerges as the most influential parameter. However, this variance also levels off after reaching 15 trajectories.

In addition to the trajectory count, the number of seeds employed holds significance in ensuring comprehensive results. Distinct seeds come into play during the creation of wave kinematics and turbulent wind generation, where the initial states are randomly chosen. Consequently, these seeds can influence outcomes. Hence, it is crucial to ascertain the number of seeds required to achieve independent outcomes. Figure 7.9 illustrates the seed independence for the hydrodynamic file. With
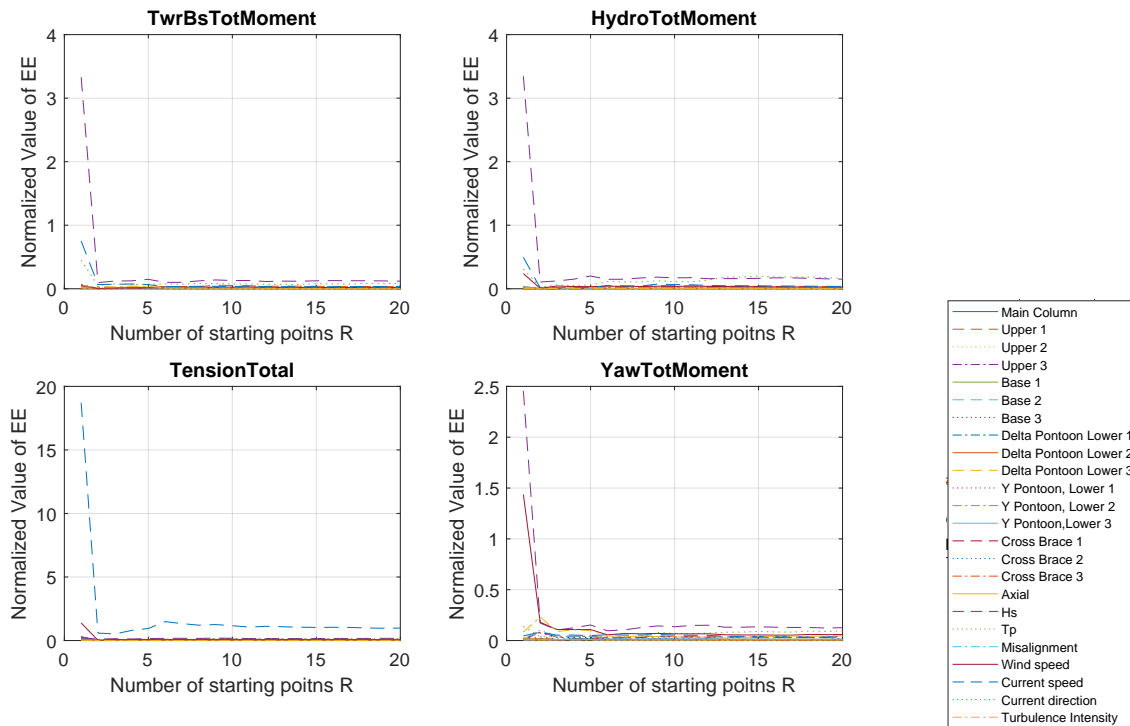
Figure 7.8: *Starting points (Trajectories) Convergence over the resulting normalized EE values of the DEL of different outputs*

each added seed, the result is averaged, encompassing all prior seeds. The graph demonstrates that after incorporating around 6-7 seeds, a state of independence is reached.

Figure 7.9: *HydrDyn file seeds Convergence over the resulting normalized EE values of the DEL of different outputs*

The wind file created using TurbSim also necessitates the assignment of seeds. However, for the studied outputs, primarily related to the floater and tower loads, no significant dependence on seeds

is evident, as depicted in Figure 7.10. The stability in the resulting EE values is achieved with just four different seeds. This stability can be attributed, in part, to the normalization of the resulting EE.
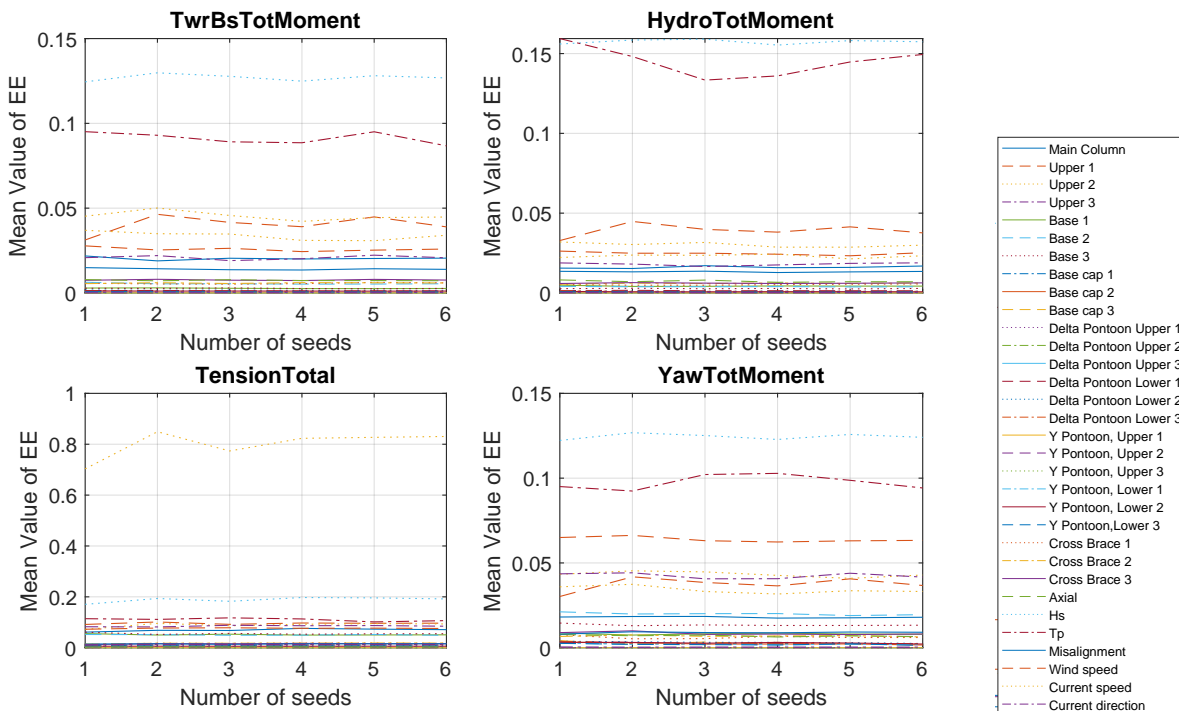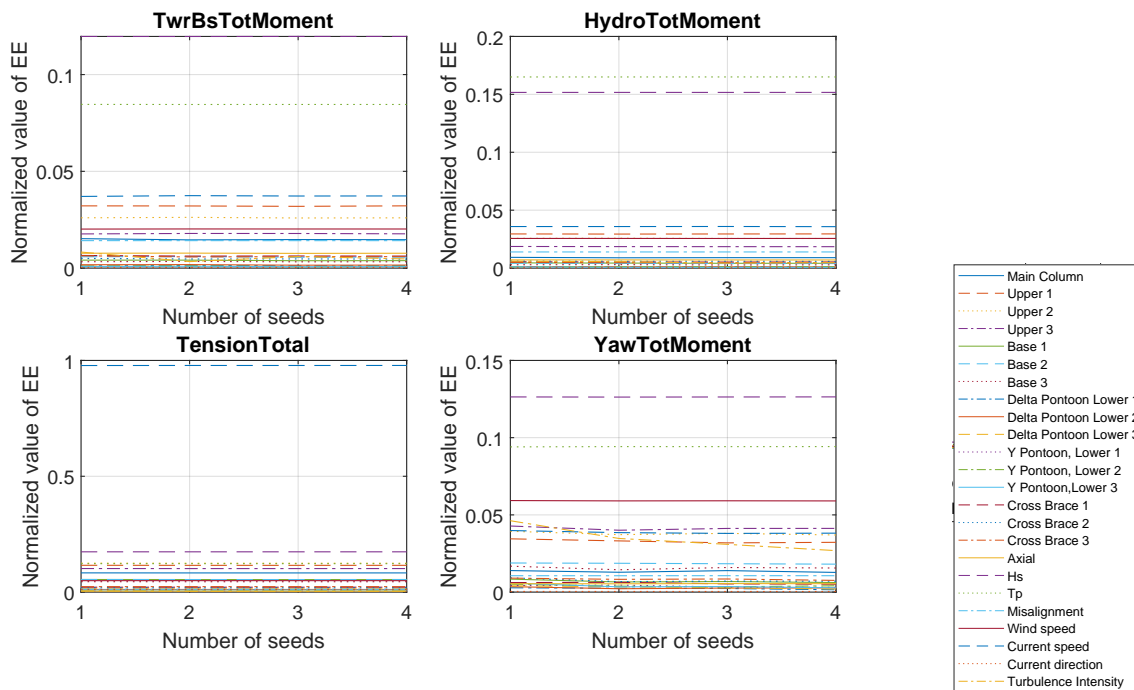

Figure 7.10: *Turbulent wind seeds Convergence over the resulting normalized EE values of the DEL of different outputs*

7.2   Spar platform sensitivity analysis

While the primary focus remained on the semisubmersible properties, it was deemed valuable to broaden the scope of the research by including a comparison with other layouts. Consequently, the choice was made to incorporate the spar platform, as outlined in the OC3 experiment, to ensure a comprehensive analysis.

7.2.1   OC3 Spar Platform

The OC3 experiments utilized the same reference NREL 5MW wind turbine, employing a tower and structural attributes that mirror those of the earlier experiment. However, a spar-buoy platform known as "Hywind," developed by Norway's Statoil, was utilized [48]. Depicted in Figure 7.11, the platform features a draft of 120 m. The OC3-Hywind spar buoy, positioned between the upper and lower sections of the platform, consists of two cylindrical segments joined by a linearly tapered conical region. The diameter of the cylinder is 6.5 m above the taper, transitioning to a larger diameter of 9.4 m below the taper. This design adjustment aims to mitigate hydrodynamic loads near the water's surface. The linearly tapered conical section extends from a depth of 4 m to 12 m below the still water level. It is essential to note that all these attributes are referenced to the platform's original position before displacement.

The spar buoy platform's layout lies in its simple structure. In the OpenFAST model, this simplicity allows for employing a uniform drag coefficient throughout the platform Additionally, owing to its slender geometry, there is no explicit axial drag coefficient referenced for the structure.
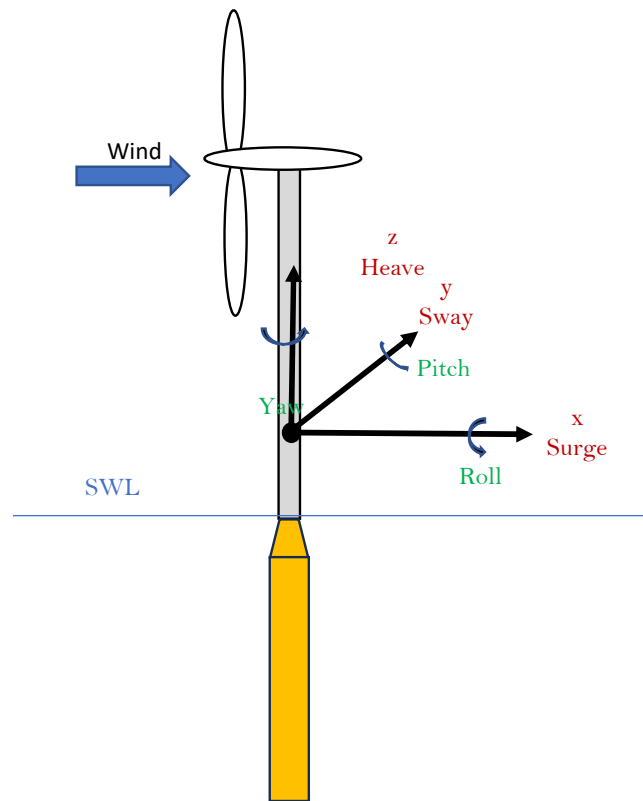
Figure 7.11: *Schematic of the Spar-buoy layout*

Table 7.1: *OC3 Spar-buoy properties [48]*

Properties	Values
Water Density (ρ)	1,025 kg/m^3
Water Depth (h)	320 m
Buoyancy Force in Undisplaced Position ($\rho g V_0$)	80,708,100 N
Hydrostatic Restoring in Heave (Hydrostatic $C_3 3$)	332,941 N/m
Hydrostatic Restoring in Roll (Hydrostatic $C_4 4$)	-4,999,180,000 Nm/rad
Hydrostatic Restoring in Pitch (Hydrostatic $C_5 5$)	-4,999,180,000 Nm/rad
Added-Mass Coefficient (Ca in Morison's Equation)	0.969954
Viscous-Drag Coefficient (Cd in Morison's Equation)	0.6
Additional Linear Damping in Surge (Linear $B_1 1$)	100,000 N/(m/s)
Additional Linear Damping in Sway (Linear $B_2 2$)	100,000 N/(m/s)
Additional Linear Damping in Heave (Linear$B_3 3$)	130,000 N/(m/s)
Additional Linear Damping in Yaw (Linear $B_6 6$)	13,000,000 Nm/(rad/s)

It is important to underline that the dynamics and stability of a spar-buoy platform differ significantly from those of a semi-submersible structure. The stability of a floating wind turbine based on a spar-type platform hinges on an entirely distinct mechanism. This mechanism is based on the platform's capacity to maintain equilibrium across diverse environmental conditions encompassing wind, waves, and currents.

Various elements such as the position of the centre of gravity, the ballast distribution, and a well-designed mooring system are pivotal in preserving stability and mitigating excessive movements that might compromise the turbine's overall efficiency and structural integrity. This might as well

have an effect on the significance of the different parameters.

For the analysis the same external conditions were used, with the wave height, the peak period, the wind speed, the misalignment, the current characteristics and the turbulence intensity as described in the semi-submersible sensitivity analysis. For the variation of the simple drag coefficient falls between 0.6 to 1.2 for cylindrical members [13].

7.2.2 Spar-buoy elementary effect method results

The normalized significant analysis outcomes across the spar-buoy configuration are depicted in Figure 7.12. The Damage Equivalent Load (DEL) values for various loads are displayed. The primary parameter influencing all of the examined outputs is the current speed, which is analogous to the semi-submersible floater scenario. Specifically, the current speed has the greatest influence on mooring line tension, followed by its impact on hydrodynamic moments.

The role of the drag coefficient differs noticeably from that of the semi-submersible structure whose averaged effect is presented in Figure 7.13. The drag coefficient has a substantial influence on the mooring line tension, hydrodynamic moments, and both the top and bottom tower moments in the case of the spar-buoy. This strong influence is emphasized by the floater's considerable submerged region, where stability is mostly determined by this coefficient. This contrast emphasizes how varied platform geometries might result in differing load sensitivity.

The sensitivity of the wave characteristics, the wave height and the peak period influence the different load outputs. In more detail, the wave height mostly affects the tower's top and base moments and in a smaller degree the hydrodynamic loads and the mooring line tension. However, it is worth mentioning that there is an effect on the rotor thrust and torque which underlies the effect on the power generation as well. On the contrary, the peak period has a small impact on the thrust and the tower moments but significantly affects the hydrodynamic forces and the rotor torque.

Figure 7.12: *Total Normalized EE significance of the input parameters (hydrodynamic drag coefficient and external conditions) with respect to the DEL values of the tower and hydrodynamic loads and mooring line tensions for Spar-buoy, OC3 FOWT*
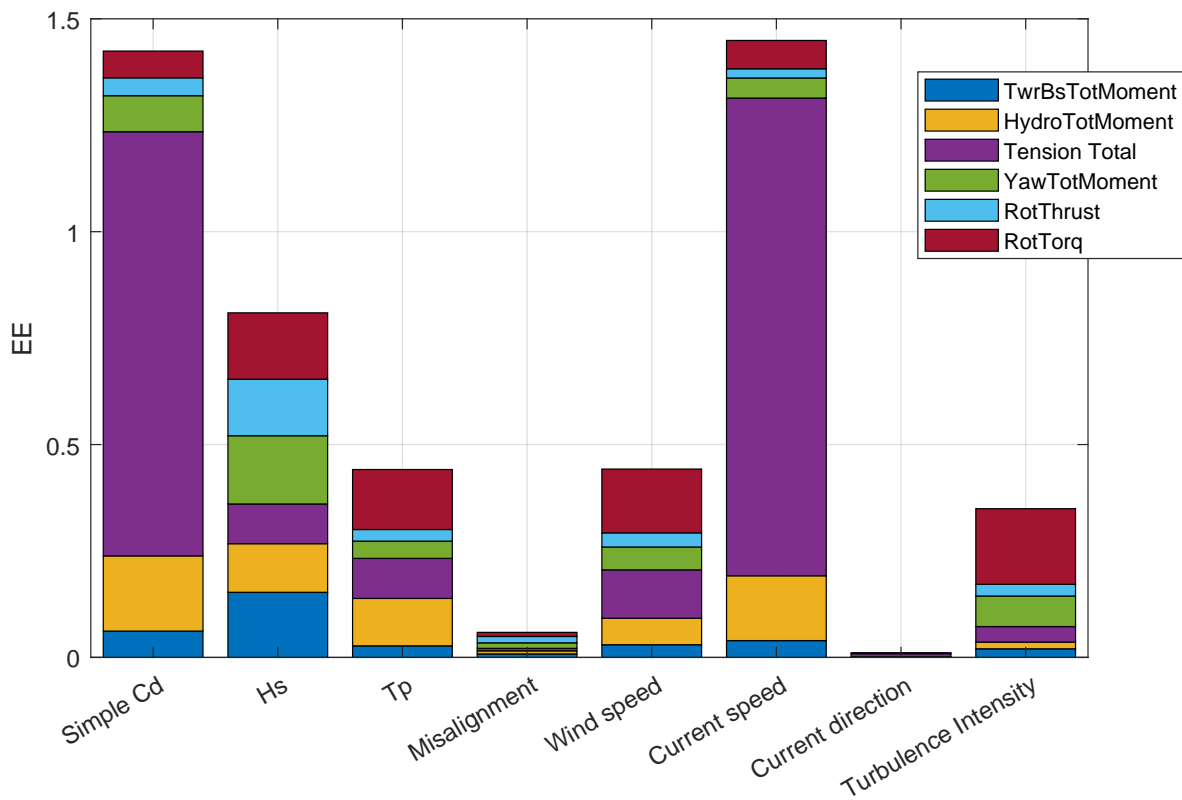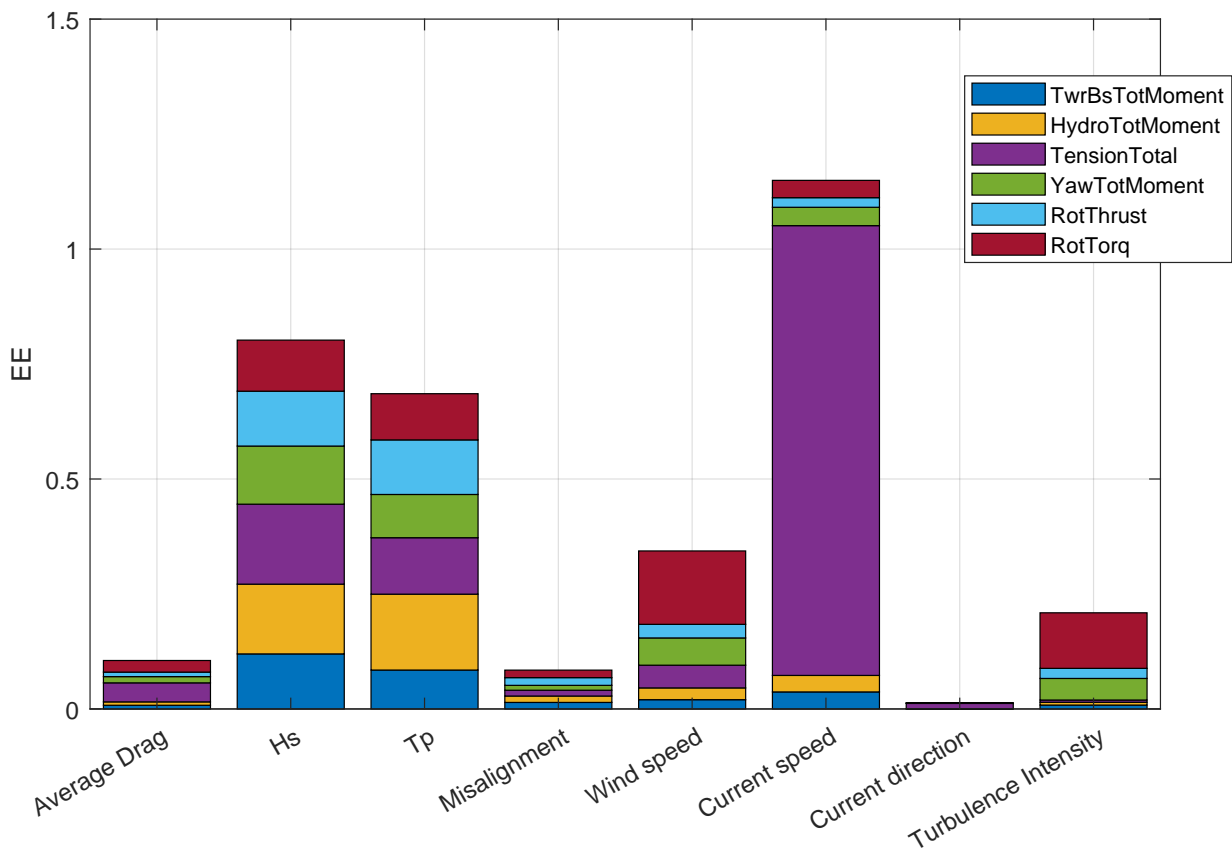
Figure 7.13: *Total Normalized EE significance of the input parameters (hydrodynamic drag coefficient and external conditions) with respect to the DEL values of the tower and hydrodynamic loads and mooring line tensions for Semisubmersible OC4 FOWT. The drag coefficient effect of all the members has been averaged*

8 Location Analysis

The sensitivity of the external environmental conditions to the different outputs underlines the need for a more structured analysis with respect to those parameters. In the initial phase of the analysis, the conditions were selected randomly between the minimum and maximum values of each parameter. However, the wave height, the peak wave parameter, the wind and wave direction as well as the wind speed are all connected and follow a joint probability of occurrence. In this chapter, the real met ocean data were processed and fitted to probability occurrences for different locations. The statistical analysis of different location data as well as their influence on the sensitivity analysis will be presented.

8.1 Location Selection

Numerous suitable places for deploying floating wind turbines have been found, indicating a promising potential. Extensive analyses are being undertaken worldwide to determine the potential of various sites for developing wind farms. Notably, the North Sea has been a research focus for several decades, mostly due to bottom-fixed offshore wind turbines. Ongoing investigations, as detailed in Life S 50+ project [49], are intensifying in places such as Scotland in Europe emphasizing the potential of those regions.

While the offshore wind industry has primarily been concentrated in Europe and the North Sea, the advent of floating wind turbine technology has extended to encompass regions such as Asia and North America. In light of this development, metocean data analysis has been undertaken, encompassing crucial parameters such as wind speed and direction, wave height, peak wave period, and wave direction from those locations.

Hourly data of 20 years between years 2002 and 2021 were derived from ERA-5 Copernicus database [50]. After an analysis of the details of the different data, three locations were selected representing moderate, medium and severe conditions. This was determined from the statistical analysis of the significant wave heights since all of the locations have a satisfying wind potential.

8.1.1 Moderate Location

The initial location exemplifies moderate metocean conditions. As a result, Nagasaki Prefecture in Japan was chosen, as it is regarded as a potential site for the establishment of floating wind farms, as has been indicated [51].

The wave rose is illustrated in Figure 8.2, revealing prevailing moderate wave conditions. A majority of the recorded significant wave heights are below 1 meter, with an average value of approximately 1.13 meters. The highest recorded value reaches 10.9 meters.

The wind speed predominantly does not exceed the rated wind speed, boasting an average value of 7.7m/s. Additionally, the wind direction spans from the northwest (NW) to the southwest (SW) as shown in Figure 8.3.

Figure 8.1: *Nagasaki Perfecture location in Japan*

Figure 8.2: *Wave Data of Nagasaki Perfecture location*

Nagasaki Perfecture (Japan)

Figure 8.3: *Wind Data of Nagasaki Perfecture location*

8.1.2   Medium Location - Gulf of Maine

Moderate conditions are represented by the Gulf of Maine in North America. The United States is strategically poised to venture into the dynamic floating win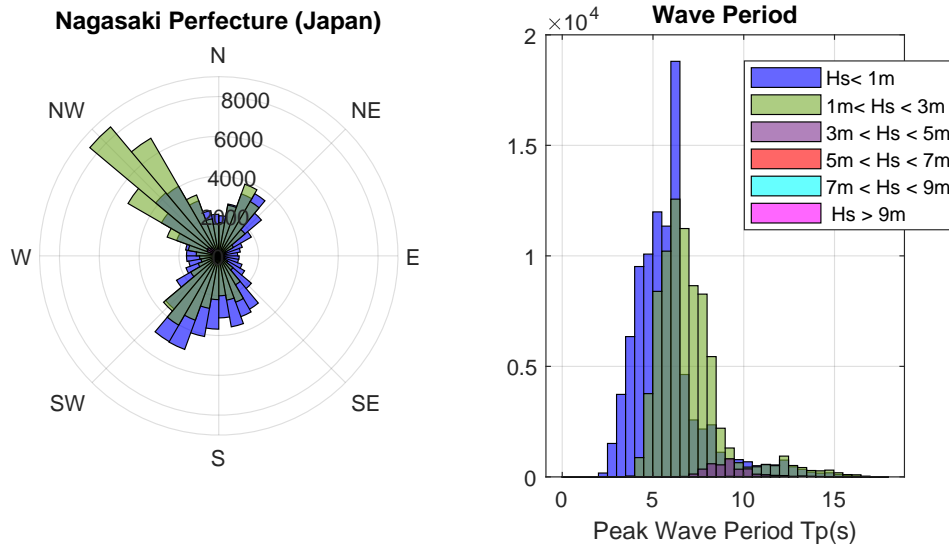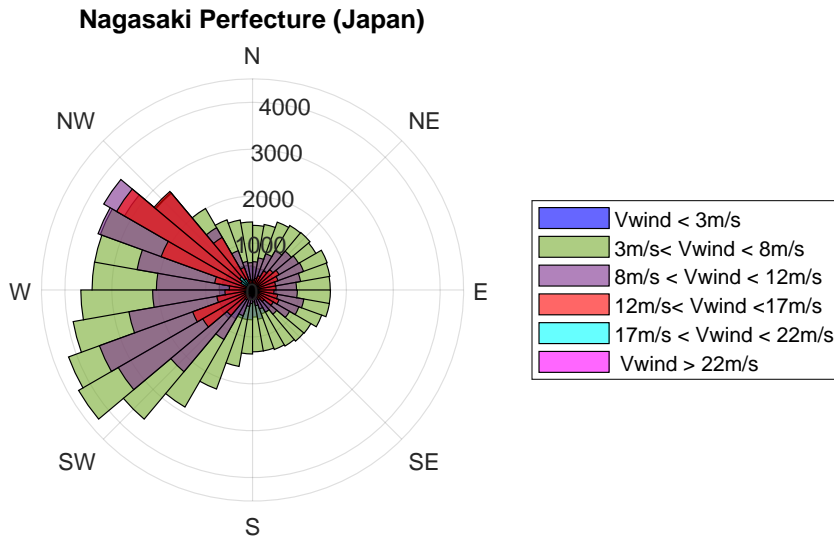d turbine market, with plans for several MW of offshore wind energy. This renders it an ideal location to comprehensively investigate the diverse effects and modelling parameters associated with floating wind turbines, thus substantiating its selection for the current study. A great interest has risen in the Gulf of Maine which is a location with great potential [52]. Plans for installing more than 144 megawatts (MW) of wind energy capacity in this area are currently in progress [53].

The wave rose depicted in Figure 8.5 vividly illustrates the prevailing influence of waves originating from the south (S) to the southeast (SE) directions. Their significant heights primarily fluctuate within the range of 1 to 3 meters, while peak periods exhibit a broader distribution between 5 and 15 seconds. In the Gulf of Maine, the mean wave height averages around 1.4 meters, with the maximum observed height being lower than that recorded in Nagasaki Prefecture, reaching a peak of 9.4 meters.

The average wind speed registers at 9 m/s, showcasing a diverse directional distribution with the most notable wind speeds occurring in the northwest (NW) and northeast (NE) directions (Figure 8.6).
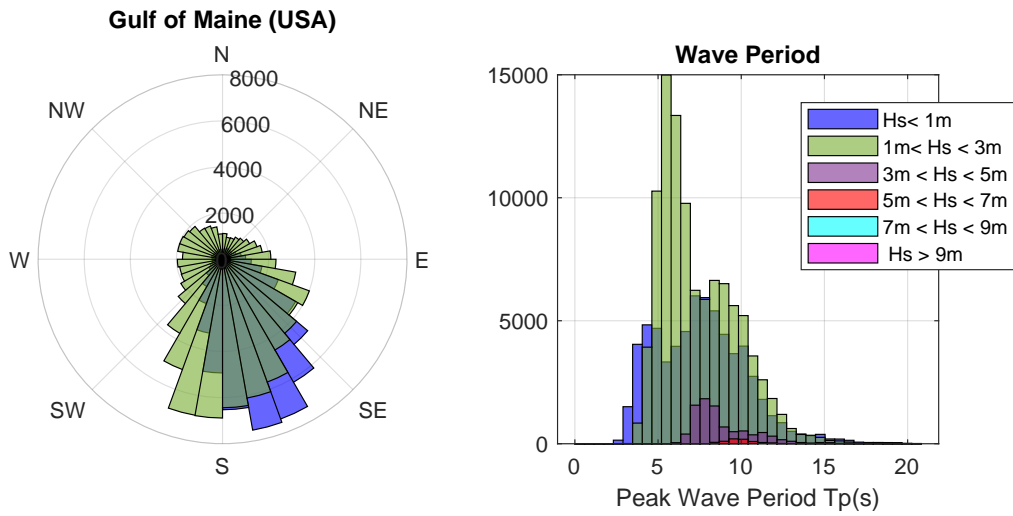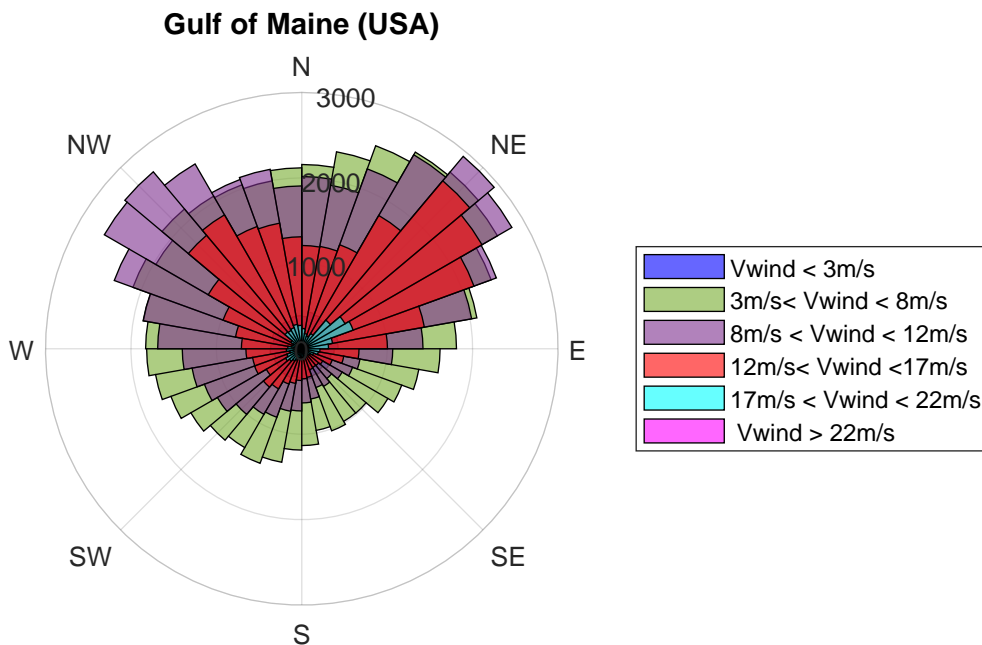

Figure 8.4: *Gulf of Maine location in USA*

69

Figure 8.5: *Wave Data of Gulf of Maine location*

Figure 8.6: *Wind Data of Gulf of Maine location*

8.1.3 Severe Location - West of Barra

The third site is characterized by the most challenging environmental conditions. Situated off the coast of Scotland, specifically to the west of Barra, this location boasts notably high wind speeds, rendering it a promising candidate for the deployment of floating wind turbines. However, the interplay between these favourable wind conditions and the potential impact of wave conditions necessitates thorough examination.

Figure 8.7: *West of Barra location in Scotland*

Figure 8.8 illustrates the wave statistics and their corresponding directions. Notably, a pronounced dominance of westerly wave directions is evident. Although a majority of the wave heights fall within the 1 to 3-meter range, examples of larger wave heights exceeding 5 meters, coupled with extended wave periods, are also observed. Through comprehensive analysis, it has been determined that the highest recorded wave height reaches 14.7 meters, while the overall average wave height for the region stands at approximately 3 meters.

Figure 8.8: *Wave Data of West of Barra location*

In contrast to wave direction (Figure 8.9), wind direction displays a wider distribution across various orientations. Interestingly, a majority of wind speeds surpass the rated speed with a mean value around 11 m/s, rendering the location particularly promising for wind farm installation.

Figure 8.9: *Wind Data of West of Barra location*

8.2   Cases Formulation

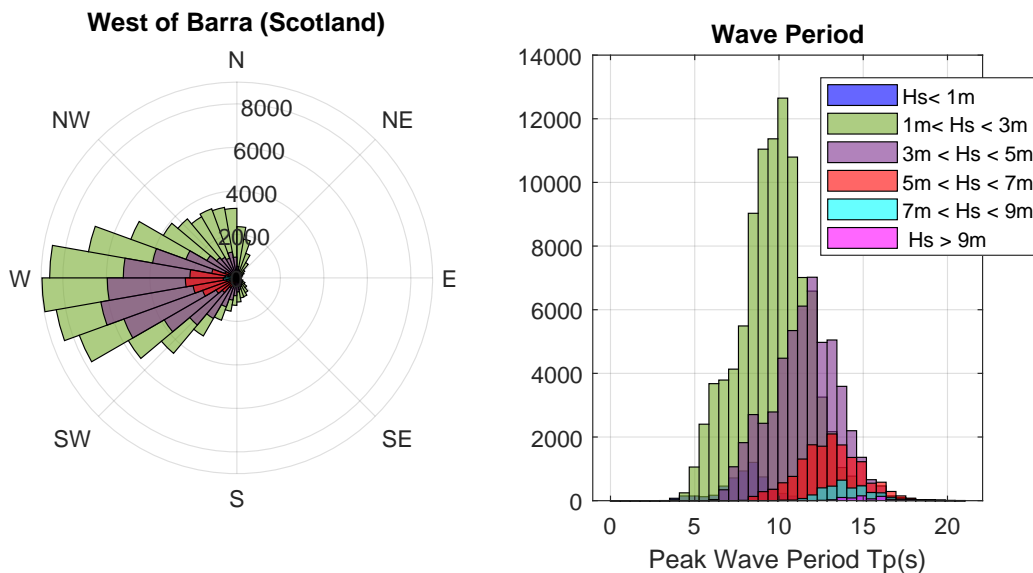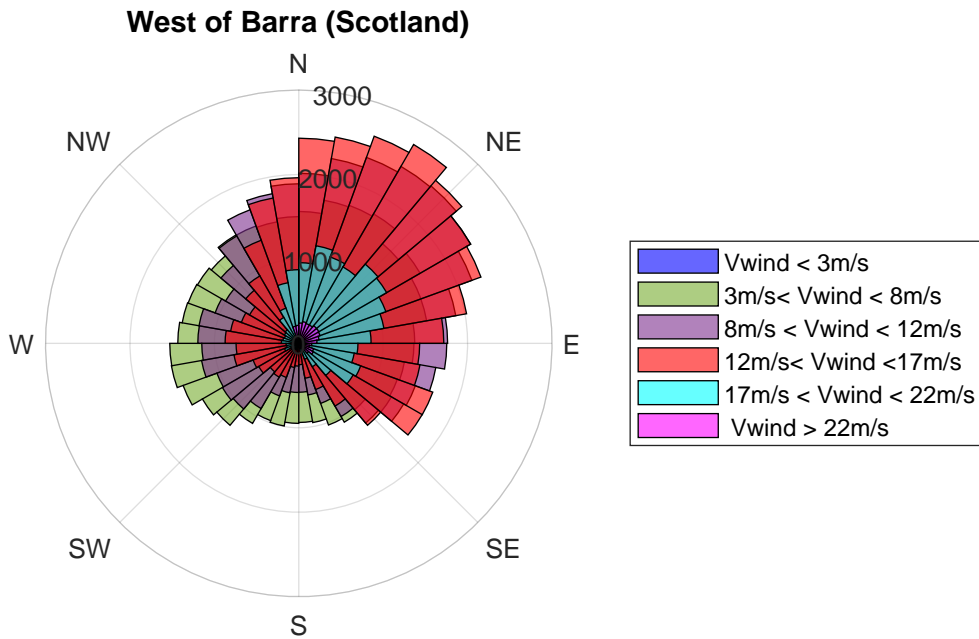To construct these cases, it was imperative to ensure that the data conformed to an appropriate probability distribution and that they were interconnected, allowing the randomly generated trajectories to follow this inherent relationship seamlessly.

It is a well-established fact that wind speed conforms to a Weibull distribution [54]. Consequently, the wind data for each location were fitted to this Weibull distribution, and new samples were generated using the parameters derived from the fitted data. Wind direction, being a circular sample, adheres to a circular distribution known as the Von-Mises distribution. Wave height and peak wave period, on the other hand, follow a gamma distribution. The formulas for these distributions are detailed in Figure 8.10. The parameters specifying the shape and scale for each distribution are also listed in the table. Utilizing the MATLAB fitting toolbox, the data from each location were fitted to these distributions. The resulting parameters for each location are presented in Table 8.1.

Following the fitting of each external parameter to its respective distribution, the process of generating various cases was conducted using Kernel Density Estimation (KDE) [55]. The bandwidth estimation, a critical factor in determining the precision of the analysis, was calculated using Silverman's Rule of Thumb [56], as detailed in Equation 8.1. This calculation incorporates both the standard deviation (σ) of the sample and the sample size (n). The resulting bandwidth value is subsequently employed in the computation of the joint probability density, facilitating a more accurate and informative analysis of the data. This methodology enabled the selection of different cases based on their joint probability distribution. In contrast to the previous approach, where the most distinct cases were chosen, this method focuses on the most probable scenarios. This approach facilitates the simulation of more realistic combinations, streamlines the case selection process, and promotes the coupling of cases together.

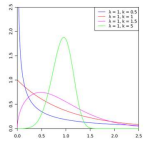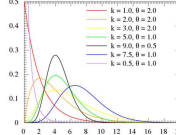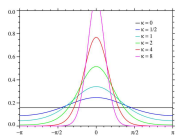$$ h = 1.06\sigma n^{-1/5} \tag{8.1} $$

Distribution	Parameters	Probability Density	Graph
Weibull	λ scale K shape	$f(x) = \dfrac{k}{\lambda}\left(\dfrac{x}{\lambda}\right)^{k-1} e^{-\left(\frac{x}{\lambda}\right)^{k}}$	
Gamma	θ scale k shape	$f(x) = \dfrac{1}{\Gamma(k)\theta^{k}} x^{k-1} e^{-x/\theta}$ $\Gamma(x)$ *Gamma function*	
Von Mises	μ mean κ	$f(x) = \dfrac{e^{\kappa \cos(x-\mu)}}{2\pi\, I_0(\kappa)}$ $I_0(x)$ *Bessel function*	

Figure 8.10: *Distributions description*

Consequently, distinct cases were developed for each location, encompassing parameters like wind speed, wind-wave misalignment (expressed as direction), significant wave height, and peak wave period, from the newly generated data fitted to the different distributions. For the remaining parameters, such as the drag coefficients, current speed and direction, and turbulence intensity, a similar methodology as in the previous simulations was applied. This involved employing random Sobol number generation techniques and selecting the most distinct sets of numbers to ensure a comprehensive and diverse range of input values. The same ranges were used with a variation of 10% among the generated cases. This approach allows for a robust exploration of the parameter space, providing a thorough understanding of their effects on the system under study. By systematically varying these parameters and conducting simulations, valuable insights into their impact on the system's behaviour and performance can be gained, contributing to a comprehensive sensitivity analysis. It is important to highlight that, particularly for current speed, accurate location-specific data were unavailable. Therefore, the same ranges as those used previously were applied, spanning from 0 to 2 m/s. However, an adjustment was made by increasing the reference depth to 20 meters, as opposed to the previous 10 meters. This alteration aimed to diminish the impact of current speed and enable better observation of the effects of other parameters.

For the cases simulated, 24 parameters were used, 15 trajectories (starting points) and the studied outputs involve top and bottom tower moments, hydrodynamic forces, mooring line tensions and rotor thrust and torque as representative of the rotor aerodynamics and power generation.

8.3 Results & Discussion

The results from the different locations were generated and compared for any distinction between them. This comprehensive approach facilitates an in-depth investigation into the location-specific effects, particularly how the varying external conditions prevalent in different geographical areas influence the sensitivity of the diverse parameters. By examining and contrasting results from multiple locations, it becomes possible to ascertain the relative significance of location-specific factors and their potential impact on the system's sensitivity to parameter variations. This analytical method enhances the understanding of how environmental conditions can shape the behaviour and response of the system, adding a valuable layer of insight to the overall study.

In the case of Nagasaki Prefecture, which represents a moderate location, Figure 8.11 illustrates a

Table 8.1: *Distribution parameters for each one of the external condition for every location*

Location	Parameters
Location 1, Nagasaki Perfecture, Japan	Wind Speed, Weibull Distribution $\lambda = 8.7351, k = 1.9527$
	Wind/Wave Misalignment Von Mises Distribution $\mu = 1.3989, \kappa = 0.3770$
	Significant wave Height Gamma Distribution k=3.0235, $\theta = 0.3770$
	Peak period Gamma Distribution k=11.1591, $\theta = 0.5774$
Location 2, Gulf of Maine USA	Wind Speed, Weibull Distribution $\lambda = 10.2568, k = 2.1252$
	Wind/Wave Misalignment Von Mises Distribution $\mu = 1.8804, \kappa = 1.1703$
	Significant wave Height Gamma Distribution k=3.7143, $\theta = 0.3831$
	Peak period Gamma Distribution k=9.8698, $\theta = 0.7650$
Location 3, West of Barra, Scotland	Wind Speed, Weibull Distribution $\lambda = 12.1721, k = 2.1932$
	Wind/Wave Misalignment Von Mises Distribution $\mu = 2.2133, \kappa = 0.0.5113$
	Significant wave Height Gamma Distribution k=3.9273, $\theta = 0.7575$
	Peak period Gamma Distribution k=18.4058, =0.5743

notable influence of significant wave height on various loads, with exceptions being mooring line tension and rotor torque. The study underscores the considerable impact of significant wave height on the tower's total base moment, making it a critical parameter affecting loading dynamics. This stands in contrast to modelling parameters like drag coefficients, which primarily affect mooring line tension and have negligible effect to the other parameters. The analysis also reveals that mooring line tension is influenced by current speed, albeit to a lesser extent than the initial simulations of Chapter 7. Moreover, turbulence intensity emerges as a significant factor, particularly in its influence on rotor thrust, a result that aligns with expectations based on the system's dynamics. These findings highlight the complex interplay of environmental and modelling parameters, shedding light on their respective roles in shaping load outcomes at this moderate location.

When comparing these findings to the conditions in the Gulf of Maine, representing a medium
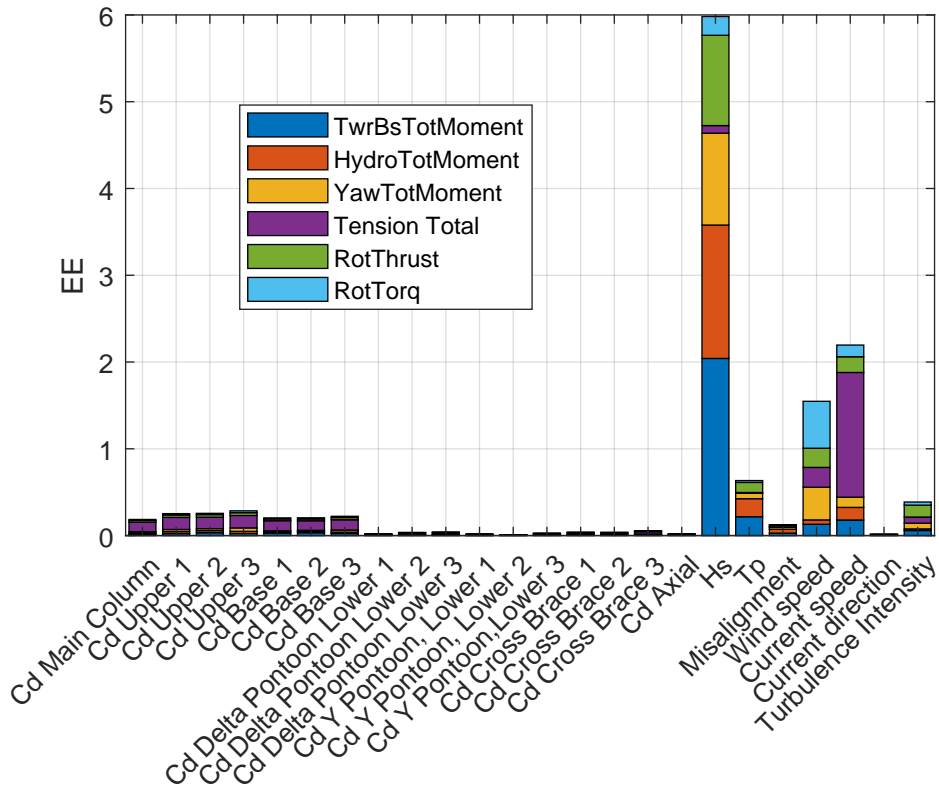
Figure 8.11: *Total Normalized EE significance of the input parameters (member hydrodynamic drag coefficients and external conditions) with respect to the DEL values of the tower and hydrodynamic loads and mooring line tensions for the moderate location at Nagasaki Perfecture*

location, some intriguing disparities emerge. As depicted in Figure 8.12, the influence of wave height remains substantial, but the distribution of its effects across different outputs appears more balanced. Interestingly, wind speed shows a relatively smaller overall impact in this location, while turbulence intensity exhibits no influence on rotor thrust. This suggests a potential interrelation between turbulence intensity and wind speed and their combined effect on rotor thrust. In contrast, the sensitivity of drag coefficients remains consistent, indicating that there may not be a coupled relationship of significance in this regard.

In the severe location off the coast of West Barra in Scotland, the sensitivity distribution takes a distinctive form (Figure 8.13). Specifically, wave height exerts a notably reduced overall effect, amounting to approximately half of that observed in other locations, although it remains the most influential parameter. Meanwhile, the drag coefficients, while still relatively modest in significance, display a more uneven distribution that depends on the specific member positions. Intriguingly, they appear to influence rotor aerodynamics as well. This could be attributed to the heightened wave conditions, which enhance the dominance of the drag term in this context. These findings underscore the diverse and location-dependent nature of parameter sensitivity and its intricate interactions with varying environmental conditions. In all three locations, the influence of the hydrodynamic drag coefficient on the rotor torque is negligible. This observation suggests that the sensitivity of the hydrodynamic drag might not significantly affect rotor dynamics. It is possible that the previous findings, which were based on more extreme and random conditions, do not accurately represent this particular effect on rotor dynamics.

Figure 8.12: *Total Normalized EE significance of the input parameters (member hydrodynamic drag coefficients and external conditions) with respect to the DEL values of the tower and hydrodynamic loads and mooring line tensions for the medium location at Gulf of Maine*
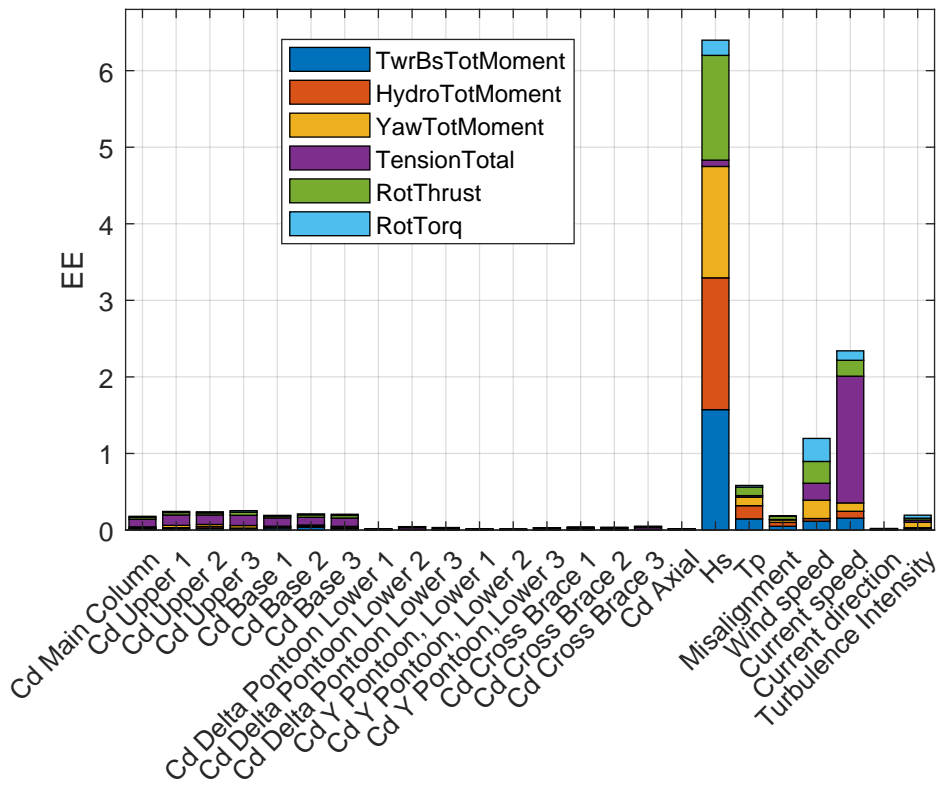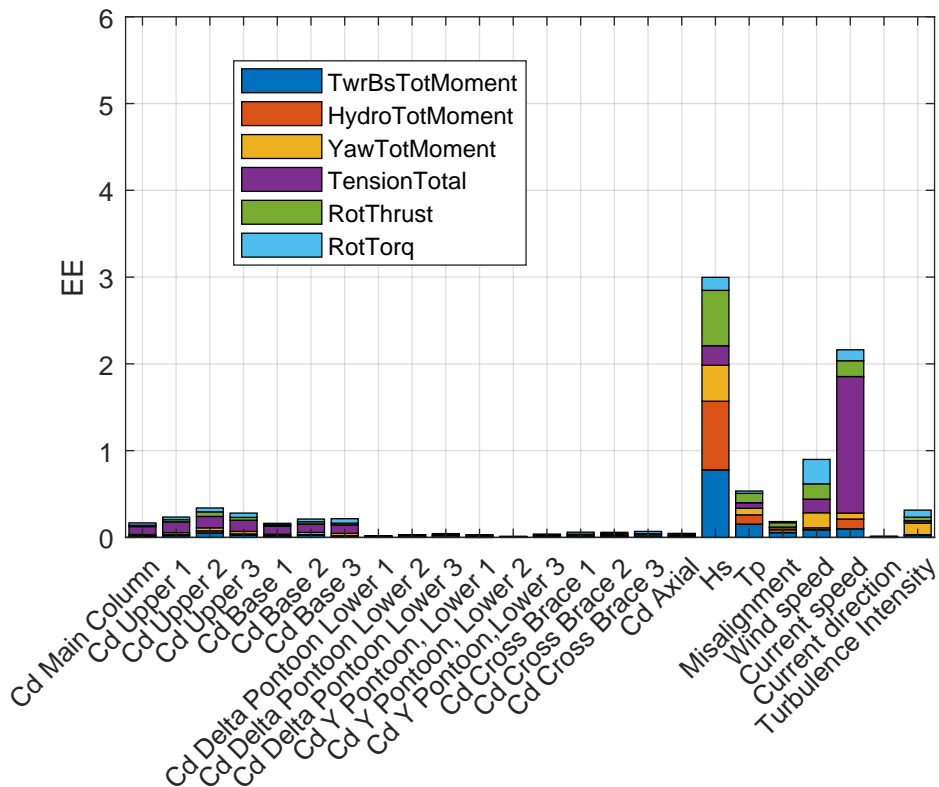

Figure 8.13: *Total Normalized EE significance of the input parameters (member hydrodynamic drag coefficients and external conditions) with respect to the DEL values of the tower and hydrodynamic loads and mooring line tensions for the severe location at West of Barra, Scotland*

9 Conclusions

The primary objective of this study is to thoroughly examine various parameters, particularly those related to hydrodynamics, and their influence on the structural and aerodynamic performance of semisubmersible floating wind turbines. This investigation is carried out through an extensive sensitivity analysis approach, employing the multi-fidelity model OpenFAST for conducting simulations on the semisubmersible floating wind turbine used in the OC4 experiment with the 5MW NREL wind turbine employed.

Throughout the course of this thesis, a significant realisation emerged: a pressing need exists for more precise predictions of the behaviour of Floating Offshore Wind Turbines (FOWTs) under diverse conditions. The uncertainty associated with various modeling parameters profoundly impacts both the generated power output and the structural robustness of FOWTs. Additionally, the scope of analyzed cases should be expanded to encompass a wide array of metocean data. In light of this, parameters such as hydrodynamic drag coefficients, significant wave height, peak period, wind speed, wind and wave misalignment, current speed and direction, as well as turbulence intensity, were identified as pivotal factors warranting thorough investigation.

The Elementary Effects (EE) method was applied to assess the significance of individual parameters by evaluating their impact on the load outputs of the floater, tower, and rotor. To ensure comprehensive results, multiple trajectories were employed, and various seeds were utilized. Over the span of 20 different starting points, independent results were achieved after 12-15 points for trajectories, while for seeds, 7 different seeds were sufficient for wave generation and 4 seeds for the wind simulation. For a more accurate representation of the findings, the Damage Equivalent Load (DEL) approach was adopted, and the effects of EE were normalized to quantify their relevant contributions to each output. The results obtained through this methodology effectively addressed the primary research inquiries.

1) *Which input parameters have a wide range of variability?*

The research study has identified several uncertain parameters. Concerning the drag coefficient, a variation ranging from 0.3 to 1.6 has been noted in the translational direction, with a notably wider range of 5 to 10 in the bottom axial drag, rendering it one of the most uncertain factors. In terms of external conditions, examination of data from various potential FOWT installation sites has revealed wave heights reaching up to 14.8 meters and peak periods spanning from 2 to 22 seconds. Wind speed and direction are traditionally chosen within the range of 0 to 25 m/s and 0 to 90 degrees, respectively, to encompass the full functional scope. Similarly, the current speed can fluctuate from 0 to 2 m/s based on the specific location, albeit with limited available data.

2) *Which are the most significant input parameters?*

Despite the varying ranges of input parameters, not all of them exert the same level of influence. Through the analysis of different cases using both the hybrid theory and the Morison equation, it is evident that, in terms of magnitude, the current speed emerges as the most impactful parameter. Its primary effect is on mooring line tension, where it exerts the greatest influence. However, this influence is considerably smaller on the other output factors. In contrast, wave parameters notably affect all the studied outputs, emphasizing the substantial role of waves in shaping the structure's

loading behaviour. In this regard, the significant wave height and the peak period can be considered the most significant parameters. The effect of the modelling parameters concerning the drag coefficients is very small in the studied range of cases.

3) *What does the addition of turbulent wind introduce?*

The inclusion of turbulent wind introduces sensitivity to turbulence intensity, which is particularly important for outputs related to rotor dynamics, specifically the rotor torque. However, the overall impact remains consistent with steady wind conditions, highlighting the significance of current speed in relation to mooring line tensions, and the importance of significant wave height and peak period in affecting tower, floating platform, rotor, and mooring line tensions. Turbulent wind simulations provide a more realistic representation of environmental conditions.

4) *What is the effect of the physical model on the significant parameter analysis??*

The sensitivity analysis of the examined parameters reveals only minor discrepancies when second-order hydrodynamic elements are excluded with a small underestimation of the sensitivity. This suggests that there's no compelling necessity to incorporate second-order elements in all simulations.

The Morison equation solution exhibits a remarkable similarity to the potential flow theory, with a key distinction being its heightened sensitivity to external environmental conditions. Furthermore, the added mass emerges as a significantly influential factor across various outputs, highlighting the critical importance of accurately determining its associated parameters. These findings underscore the superior performance of the hybrid theory in capturing the intricate dynamics of floating wind turbines under differing conditions, making it a more robust choice for analysis and design considerations.

5) *Can similar conclusions be drawn when applying this analysis to a different type of platform?*

The comparison of the semi-submersible and the spar platform leads to similar behaviour in terms of the current speed and the effect on the mooring line tension. However, the order of significance in different outputs is different between the two platforms. Notably, rotor thrust is minimally affected by the significant wave height and peak period in the spar platform, whereas in the semi-submersible platform, these factors have a more evenly distributed effect on different outputs. The sensitivity to turbulence intensity is also more significant in the spar platform. In addition, the modelling approach and the selected hydrodynamic drag that is used are crucial for the resulting loads. In these terms, the spar is much more sensitive and the selection of the parameters has to be made carefully.

6) *What does the location correlation add to the sensitivity analysis study?*

Incorporating various locations into the study serves the fundamental purpose of simulating a broader range of realistic conditions, all while maintaining a consistent set of parameters governing wind and wave characteristics. The outcomes of these diverse locations shed light on the primary driver of parameter sensitivity, which consistently proves to be wave height. Wave height demonstrates a substantial influence on the dynamics of floater, tower, and rotor loads across all locations. Current speed primarily comes into play with mooring line tensions, whereas the sensitivity of drag coefficients is more pronounced in severe conditions, contrasting with their lesser significance in moderate and medium locations. These location-specific variations underscore the complex interplay between environmental conditions and parameter sensitivity, offering valuable insights for the design and operation of floating wind turbines across diverse geographical settings.

In the location analysis, it is important to clarify that the selection of cases was performed using probability distributions, resulting in a choice of cases that represent lower (moderate) but more possible conditions. However, for a more comprehensive analysis, a wider range of diverse cases should have been selected while still following the probability distribution. As a result, we cannot draw definitive conclusions based on the current analysis, and further investigation is necessary for more robust results.

10   Recommendations

The research has led to several recommendations that can enhance the reliability and comprehensiveness of the study.

Firstly, it is important to emphasize that the uncertainty surrounding several parameters significantly impacts the outputs. This, in turn, affects fatigue analysis and the efficiency of power extraction from wind turbines, both of which are critical in the design and widespread deployment of floating wind farms. While external metocean conditions are readily associated with installation location, it is imperative to establish a correlation between these conditions and other parameters like drag and added mass coefficients. This correlation will integrate the influence of each environmental condition on the selection of these parameters, ultimately reducing uncertainty and its impact on structural loading.

To achieve these more robust experimental results, higher fidelity models should be employed. It is worth noting that there is a shortage of experimental data for scale-modified models, highlighting the need for more research in this area. Higher fidelity models have the potential to yield more realistic results while mitigating uncertainty. Consequently, conducting a comprehensive parameter analysis using these advanced models to validate results would be worthwhile.

In addition to addressing the uncertainty associated with modelling parameters, it is crucial to focus on refining the data related to the most significant parameters: current speed and significant wave height. Obtaining more accurate data for these parameters is essential. Particularly for hydrodynamic loads and mooring line tensions, which can be tailored to the installation location, simulating cases that align with specific installation locations can be highly beneficial. Even small adjustments in these parameters can have a substantial impact on the resulting DEL. Therefore, a location-specific approach can lead to more precise predictions and optimized designs for floating wind turbines.

Finally, the comparative analysis of significant parameters between the semi-submersible and the spar platform has unveiled another level that worth researching, particularly concerning platform types. The distinct mechanisms governing the motion of each platform type significantly influence parameter sensitivity. From this perspective, it would be valuable to investigate other platform types and possibly different scales. For instance, the 15 MW IEA platform presents an intriguing subject for future study.

Bibliography

[1] International Energy Agency, "Offshore Wind Outlook 2019: World Energy Outlook Special Report," 2019. [Online]. Available: `www.iea.org/t&c/`, (accessed: 01.12.2022).

[2] European Commission. "Offshore renewable energy." (2022), [Online]. Available: `https://energy.ec.europa.eu/topics/renewable-energy/offshore-renewable-energy`. (accessed: 05.12.2022).

[3] "Global offshore wind report 2022." [Online]. Available: `www.gwec.net`.

[4] J. Cruz and M. Atcheson, *Floating Offshore Wind Energy: The Next Generation of Wind Energy*. Springer, 2016. [Online]. Available: `http://www.springer.com/series/8059`.

[5] DNV, Det Norske Veritas, "Floating Offshore Wind: The Next Five Years."

[6] C. M. Wang, T. Utsunomiya, S. C. Wee, and Y. S. Choo, *Research on floating wind turbines: A literature survey*, 2010. DOI: `10.1080/19373260.2010.517395`.

[7] United Nations. "Floating wind turbines: a new player in cleantech." (2022), [Online]. Available: `https://unric.org/en/floating-wind-turbines-a-new-player-in-cleantech/`. (accessed: 05.12.2022).

[8] Cleantech Group. "Floating Offshore Wind – The Race to Scale." (2021), [Online]. Available: `https://www.cleantech.com/floating-offshore-wind-the-race-to-scale/`. (accessed: 06.12.2022).

[9] S. Butterfield, W. Musial, J. Jonkman, and P. Sclavounos, "Engineering Challenges for Floating Offshore Wind Turbines," 2005. [Online]. Available: `http://www.osti.gov/bridge`.

[10] GustoMSC | NOV. "Tri-Floater Floating Offshore Wind Turbine Foundation." (), [Online]. Available: `https://www.nov.com/products/tri-floater-floating-offshore-wind-turbine-foundation`. (accessed: 20.12.2022).

[11] R. James and M. C. Ros, "Floating Offshore Wind: Market and Technology Review," 2015. [Online]. Available: `https://www.carbontrust.com/our-work-and-impact/guides-reports-and-tools/floating-offshore-wind-market-technology-review`.

[12] Principle Power. "Wind Float." (), [Online]. Available: `https://www.principlepower.com/windfloat`. (accessed: 20.12.2022).

[13] J. M. J. Journée and W. W. Massie, "OFFSHORE HYDROMECHANICS," 2001.

[14] International Electrotechnical Commission, *Wind energy generation systems. Part 3-1 : design requirements for fixed offshore wind turbines*, p. 148, ISBN: 9782832266007.

[15] DNV, Det Norske Veritas, "Recommended practice DNV-RP-C205, Environmental Conditions and Environmental Loads," 2010. [Online]. Available: `http://www.dnv.com`.

[16] A. Otter, J. Murphy, V. Pakrashi, A. Robertson, and C. Desmond, "A review of modelling techniques for floating offshore wind turbines," *Wind Energy*, vol. 25, no. 5, pp. 831–857, 2022. DOI: `https://doi.org/10.1002/we.2701`. eprint: `https://onlinelibrary.wiley.com/doi/pdf/10.1002/we.2701`. [Online]. Available: `https://onlinelibrary.wiley.com/doi/abs/10.1002/we.2701`.

[17] "Wamit, Inc. - The State of the Art in Wave Interaction Analysis." (), [Online]. Available: `https://www.wamit.com/`.

[18] "NEMOH-Presentation - LHEEA." (2022), [Online]. Available: `https://lheea.ec-nantes.fr/research-impact/software-and-patents/nemoh-presentation`.

[19] "Ansys | Engineering Simulation Software." (), [Online]. Available: `https://www.ansys.com/`.

[20] A. Robertson, J. Jonkman, F. Vorpahl, *et al.*, "Offshore Code Comparison Collaboration, Continuation within IEA Wind Task 30: Phase II Results Regarding a Floating Semisubmersible Wind System," 2014. [Online]. Available: `www.nrel.gov/publications.`.

[21] A. N. Robertson, F. Wendt, J. M. Jonkman, *et al.*, "OC5 Project Phase II: Validation of Global Loads of the DeepCwind Floating Semisubmersible Wind Turbine," *Energy Procedia*, vol. 137, pp. 38–57, Oct. 2017, ISSN: 1876-6102. DOI: `10.1016/J.EGYPRO.2017.10.333`.

[22] A. N. Robertson, S. Gueydon, E. Bachynski, *et al.*, "OC6 Phase I: Investigating the underprediction of low-frequency hydrodynamic loads and responses of a floating wind turbine," *Journal of Physics: Conference Series*, vol. 1618, 3 Sep. 2020, ISSN: 17426596. DOI: `10.1088/1742-6596/1618/3/032033`.

[23] M. I. Kvittem, P. Berthelsen, L. Eliassen, and M. Thys, "Calibration of Hydrodynamic Coefficients for a Semi-Submersible 10 MW Wind Turbine," V010T09A080, Jun. 2018. DOI: `10.1115/OMAE2018-77826`.

[24] P. Berthelsen, R. Baarholm, C. Pâkozdi, *et al.*, "Viscous Drift Forces and Responses on a Semisubmersible Platform in High Waves," *Proceedings of the International Conference on Offshore Mechanics and Arctic Engineering - OMAE*, vol. 1, Jan. 2009. DOI: `10.1115/OMAE2009-79483`.

[25] H. Li and E. Bachynski-Polić, "Analysis of difference-frequency wave loads and quadratic transfer functions on a restrained semi-submersible floating wind turbine," *Ocean Engineering*, vol. 232, p. 109 165, Jul. 2021. DOI: `10.1016/j.oceaneng.2021.109165`.

[26] L. Wang, A. Robertson, J. Jonkman, and Y.-H. Yu, "OC6 phase I: Improvements to the Open-FAST predictions of nonlinear, low-frequency responses of a floating offshore wind turbine platform," *Renewable Energy*, vol. 187, Jan. 2022. DOI: `10.1016/j.renene.2022.01.053`.

[27] A. Srinivas, B. Robertson, J. Gadasi, B. Simpson, P. Lomonaco, and J. Ilzarbe, "Impact of Limited Degree of Freedom Drag Coefficients on a Floating Offshore Wind Turbine Simulation," *Journal of Marine Science and Engineering*, vol. 11, Jan. 2023. DOI: `10.3390/jmse11010139`.

[28] Y. Alkarem and B. Ozbahceci, "A Complemental Analysis of Wave Irregularity Effect on the Hydrodynamic Responses of Offshore Wind Turbines With the Semi-submersible Platform," *Applied Ocean Research*, vol. 113, p. 102 757, 2021, ISSN: 0141-1187. DOI: `https://doi.org/10.1016/j.apor.2021.102757`. [Online]. Available: `https://www.sciencedirect.com/science/article/pii/S0141118721002339`.

[29] I. Sandua-Fernández, F. Vittori, I. Eguinoa, and P. Cheng, "Impact of hydrodynamic drag coefficient uncertainty on 15 MW floating offshore wind turbine power and speed control," *Journal of Physics: Conference Series*, vol. 2362, p. 012 037, Nov. 2022. DOI: `10.1088/1742-6596/2362/1/012037`.

[30] W. Shi, L. Zhang, M. Karimirad, C. Michailides, Z. Jiang, and X. Li, "Combined effects of aerodynamic and second-order hydrodynamic loads for floating wind turbines at different water depths," *Applied Ocean Research*, vol. 130, p. 103 416, 2023, ISSN: 0141-1187. DOI: `https://doi.org/10.1016/j.apor.2022.103416`. [Online]. Available: `https://www.sciencedirect.com/science/article/pii/S0141118722003455`.

[31] W. Wiley, J. Jonkman, A. Robertson, and K. Shaler, "Sensitivity analysis of numerical modeling input parameters on floating offshore wind turbine loads," *Wind Energy Science Discussions*, vol. 2023, pp. 1–35, 2023. DOI: `10.5194/wes-2023-49`. [Online]. Available: `https://wes.copernicus.org/preprints/wes-2023-49/`.

[32] A. N. Robertson, K. Shaler, L. Sethuraman, and J. Jonkman, "Sensitivity analysis of the effect of wind characteristics and turbine properties on wind turbine loads," *Wind Energ. Sci*, vol. 4, pp. 479–513, 2019. DOI: `10.5194/wes-4-479-2019`. [Online]. Available: `https://doi.org/10.5194/wes-4-479-2019`.

[33] J. M. Jonkman, A. N. Robertson, and G. J. Hayman, "Hydrodyn user's guide and theory manual," [Online]. Available: `www.nrel.gov/publications..`

[34] P. J. Moriarty and A. C. Hansen, *Aerodyn theory manual*, 2005. [Online]. Available: `http://www.osti.gov/bridge.`

[35] E. Petersen, N. Mortensen, L. Landberg, J. Højstrup, and H. Frank, "Wind power meteorology. part 1: Climate and turbulence," English, *Wind Energy*, vol. 1, pp. 2–22, 1998, ISSN: 1095-4244.

[36] International Electrotechnical Commission, *Wind energy generation systems - part 1: Design requirements*, p. 148.

[37] J. Jonkman, S. Butterfield, W. Musial, and G. Scott, "Definition of a 5-MW reference wind turbine for offshore system development," *Contract*, February 2009, ISSN: 01487299.

[38] A. N. Robertson, J. M. Jonkman, and M. D. Masciola, "Definition of the Semisubmersible Floating System for Phase II of OC4," 2014.

[39] A. Robertson, J. Jonkman, F. Wendt, A. Goupee, and H. Dagher, "Definition of the OC5 DeepCwind Semisubmersible Floating System," *Annals of Finance*, vol. 3, p. 44, 4 2016, ISSN: 16142446. [Online]. Available: `http://www.osti.gov/servlets/purl/1155123/.`

[40] "OC6 Phase I-CFD Modeling Specification."

[41] M. Böhm, A. Robertson, C. Hübler, R. Rolfes, and P. Schaumann, "Optimization-based calibration of hydrodynamic drag coefficients for a semisubmersible platform using experimental data of an irregular sea state," *Journal of Physics: Conference Series*, vol. 1669, 1 Oct. 2020, ISSN: 17426596. DOI: `10.1088/1742-6596/1669/1/012023.`

[42] A. Saltelli, *Sensitivity analysis in practice : A guide to assessing scientific models*. Wiley, 2004, p. 219, ISBN: 0470870931.

[43] *Validation of Hydrodynamic Load Models Using CFD for the OC4-DeepCwind Semisubmersible*, vol. Volume 9: Ocean Renewable Energy, International Conference on Offshore Mechanics and Arctic Engineering, May 2015, V009T09A037. DOI: `10.1115/OMAE2015-41045.` eprint: `https://asmedigitalcollection.asme.org/OMAE/proceedings-pdf/OMAE2015/56574/V009T09A037/4435019/v009t09a037-omae2015-41045.pdf.` [Online]. Available: `https://doi.org/10.1115/OMAE2015-41045.`

[44] L. R. Reddy, D. Milano, J. Walker, and A. Viré, "Validation of cfd determined hydrodynamic coefficients for a semisubmersible floating offshore wind turbine," *Journal of Physics: Conference Series*, vol. 2265, no. 4, p. 042012, May 2022. DOI: `10.1088/1742-6596/2265/4/042012.` [Online]. Available: `https://dx.doi.org/10.1088/1742-6596/2265/4/042012.`

[45] *Morris screening method — gsa-module 0.5.3 documentation.* [Online]. Available: `https://gsa-module.readthedocs.io/en/stable/implementation/morris_screening_method.html.`

[46] M. Xie, S. Li, Y. Mu, *et al.*, "Experimental investigation on the mooring dynamics of the flexible trash intercept net under wave-current combined actions," *Ocean Engineering*, vol. 268, p. 113544, 2023. DOI: `https://doi.org/10.1016/j.oceaneng.2022.113544.` [Online]. Available: `https://www.sciencedirect.com/science/article/pii/S002980182202827X.`

[47] D. Milano, C. Peyrard, and M. Capaldo, "Numerical prototyping of floating offshore wind turbines: Virtual operation in real environmental conditions," Aug. 2020. DOI: `10.1115/OMAE2020-18174.`

[48] J. Jonkman, *Definition of the floating system for phase iv of oc3*, 2010. [Online]. Available: `http://www.osti.gov/bridge.`

[49] G. Sánchez, A. Llana, and G. Gonzalez, *Qualification of innovative floating substructures for 10mw wind turbines and water depths greater than 50m*, 2015.

[50] Hersbach, H., Bell, B., Berrisford, P., Biavati, G., Horányi, A., Muñoz Sabater, J., Nicolas, J., Peubey, C., Radu, R., Rozum, I., Schepers, D., Simmons, A., Soci, C., Dee, D., Thépaut, J-N., *Era5 hourly data on single levels from 1940 to present. copernicus climate change service (c3s) climate data store (cds)*, 2023. DOI: 10.24381/cds.adbb2d47. [Online]. Available: `https://cds.climate. copernicus.eu`, (accessed: 01.03.2023).

[51] T. Utsunomiya, I. Sato, and T. Shiraishi, "Floating offshore wind turbines in goto islands, nagasaki, japan," in *WCFS2019*, C. M. Wang, S. H. Lim, and Z. Y. Tay, Eds., Singapore: Springer Singapore, 2020, pp. 359–372, ISBN: 978-981-13-8743-2.

[52] *Gulf of maine floating offshore wind research array | governor's energy office*. [Online]. Available: `https://www.maine.gov/energy/initiatives/offshorewind/researcharray`.

[53] *Maine files for federal lease to build first us floating wind research project | offshore wind*. [Online]. Available: `https://www.offshorewind.biz/2021/10/04/maine-files-for-federal-lease- to-build-first-us-floating-wind-research-project/`.

[54] G. M. Stewart, A. Robertson, J. Jonkman, and M. A. Lackner, "The creation of a comprehensive metocean data set for offshore wind turbine simulations," *Wind Energy*, vol. 19, no. 6, pp. 1151– 1159, 2016. DOI: `https://doi.org/10.1002/we.1881`. eprint: `https://onlinelibrary.wiley. com/doi/pdf/10.1002/we.1881`. [Online]. Available: `https://onlinelibrary.wiley.com/ doi/abs/10.1002/we.1881`.

[55] S. M. Scott, C. E. Middleton, and E. N. Bodine, "Chapter 1 - an agent-based model of the spatial distribution and density of the santa cruz island fox," in *Integrated Population Biology and Modeling, Part B*, ser. Handbook of Statistics, A. S. Srinivasa Rao and C. Rao, Eds., vol. 40, Elsevier, 2019, pp. 3–32. DOI: `https://doi.org/10.1016/bs.host.2018.10.001`. [Online]. Available: `https://www.sciencedirect.com/science/article/pii/S0169716118300889`.

[56] B. Silverman, "Density estimation for statistics and data analysis," *School of Mathematics University of Bath, UK, Monographs on Statistics and Applied Probability, London: Chapman and Hall*, 1986.